STYRELSEN FÖR

VINTERSJÖFARTSFORSKNING

WINTER NAVIGATION RESEARCH BOARD

Research Report No 21

MEASUREMENT AND ANALYSIS OF ICE-INDUCED STRESSES IN THE SHELL OF AN ICEBREAKER

Sjöfartsstyrelsen
Finland

Finnish Board of Navigation

Sjöfartsverket
Sverige

Swedish Administration
of Shipping and Navigation

F O R E W O R D

The Winter Navigation Research Board presents its report No 21. The report deals with the measurement of the structural response to ice impacts on the plating of the icebreaker URHO. This is the first stage of an undertaking to investigate the real ice induced stresses on the hull of a ship when advancing in ice. The work is done by Oy Wärtsilä Ab Helsinki Shipyard under direction of mr Petri Varsta. The Winter Navigation Researh Board expresses its thanks to the research team, the personnel of the icebreaker and others who have contributed to this work.

Helsingfors and Stockholm August 1977.

Jan-Erik Jansson

Lennart Johansson

CONTENTS

PART 1

CONTINUOUS MEASUREMENT OF ICE - INDUCED STRESSES IN SHELL OF ICEBREAKER URHO IN 1976.

Petri Varsta

SUMMARY

This paper deals with the continuous measurement of the structural response due to ice impacts on the plating of the icebreaker Urho on the Gulf of Bothnia in 1976.

The measuring system is described at the beginning.

The measured stress levels are shown in the form of histograms. The three-parameter Weibull distribution is fitted to the measured data.

Lastly the pressure due to ice impact on the plating is calculated from the measured data.

CONTENTS

1. BACKGROUND

It is generally known that the phenomenon of ice impacts on the shell of an icegoing ship is very complicated. There are several parameters of ice, the effects of which on ice load are still unknown. When looking at the icebreaker the problem becomes more complicated as the shell has to bear all ice loads appearing on the operation area. Due to this the structural design of an icebreaker today is mainly based on experience.

As new demands for an icebreaker have come up, such as navigation in shallow water, the selection of design pressures of shell has become more important to avoid overweight of steel structure. These demand increased knowledge about ice loads on the shell of an icebreaker.

The measurements were planned to be performed on the Baltic icebreaker Urho, which is owned by the Finnish Board of Navigation.

The main dimensions of the icebreaker Urho are the following:

- length max 104.6 m
- breadth max 23.8 m
- draught max 8.3 m
- draught at CWL 7.3 m
- power 16.2 MW

Figure 1 shows the icebreaker Urho operating on the Gulf of Bothnia.

2. DESCRIPTION OF THE RECORDING SYSTEM

The main requirements for the measuring system were the following:

- measuring time 24 hours per day
- automatic operation during recording and analysing.

The scheme of the measuring system is shown in figure 2. The recording unit was a multichannel pulse analyser, type LP 4840, made by Nokia. The analyser is shown in figure 3. The store of the central unit of the analyser included 800 channels divided into four groups. Owing to this, it was possible to measure stresses from four strain gages at the same time. The memory capacity of the store was 10^6 counts per channel. Figure 4 shows the principle of sample taking. The analyser was programmed to print the analysed data on tape once a day. The frequency of sampling was 1 kHz.

In figure 5 the places of strain gages are shown. These are mounted on the shell plating. The measuring direction of the gages was horizontal. The strain gage configuration was V-shaped as figure 5 shows. The angle between gages was 56°.

The theoretical background for this configuration of strain gages is represented in the Appendix.

3. PRESENTATION OF THE MEASURED DATA

3.1 General

The analyser was installed 1976-02-19. From the beginning it was noticed that the automatic printing unit did not tolerate conditions onboard. Owing to this there were only four successful measuring periods.

In table 6 the weather conditions during measurements are represented. It can be seen that during measurement 3 the wind has been heavy, 11 m/s from the south.

The winter was mild. Owing to this the frozen area of the Gulf of Bothnia was small. The thickness of ice on the coast south of Kemi was about 80 cm and at the open sea about 30 cm---70 cm. Figures 7, 8 and 9 show the ice conditions during measurements. In these figures it can be seen that the ice conditions were typical for the northern part of the Gulf of Bothnia including level ice and pack ice with ridges. In figures 7, 8 and 9 the routes of the icebreaker during measurements are also drawn. This information was taken from the log book of the ship.

During measurements 1, 2 and 3 the icebreaker was assisting merchant ships. The measurement 4 was done during the shipyards full scale tests.

Table 10 represents the total duration of measurement, effective measuring time, which means the time the ship was moving, and travelled voyage during measurement. In table 10 it can be found that there is a lot of time when the stress on the shell plating is zero due to the ship not moving. This has to be subtracted from final results.

Table 11 shows the measuring points at the different measurements.

3.2 Distributions of measured stresses

Figures 12 to 23 show the histograms of measured stresses in the shell plating. The stress values are divided by the yield stress of the plate (σy) which is 235 N/mm^2. In the figures the scale of calculative ice pressure is also shown. The question of the calculative ice pressure is treated more deeply in the following chapter. The zero stresses due to stops of the icebreaker are reduced from the pillar of zero stress. As the memory capacity of the analyser was 10^6 counts per channel, overflow at channels near zero stress has occurred. Owing to this the heights of these pillars are estimated from the total number of counts.

As the histograms show, these are non-symmetric and are skewed to the right. The negative stress pillars are due to impacts hitting on the nearby plate fields. In figures 20 to 23 it can be seen that the shape of the histograms of the measuring point 5 varies much from one measurement to another. This may arise from the fluctuation of ice conditions and the draught of the icebreaker.

The histograms show that the dominating stress level as an absolute value is low. Table 24 illustrates maximum stress values and averages of the 100 highest stress values at the different measuring points. In the table strong variation of maximum stress at the fore-body of the icebreaker from 0.28 to 0.70 can be recognised.

On the basis of these measurements it was not possible to draw conclusions about stress levels as a function of the places of strain gages.

As figures 12---23 indicate the aim was to fit a theoretical distribution to the measured data. The three-parameter Weibull distribution was used. The mathematical form of the Weibull distribution is the following:

$$f(x) = \frac{\eta}{\lambda}\left(\frac{x - \varepsilon}{\lambda}\right)^{\eta-1} e^{-\left(\frac{x - \varepsilon}{\lambda}\right)^{\eta}} \qquad (1)$$

where $f(x)$ = Weibull probability distribution
x = $\sigma/\sigma y$
ε = location parameter
λ = scale parameter
η = shape parameter

Table 25 shows the values of the parameters of the Weibull distribution which give best fits between distributions and histograms. Figures 12---23 show that on the whole the shapes of the Weibull distributions are good when compared to the measured data. The Kolmogorov-Smirnov test was also used to get a mathematical confidence to the goodness of fits. For the 95 percent Kolmogorov-Smirnov limit was chosen 0.136.

Table 25 shows the maximum deviations between the sample and the assumed cumulative distribution. The tests show clearly that the Weibull distribution at figures 20 and 21 does not fit very well but other distributions fulfil the test better.

3.3 Calculative ice pressure

To get some idea about the ice pressure some assumptions were made about the structural behaviour of the shell plate and the load area. The measurements made with three strain gages on a plate field /6/ showed that the maximum stress is in the middle of the plate field as figure 26 shows. On the basis of measurements made with several strain gages on the same frame /6/ and of data about ice thickness during measurements, it was decided to use load area 400 mm x 400 mm at the calculations as figure 26 shows.

Using this load area the structural response was calculated with the finite element method /2/. The effect of frames was also taken into consideration at the calculations. In figure 26 the result of the calculation drawn with broken line is shown. The calculated curve fits quite well to the measured stresses. The calculations give the following dependency between stress in the middle of plate and pressure, at this load configuration:

$$p = \frac{t^2 \times \sigma}{6 \times k \times h \times s} \qquad (2)$$

where
- p = pressure
- t = plate thickness
- s = width of load = 400 mm
- h = height of load = 400 mm
- k = constant = 0.067
- σ = stress in the middle of plate

For a simply supported infinitely long plate the constant k gets a value of 0.084 with this load configuration.

Using the formula 2 the maximum and average of 100 highest pressure values were calculated. The results are given in table 27. These values are divided by the allowed pressure, when the load area is 400 mm x 400 mm.

On the basis of figure 26, the stress value in the middle of the span of the plate can be regarded as a dimensioning value at the elastic range. Owing to this, the scale of pressure divided by the allowed pressure p_a has also been added in figures 12 to 23. The positive parts of the histograms have only meaning in this case.

4. CONCLUSIONS

The measurements of structural response of the shell of the ice-breaker Urho with equipment automatically and continuously analysing data gave encouraging experiences in spite of technical difficulties at the measuring system.

As the frequency of sample taking is high and the equipment measures all the time, it is possible to record all ice loads and the risk of missing peak loads is out of question.

The total effective measuring time was 62.2 hours. On the basis of these measurements it seems that the maximum ice pressure on the shell plating is approximately equal to the crushing strength of ice. From the literature it can be found that the crushing strength of ice of the Baltic is about 2.8 N/mm^2 for a load configuration approximately describing impact between ship and ice /4,5/.

THEORETICAL BACKGROUND OF V-SHAPED GAGES

The theory of strain at the two-dimensional case gives the following formula (see also figure 5):

$$\varepsilon_{\phi} + \varepsilon_{-\phi} = 2 \cos^2\phi(\varepsilon_x + \tan^2\phi\ \varepsilon_y)$$

The dependency between stress in the direction of x-axis and strains is given by

$$\sigma_x = \frac{E}{1 - \nu^2}(\varepsilon_x + \nu\ \varepsilon_y)$$

where E = Young's modulus

ν= Poisson's ratio

These two formulae give the following equation

$$\tan^2\phi = \nu$$

when $\nu = 0.285$ for steel the value of the angle ϕ is about 28^{o}.

The formula of σ_x can be written as follows:

$$\sigma_x = \frac{E}{2(1 - \nu)}\ (\varepsilon_{\phi} + \varepsilon_{-\phi})$$

5. REFERENCES

/1/ Askren, W.B. — Mathematical Modelling of Human Performance Errors for Reliability Analysis of System, Aerospace Medical Research Laboratory, Ohio, 1969.

/2/ Hakala, M.K. — Jäykistämättömien ja jäykistettyjen laattojen analysointi kahdeksansolmuisilla levy- ja laattaelementeillä (An Analysis of Unstiffened and Stiffened Plates with Eight-Node Plane and Plate Elements) Thesis, Helsinki University of Technology, 1974.

/3/ McGrath, E.J. — Techniques for Efficient Monte Carlo Simulation. Volume I. Selecting Probability Distribution, SAI-72-590-LJ, 1973.

/4/ Rantamäki, J — Jään kuormituskokeita talvella 1971-72 Oulu- Kemi syväväylää varten (Loading tests of ice in the winter 1971-72 for deep fairway between Oulu - Kemi), Oulu, 1972 (unpublished).

/5/ Ruck, K-W., Freund, H. — Ergebnisse und Untersuchungen über Festigkeiten von Ostsee- und Südwasser-Eis, Der Bauingenieur Heft 9, 1969.

/6/ Varsta, P. — Analysis of Short-Term Ice-Induced Stresses in The Hull of Icebreaker Urho in 1976. (In preparation)

6. FIGURES AND TABLES

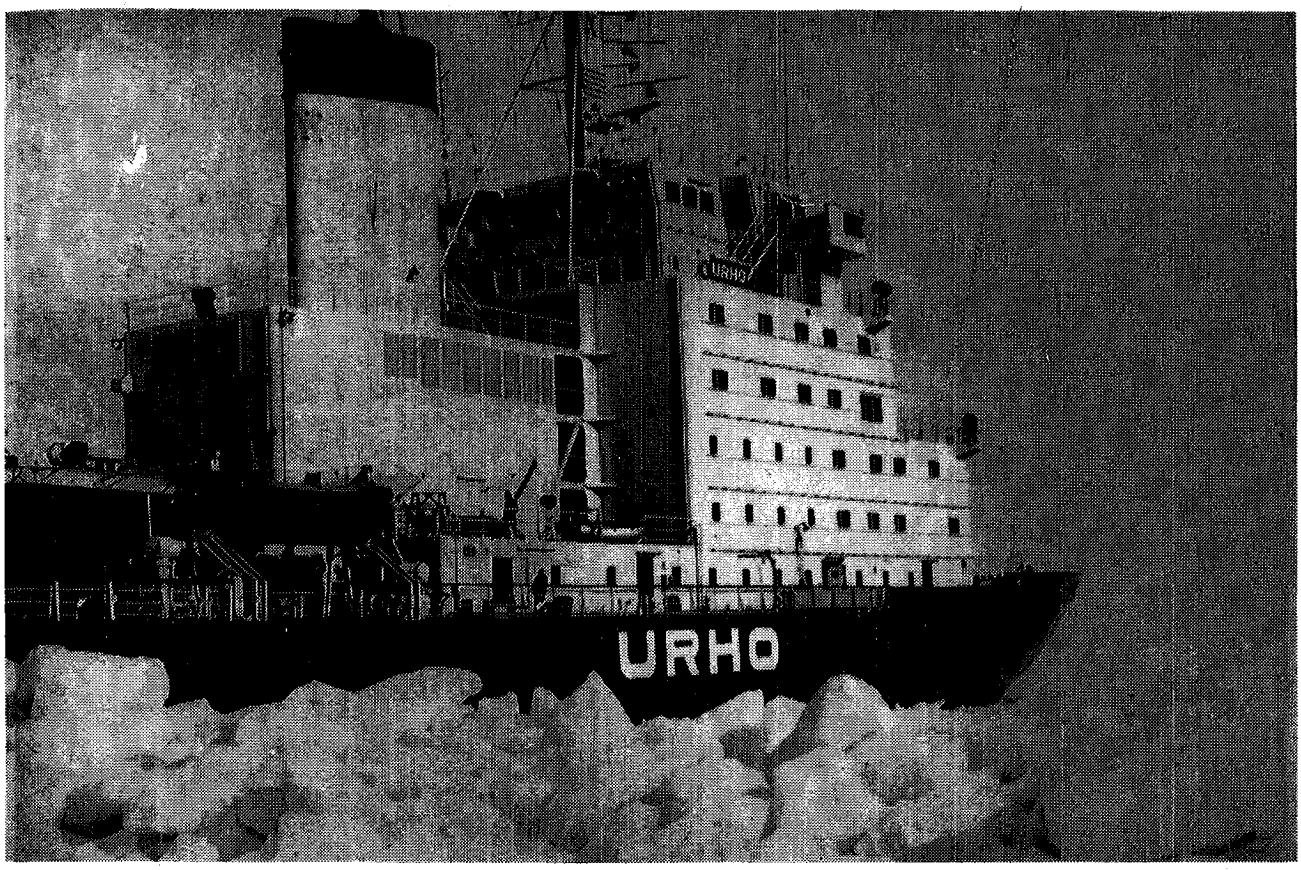

Figure 1. Icebreaker Urho

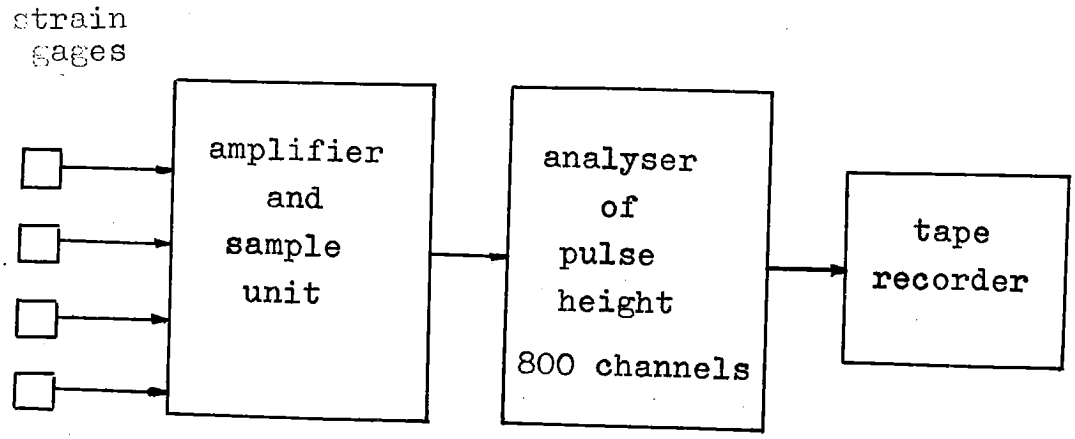

Figure 2. The scheme of the measuring system

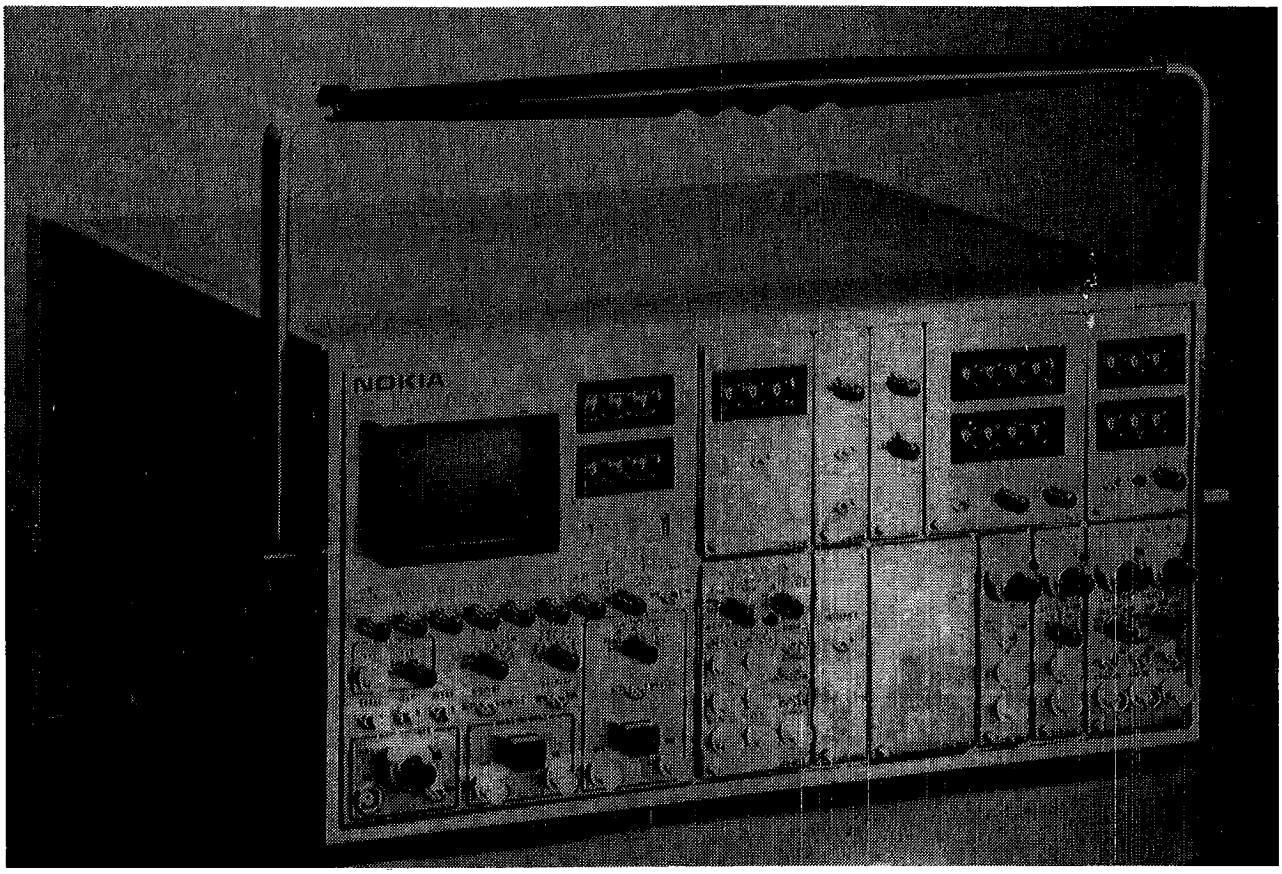

Figure 3. The multichannel pulse analyser

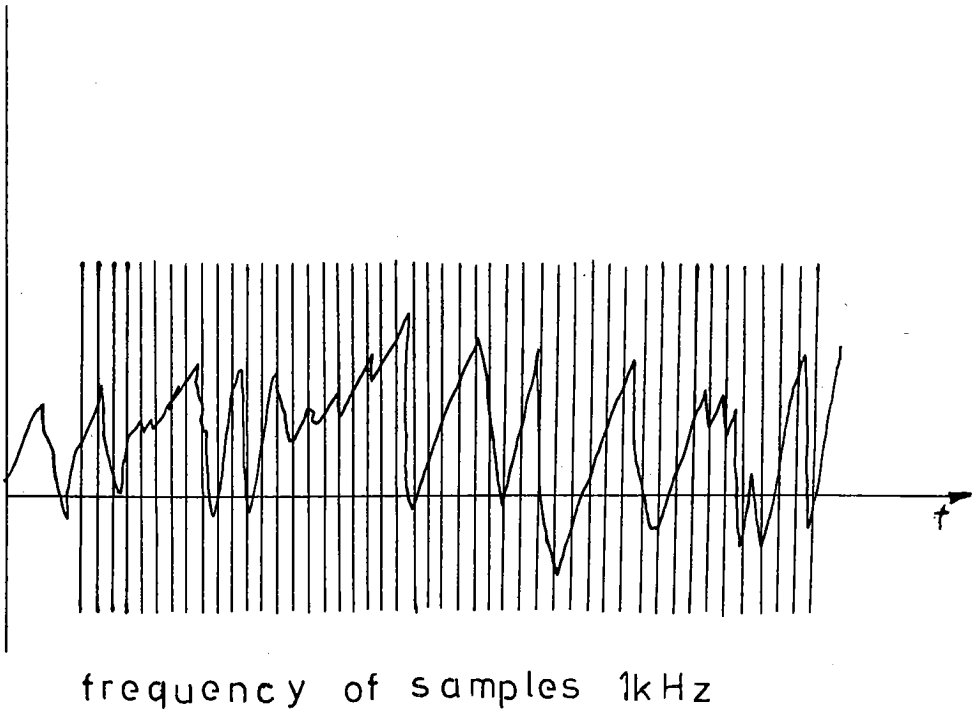

Figure 4. The principle of sample taking

M. point	Frame	Dist. from BL/m
1	88 + 200 mm	6.75
2	88 + 200 mm	5.90
3	97 + 200 mm	6.75
4	97 + 200 mm	5.90
5	111.5 + 200 mm	6.95

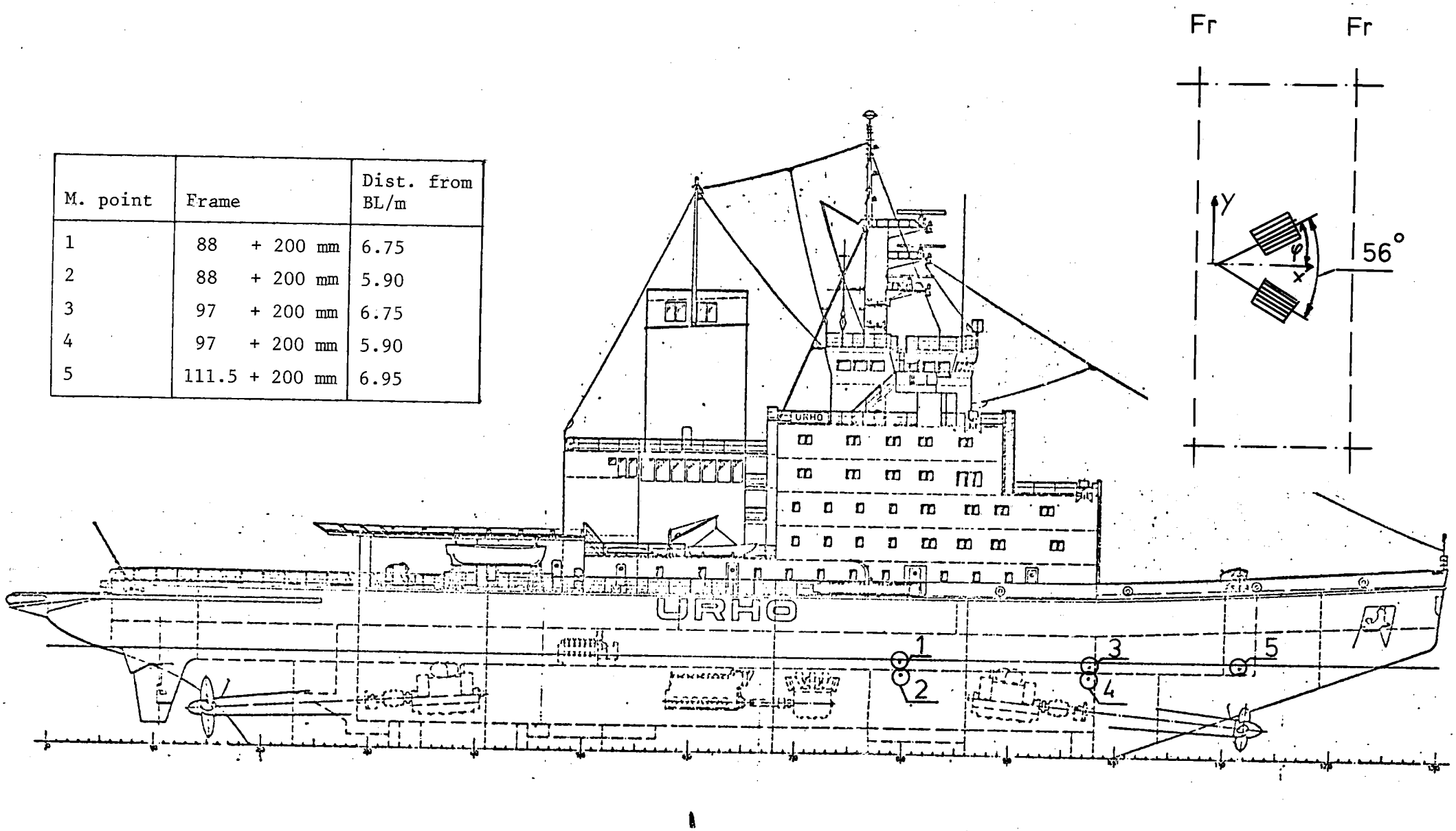

Figure 5. The places of strain gages and the mounting principle

Table 6. Weather conditions during measurements

Measurement	Date of measurement	Temperature of air/°C min	max	aver	Wind speed/ m/s
1	20.2., 5.30-21.2., 5.30	-7	-2	-3.7	calm
2	22.2., 5.30-23.2., 5.30	-4	-4	-4.0	3
3	23.2., 5.30-24.2., 5.30	-5	-2	-3.2	11
4	29.3.,13.15-30.3., 9.50	-4	+4	-2.0	4

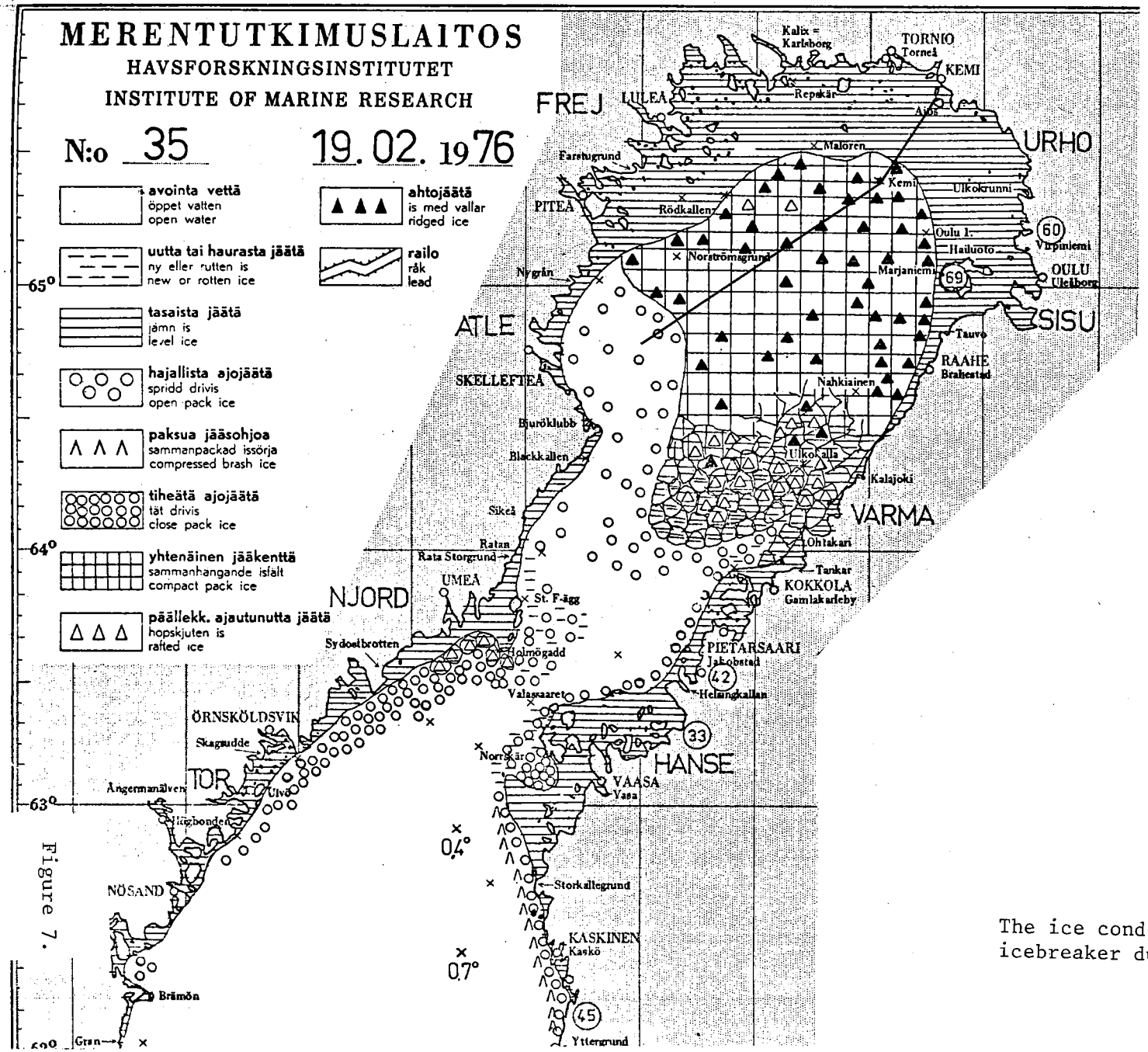

Figure 7.

The ice condition and the route of the icebreaker during the measurement 1

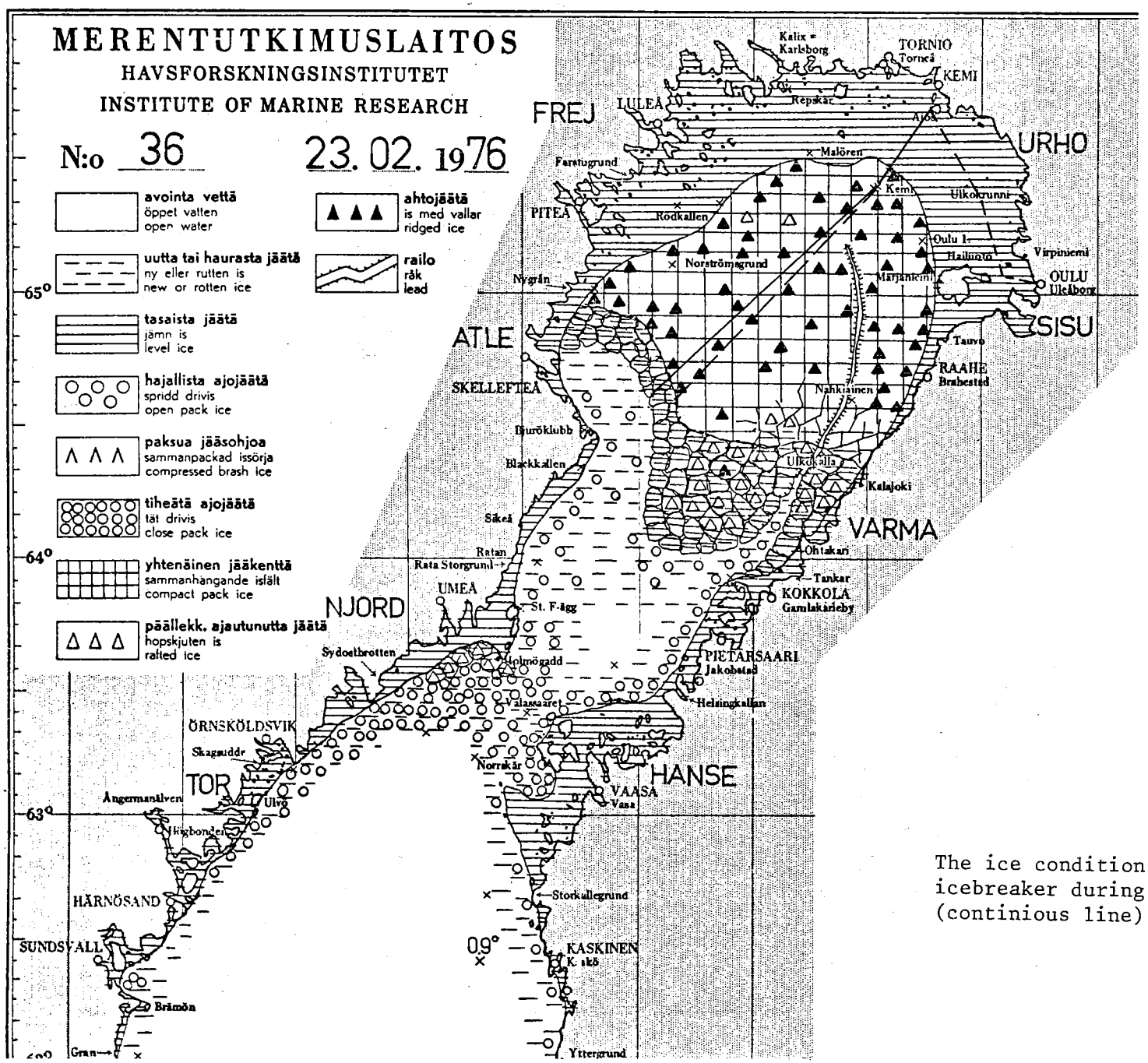

Figure 8.

The ice condition and the routes of the icebreaker during the measurements 2 (continious line) and 3 (broken line)

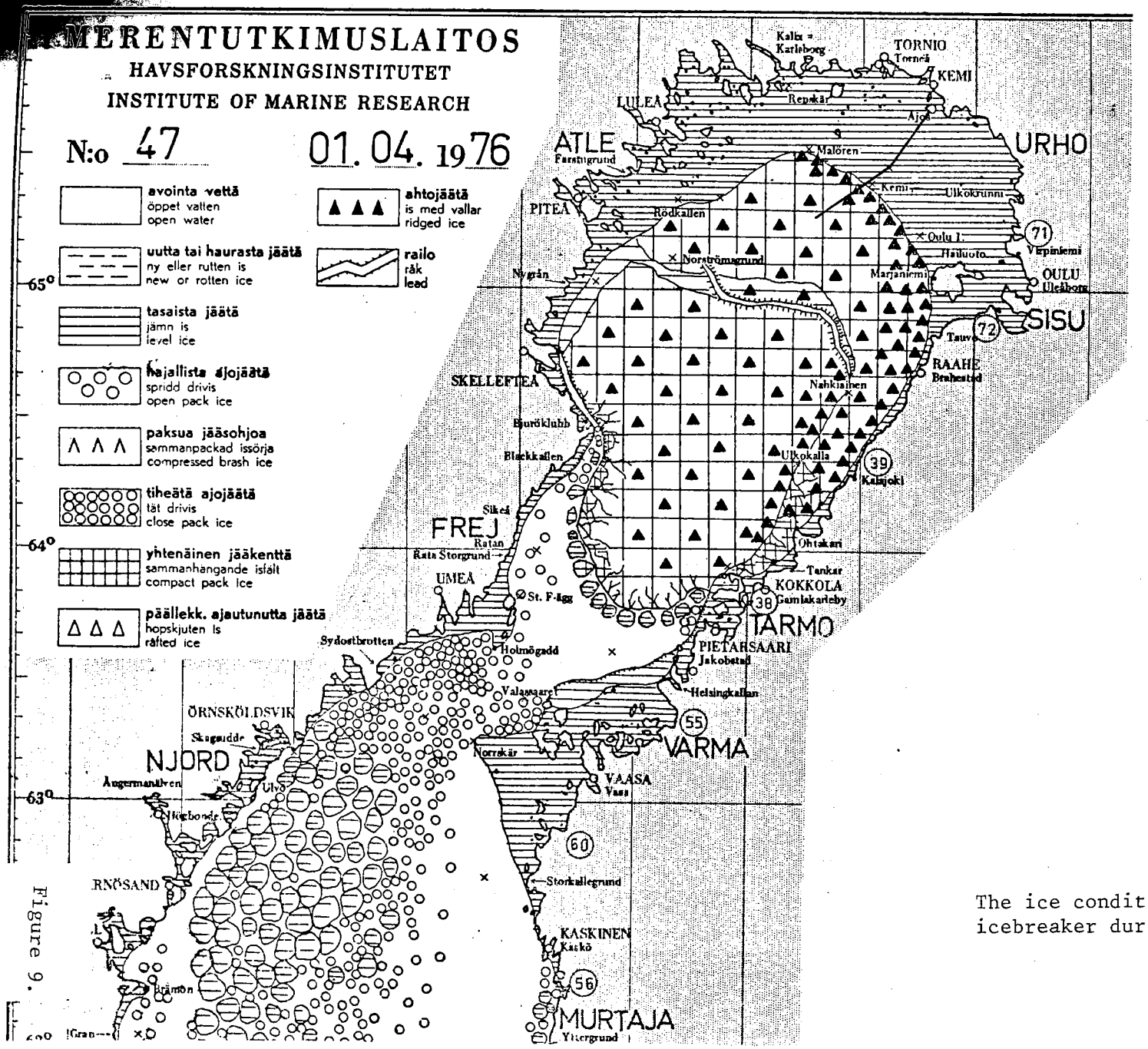

Figure 9.

The ice condition and the route of the icebreaker during the measurement 4

Table 10. Data from the log book

Measurement	Total duration of measurement	Effective measuring time	Travelled vouage/ n. miles
1	24 h	11 h 40 min	99
2	24 h	12 h 50 min	134
3	24 h	21 h 55 min	230
4	20 h 35 min	15 h 45 min	44

Table 11. The measuring points

Measurement	Measuring point
1	-, 3, -5
2	-, 3, 4, 5
3	-, 3, 4, 5
4	1, 3, 4, 5

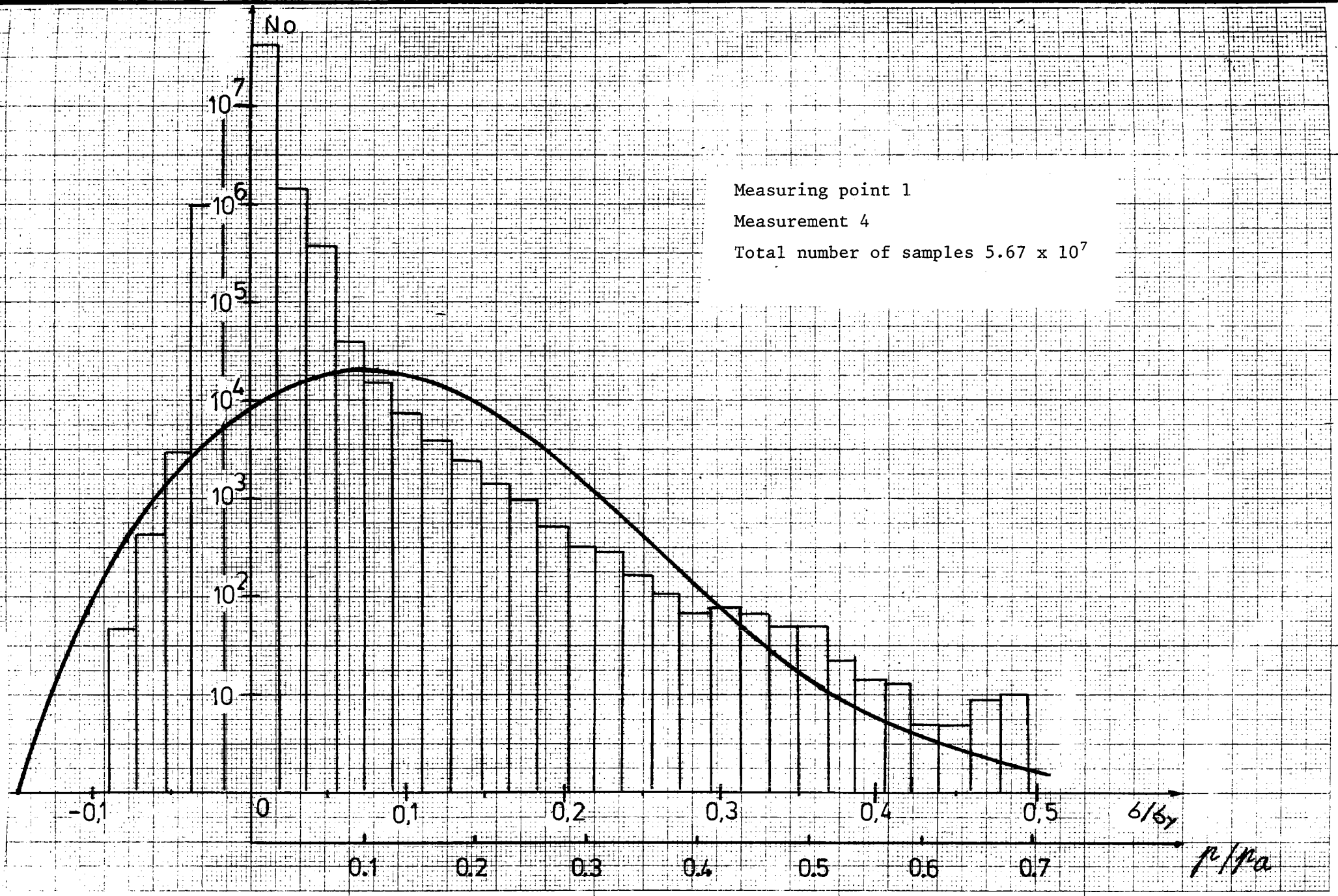
No
10^7
10^6
10^5
10^4
10^3
10^2
10
-0,1
0
0,1
0,2
0,3
0,4
0,5
σ/σ_y
0.1
0.2
0.3
0.4
0.5
0.6
0.7
p/p_a
Measuring point 1
Measurement 4
Total number of samples 5.67×10^7

Figure 12.

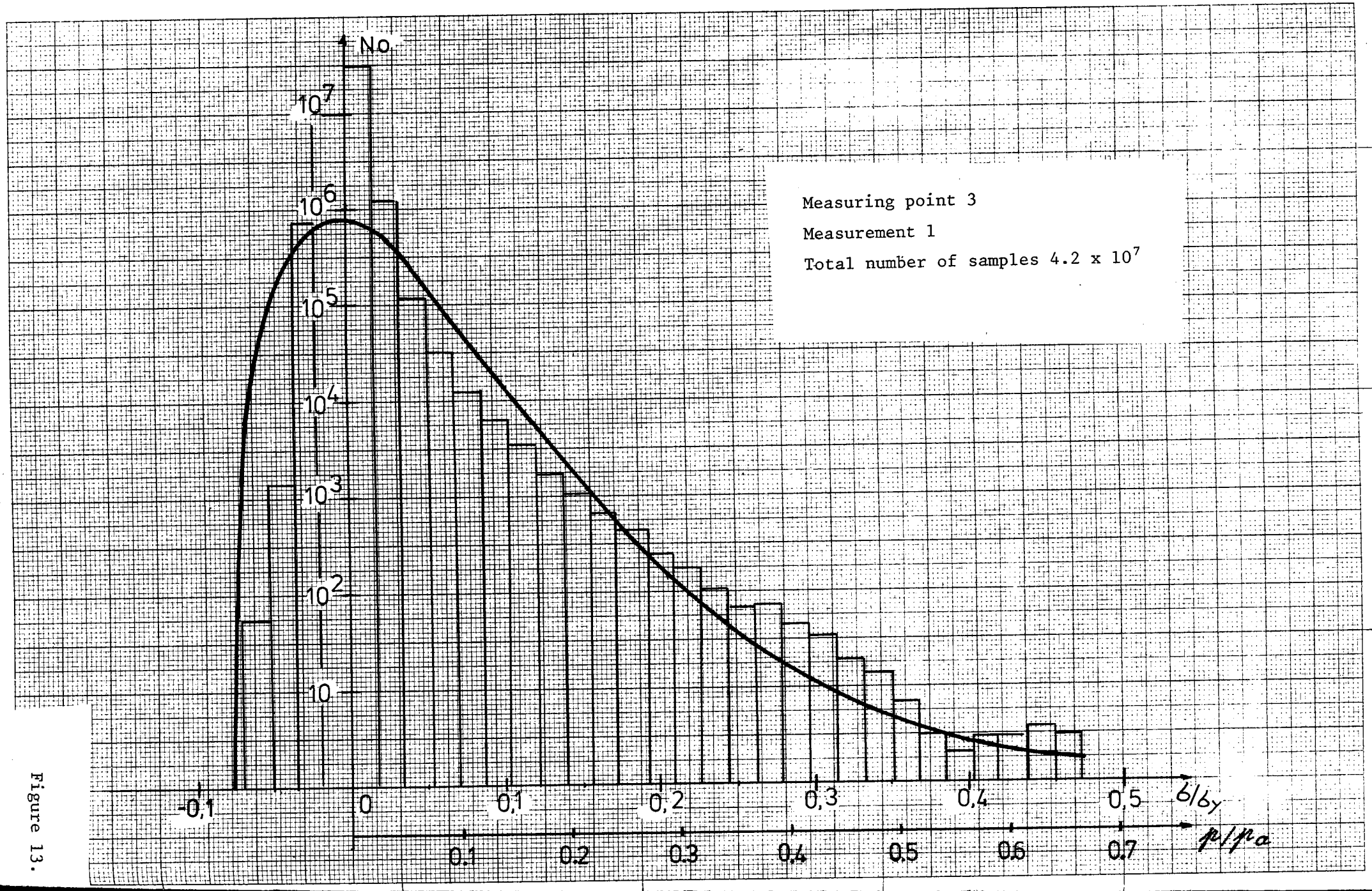
No
10^7
10^6
10^5
10^4
10^3
10^2
10
-0,1
0
0,1
0,2
0,3
0,4
0,5
σ/σ_y
0.1
0.2
0.3
0.4
0.5
0.6
0.7
p/p_a
Measuring point 3
Measurement 1
Total number of samples 4.2×10^7

Figure 13.

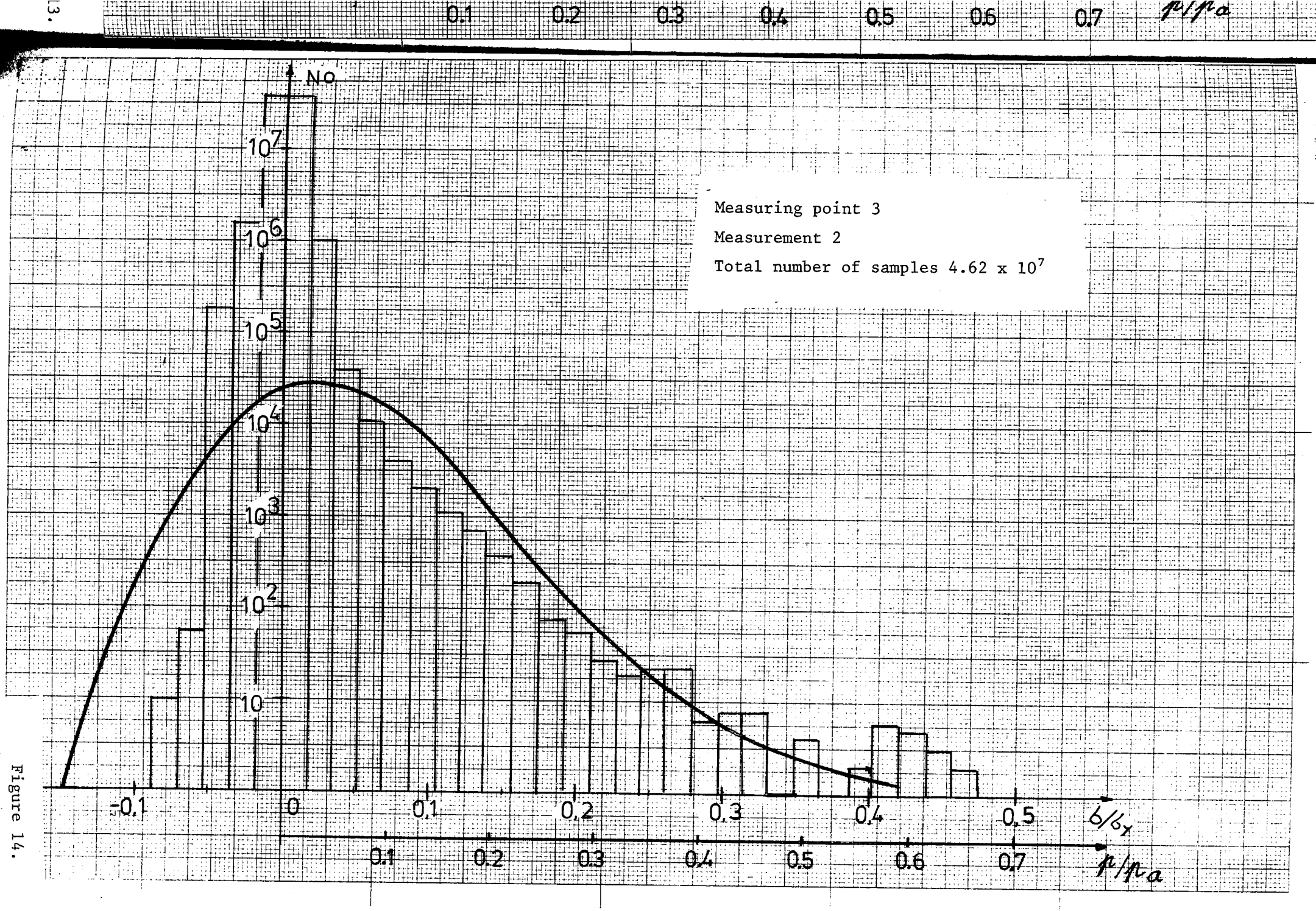
No
10^7
10^6
10^5
10^4
10^3
10^2
10
Measuring point 3
Measurement 2
Total number of samples 4.62×10^7
-0.1
0
0.1
0.2
0.3
0.4
0.5
6/6x
0.1
0.2
0.3
0.4
0.5
0.6
0.7
p/pa

Figure 14.

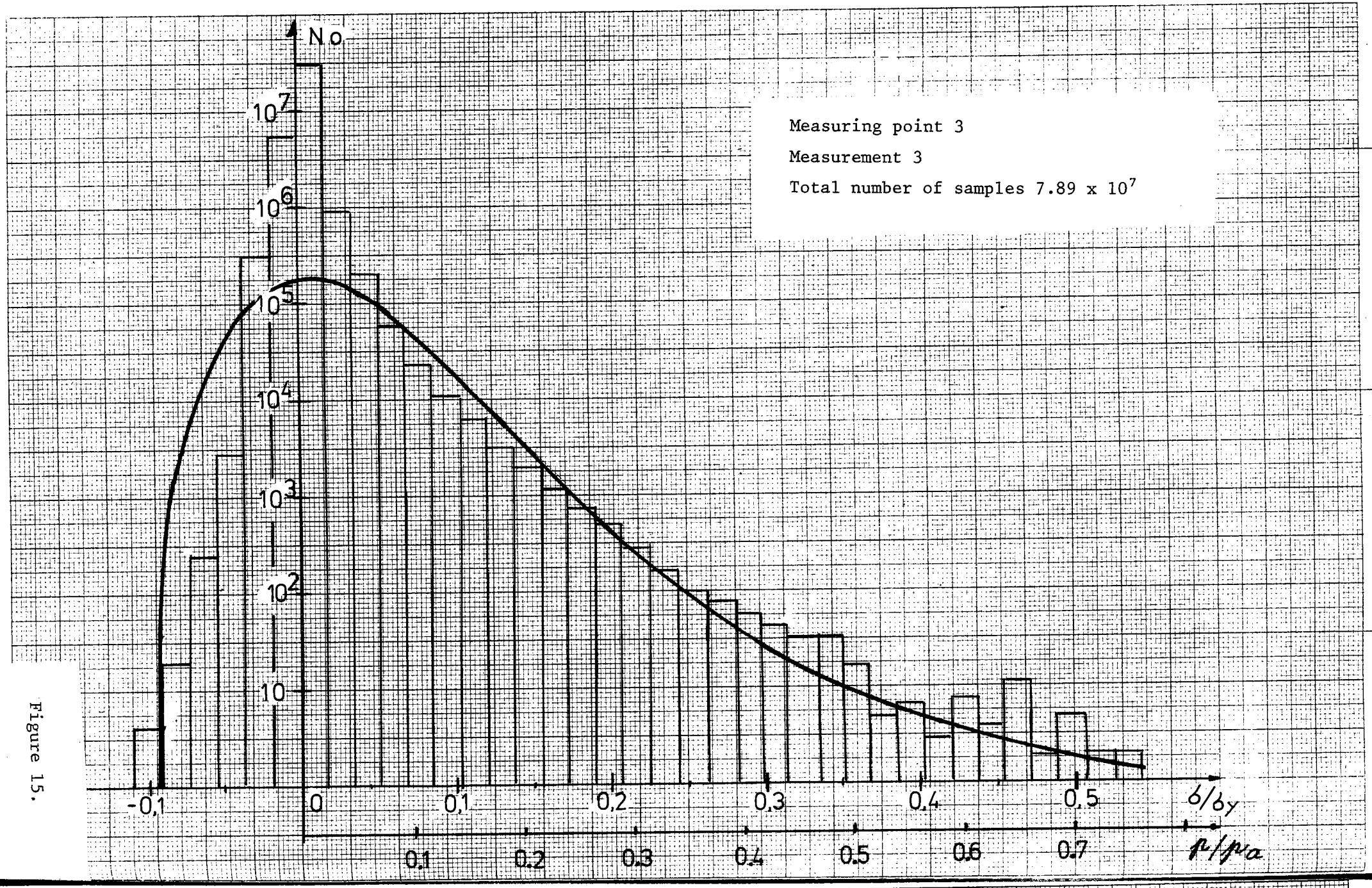

Measuring point 3

Measurement 3

Total number of samples 7.89×10^7

Figure 15.

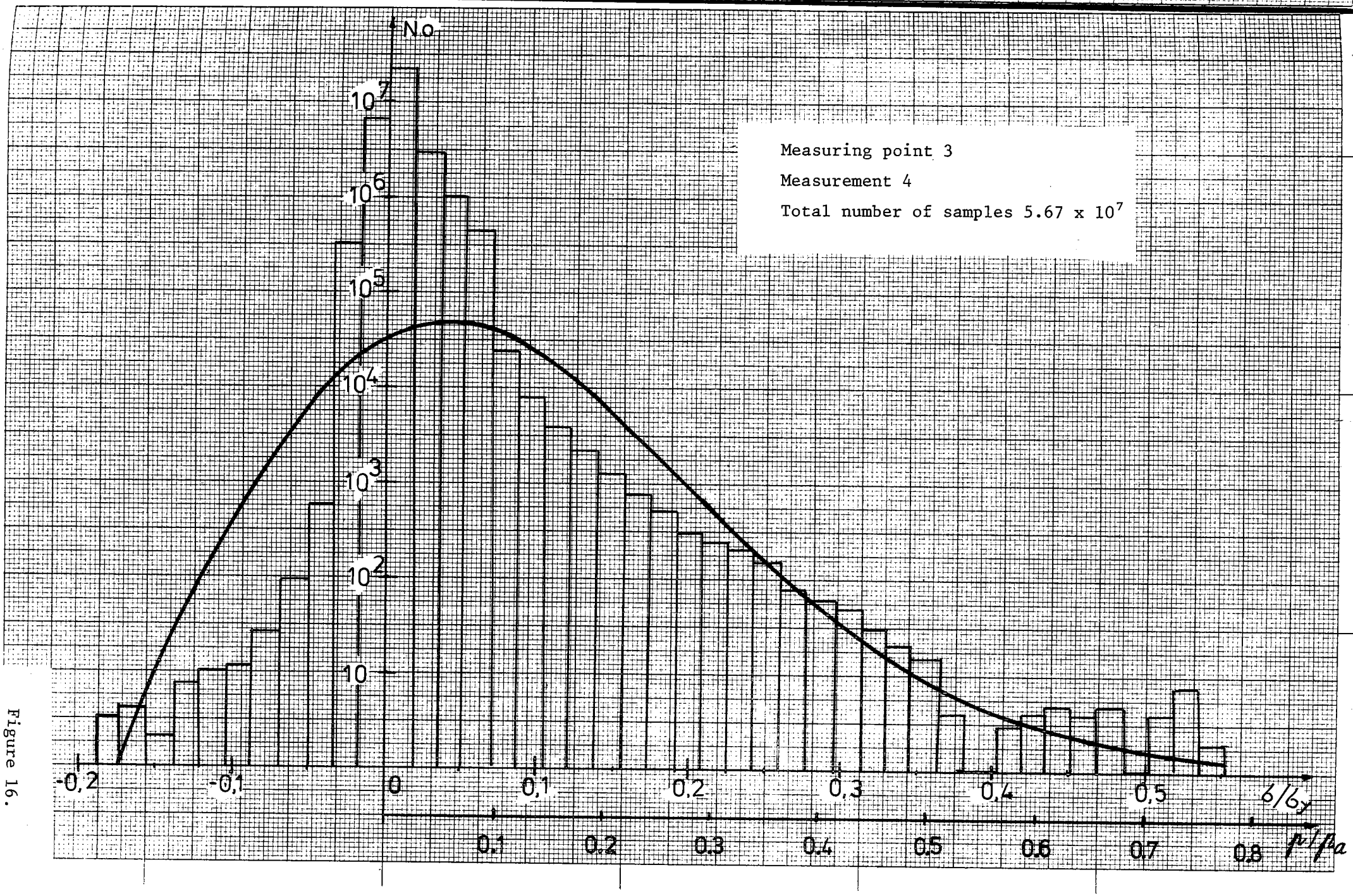
No.
10^7
10^6
10^5
10^4
10^3
10^2
10
Measuring point 3
Measurement 4
Total number of samples 5.67×10^7
-0,2
-0,1
0
0,1
0,2
0,3
0,4
0,5
0,6
0,7
0,8
p/p_a

Figure 16.

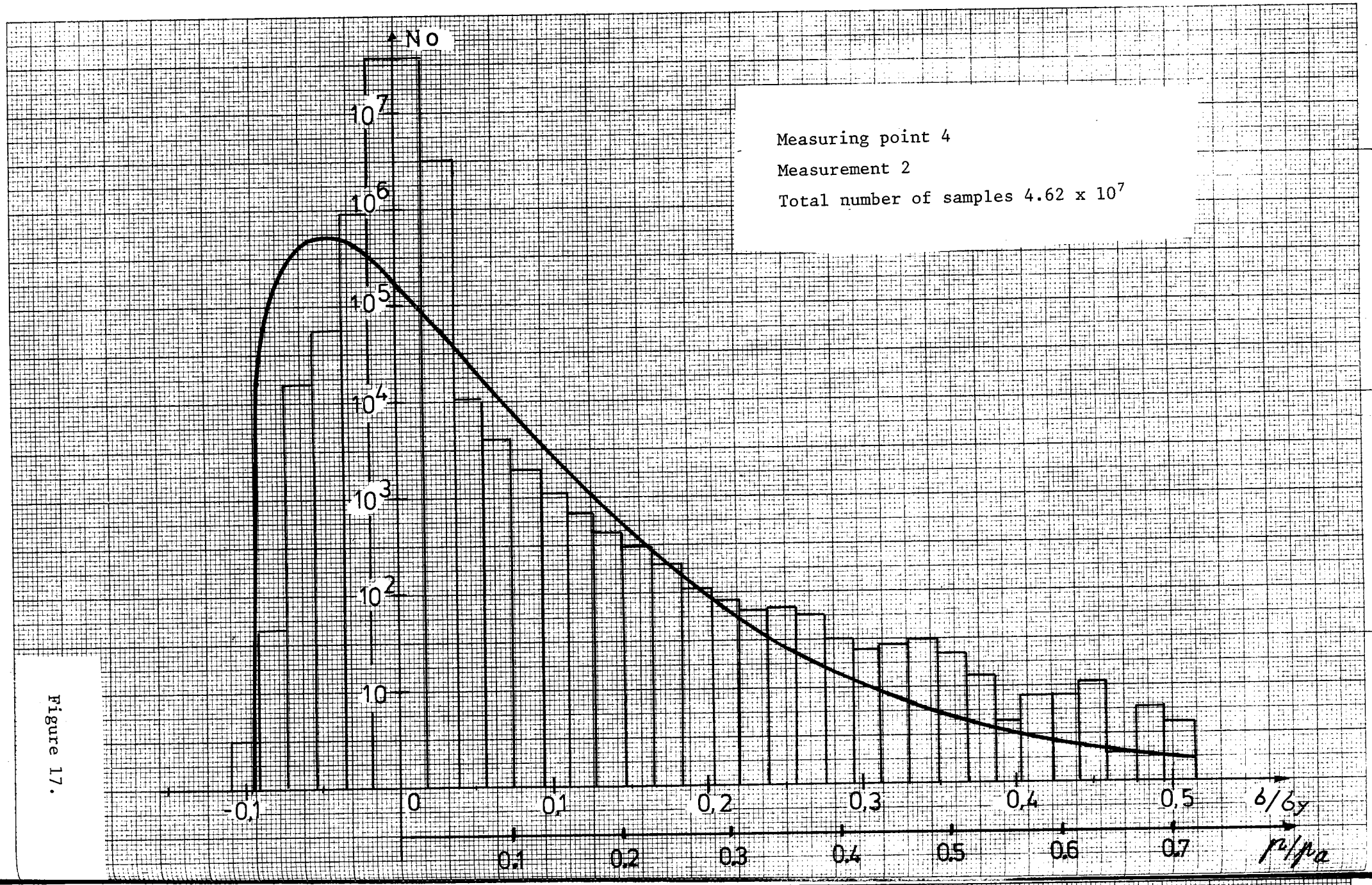
No
10^7
10^6
10^5
10^4
10^3
10^2
10
-0,1
0
0,1
0,2
0,3
0,4
0,5
6/6y
0.1
0.2
0.3
0.4
0.5
0.6
0.7
p_a/p_a
Measuring point 4
Measurement 2
Total number of samples 4.62×10^7

Figure 17.

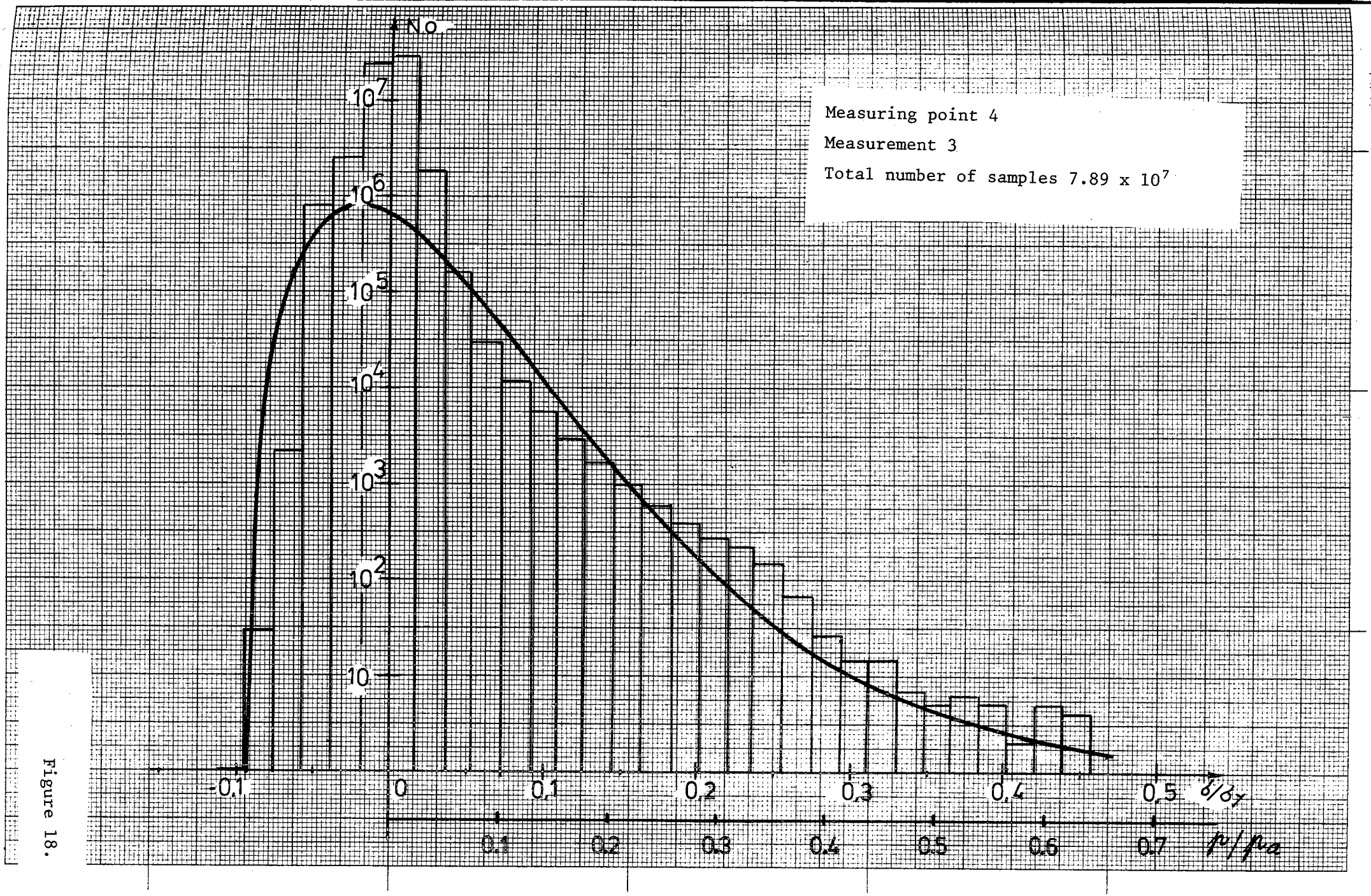
No
10^7
10^6
10^5
10^4
10^3
10^2
10
Measuring point 4
Measurement 3
Total number of samples 7.89×10^7
-0.1
0
0.1
0.2
0.3
0.4
0.5
δ/δ1
0.1
0.2
0.3
0.4
0.5
0.6
0.7
p'/pa

Figure 18.

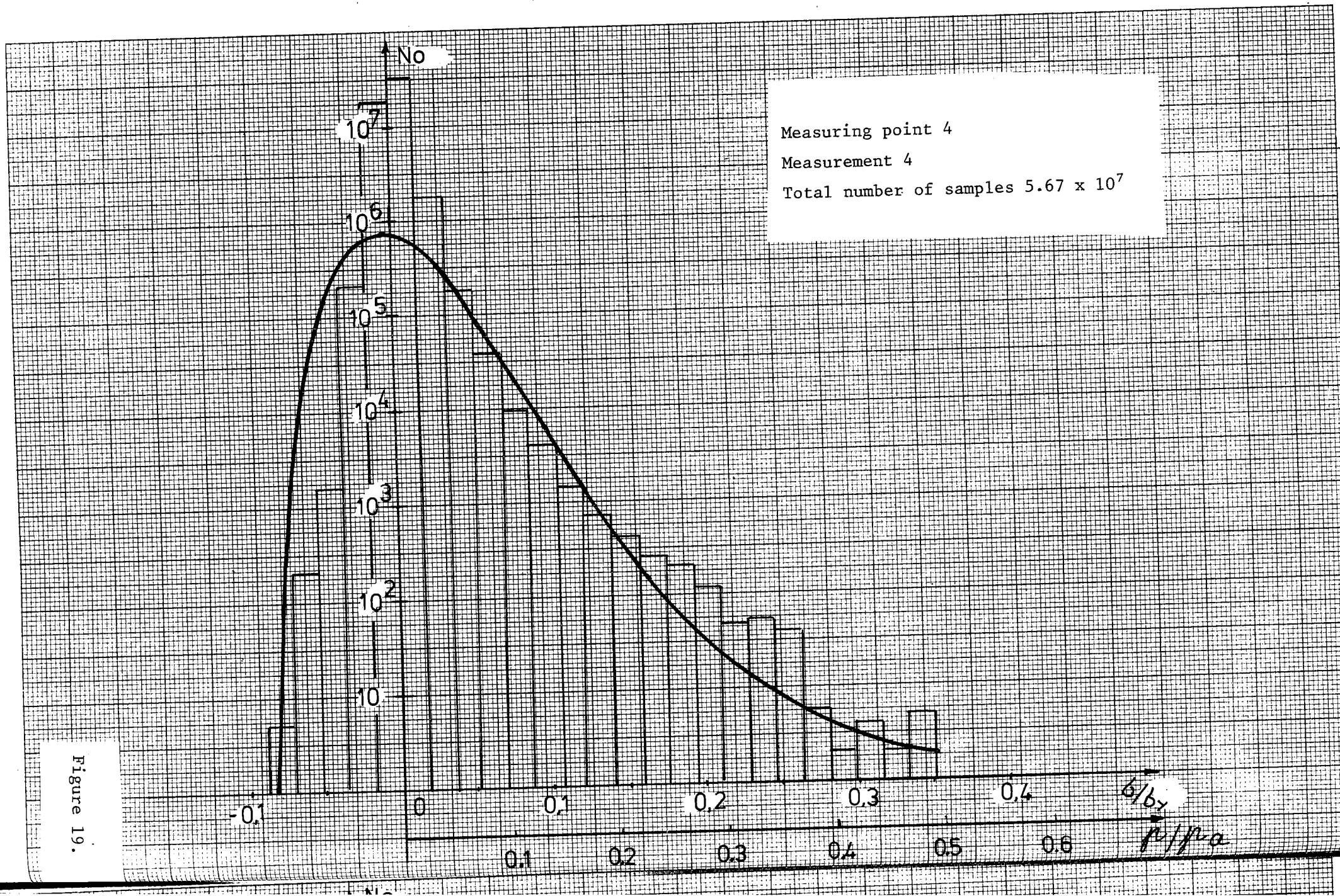

Figure 19.

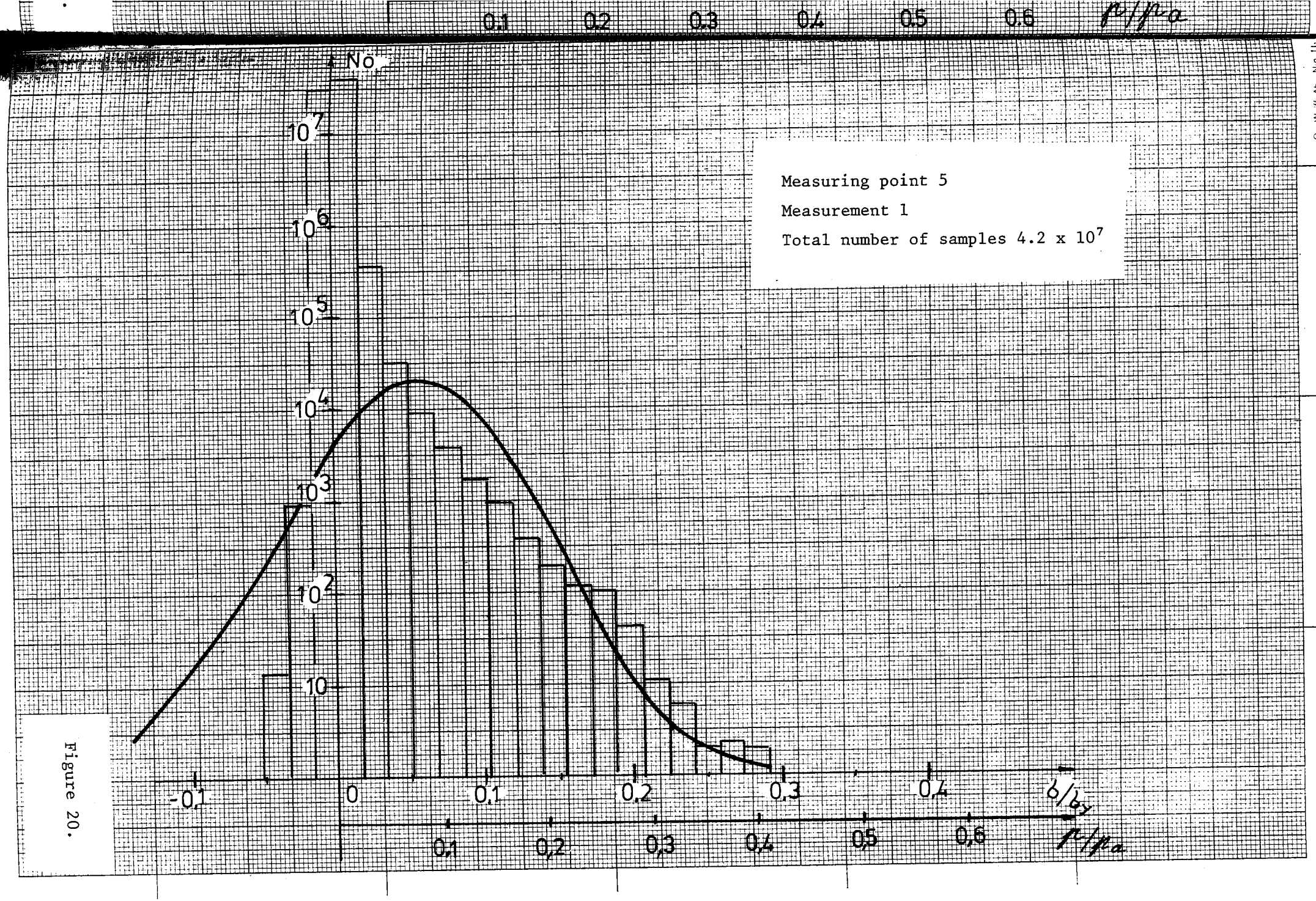
0.1
0.2
0.3
0.4
0.5
0.6
σ_a/σ_{-1}
No
10^7
10^6
10^5
10^4
10^3
10^2
10
-0,1
0
0,1
0,2
0,3
0,4
σ/σ_y
0,1
0,2
0,3
0,4
0,5
0,6
σ_a/σ_{-1}
Measuring point 5
Measurement 1
Total number of samples 4.2×10^7

Figure 20.

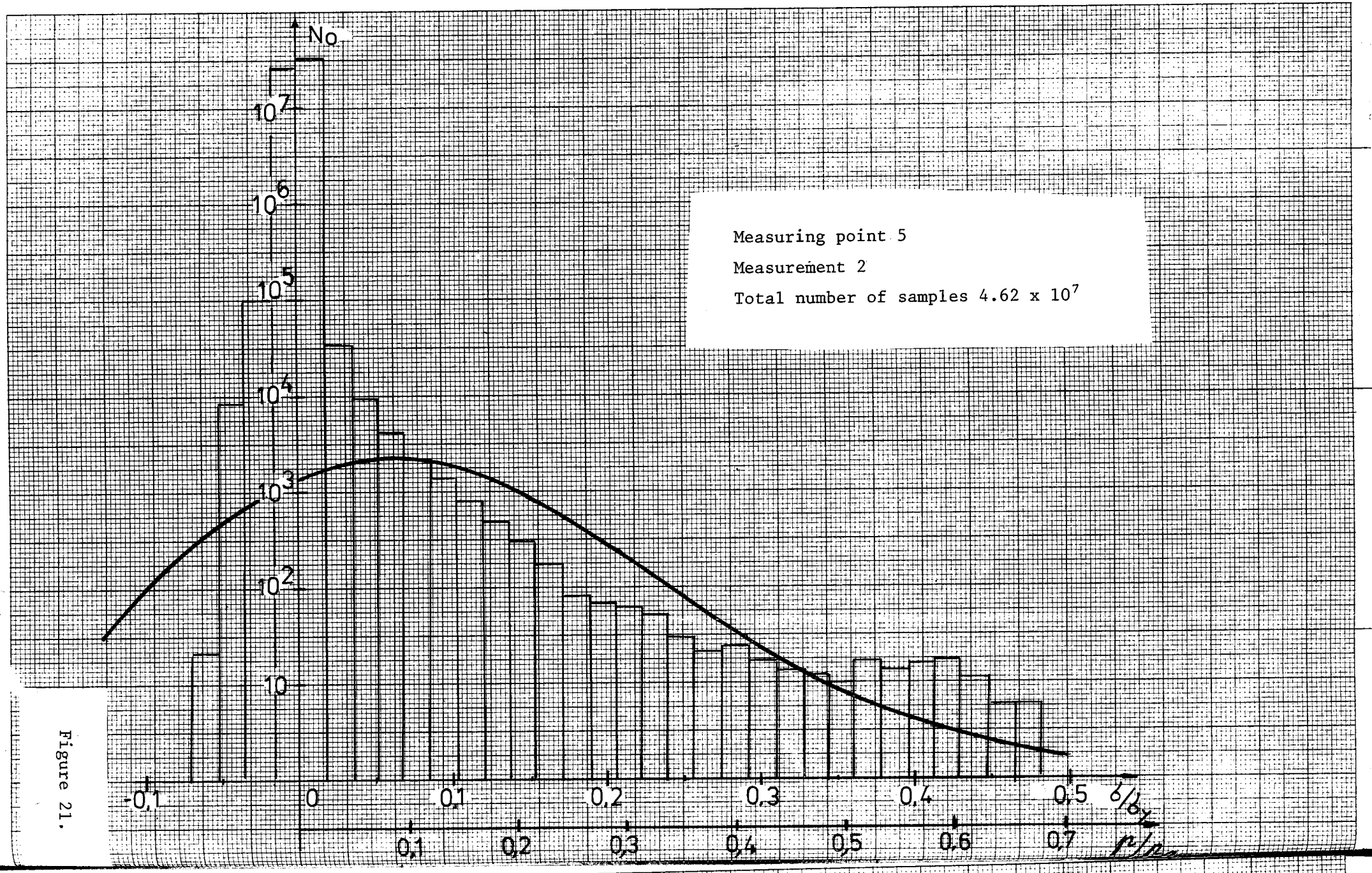

Measuring point 5

Measurement 2

Total number of samples 4.62×10^7

Figure 21.

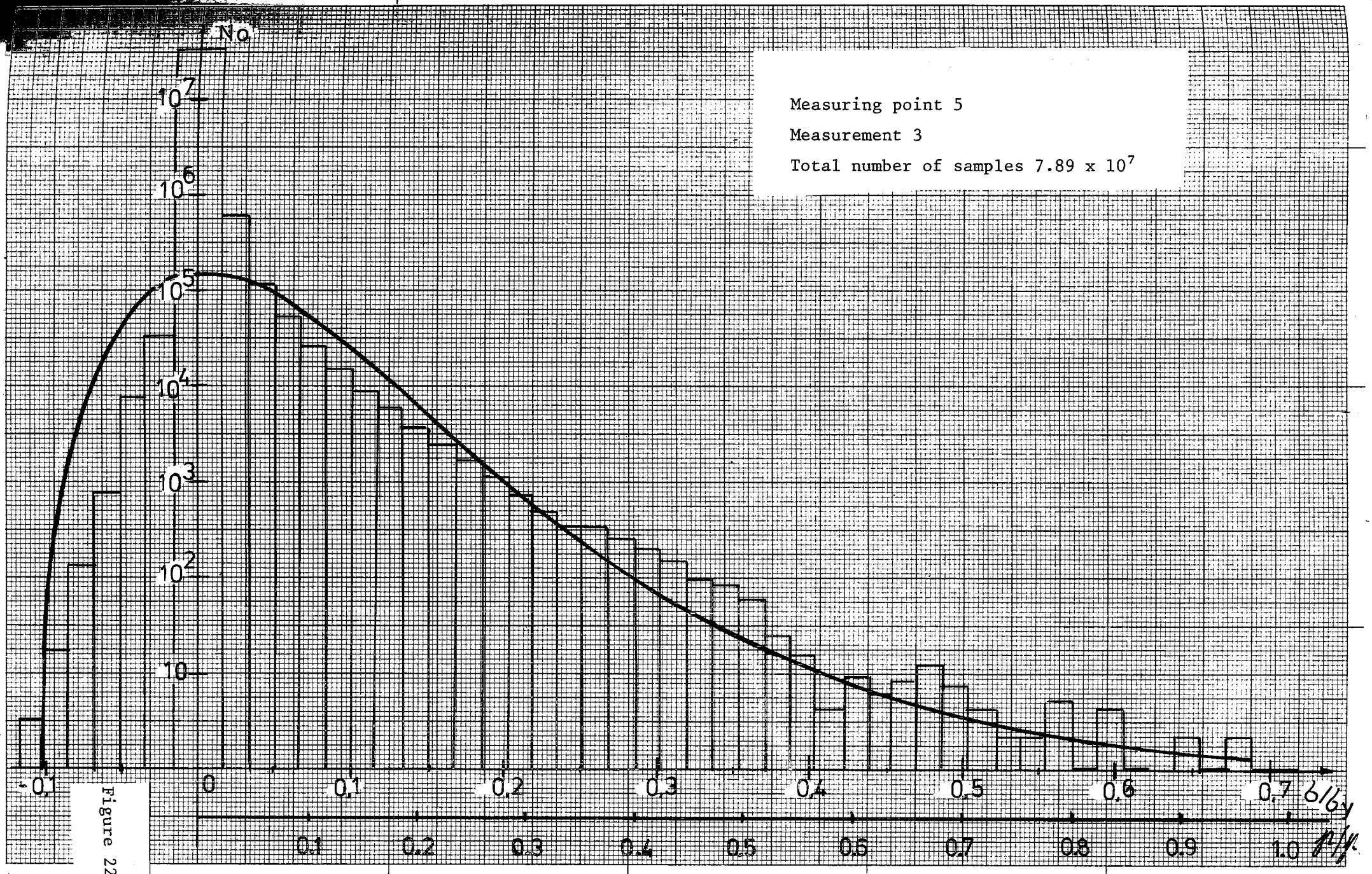
No
10^7
10^6
10^5
10^4
10^3
10^2
10
Measuring point 5
Measurement 3
Total number of samples 7.89×10^7
-0,1
0
0,1
0,2
0,3
0,4
0,5
0,6
0,7
σ/σ_y
0.1
0.2
0.3
0.4
0.5
0.6
0.7
0.8
0.9
1.0
σ/σ_y

Figure 22.

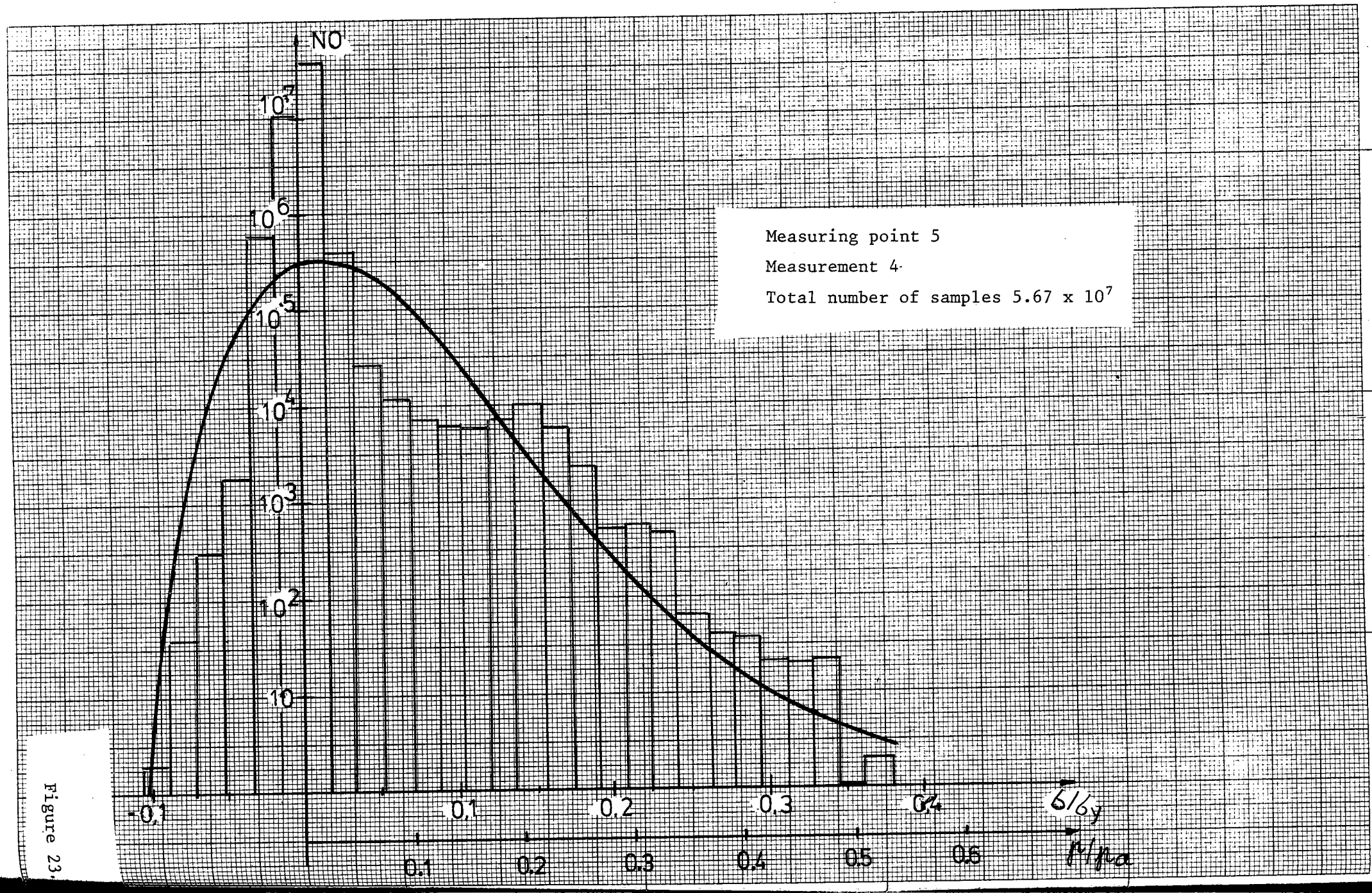

Figure 23.

Table 24. Maximum and average of 100 highest stress values

Measure-ment	Point 1 $\sigma_{max}/\sigma y$	$\sigma_{100}/\sigma y$	Point 3 $\sigma_{max}/\sigma y$	$\sigma_{100}/\sigma y$	Point 4 $\sigma_{max}/\sigma y$	$\sigma_{100}/\sigma y$	Point 5 $\sigma_{max}/\sigma y$	$\sigma_{100}/\sigma y$
1	-	-	0.46	0.34	-	-	0.28	0.20
2	-	-	0.46	0.30	0.50	0.39	0.47	0.40
3	-	-	0.53	0.40	0.45	0.33	0.70	0.47
4	0.49	0.41	0.54	0.39	0.34	0.26	0.40	0.31

Table 25. The values of parameters of the Weibull distribution

ε = location parameter
λ = scale "
η = shape "

Measuring point	Measure-ment	ε	λ	η	Max deviation
1	4	-0.2554	0.4033	2.506	0.096
3	1	-0.0751	0.1865	1.335	0.031
	2	-0.1659	0.2603	2.047	0.106
	3	-0.0956	0.2272	1.440	0.029
	4	-0.1783	0.3065	2.005	0.068
4	2	-0.0978	0.1953	1.229	0.072
	3	-0.0937	0.1927	1.373	0.025
	4	-0.0826	0.1621	1.514	0.025
5	1	-0.3002	0.3821	4.483	0.134
	2	-0.2256	0.3700	2.238	0.134
	3	-0.1017	0.2577	1.404	0.028
	4	-0.0980	0.2046	1.617	0.033

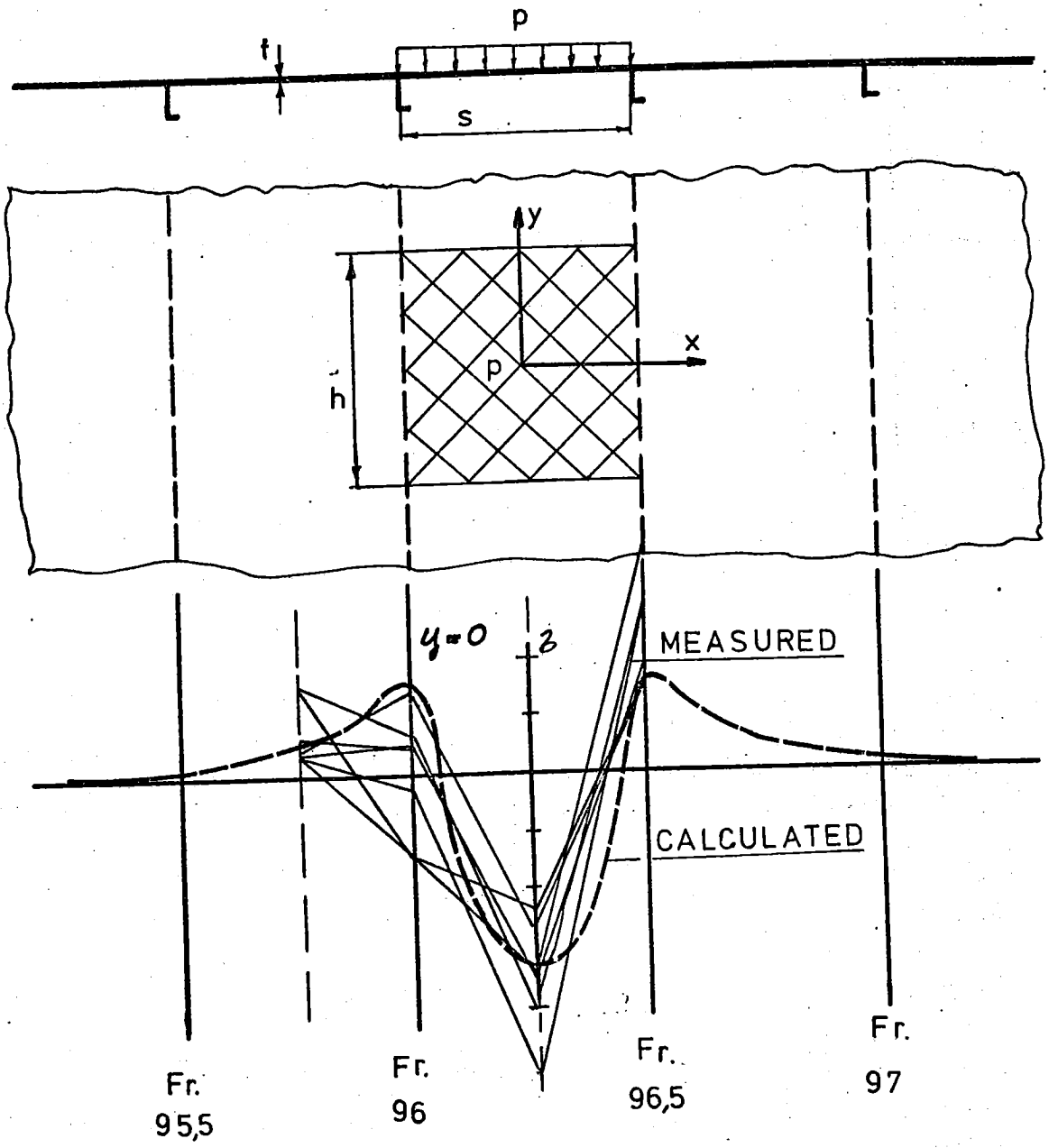

Figure 26. Calculated and measured stress distributions of the shell plate

Table 27. Maximum and average of 100 highest values of calculative pressure (p/p_a).

p_a = allowed pressure at this load configuration

Measurement	Point 1		Point 3		Point 4		Point 5	
	p_{max}/p_a	p_{100}/p_a	p_{max}/p_a	p_{100}/p_a	p_{max}/p_a	p_{100}/p_a	p_{max}/p_a	p_{100}/p_a
1	-	-	0.65	0.48	-	-	0.39	0.28
2	-	-	0.65	0.42	0.70	0.55	0.66	0.56
3	-	-	0.37	0.56	0.63	0.47	0.98	0.66
4	0.69	0.58	0.76	0.55	0.48	0.37	0.56	0.44

PART 2

ANALYSIS OF SHORT-TERM ICE-INDUCED STRESSES IN THE HULL OF ICEBREAKER URHO IN 1976

Petri Varsta

SUMMARY

This paper deals with the analysis of short-term samples of the measured ice load data from the icebreaker Urho in 1976. The measurements were done on the northern part of the Gulf of Bothnia. The data collection and reduction system are described. Different statistical stress distributions are shown. The vertical and horizontal stress distributions on the shell structure are represented and discussed. Calculative loads with different widths of load area are derived from the measured data. Lastly the results of spectral analysis with an FFT analyser are represented.

CONTENTS

I INTRODUCTION

The progress of winter navigation in the Baltic has been rapid in the last years. A merchant fleet for winter navigation has been built, and powerful icebreakers have been delivered to the Finnish and Swedish states. Thus it is possible today to keep open the northern harbours of the Gulf of Bothnia all winter.

At the study of ice loads on the hull of a ship the following ways of approach can be found:

- theoretical treatment
- measurements and observations in full-scale
- collecting empirical data from built ice-going ships.

An excellent example of the third one is the "Finnish-Swedish Ice Rules 1971". In the icebreaker branch the third has also been most often the way of approach. The mechanism of ice during impact is not yet very well known to give satisfactory results with theoretical treatment compared with empirical data. This is mainly due to the lack of data from full-scale measurements.

To get statistical data from ice-induced stresses in the shell, it was decided to start measurements on the ice-breaker Urho. The purpose of measurements was to clarify the following factors in the fore part of an icebreaker:

- stress level in the plating and frame
- vertical and horizontal distribution of structural response in the shell
- magnitude of ice load on the shell
- frequency response of shell structure.

It was also seen that it is important to collect practical experience on measuring and analysing techniques.

The main dimensions of the icebreaker Urho are the following:

- length, max	104.6 m
- length, cwl	96.0 m
- breadth, max	23.8 m
- breadth, cwl	22.5 m
- draught, max	8.3 m
- draught, cwl	7.3 m
- power	16.2 MW
- two stern and bow propellers	

Figure I.1 shows a side view of the icebreaker Urho.

The shell structure of the icebreaker Urho consists of plating, frames (s = 400 mm), horizontal stringers and webframes (s = 2400 mm). The frames are at the right angle to the symmetry plane of the ship. The yield stresses of the steel materials of the shell are the following:

- plate σ_y = 235 N/mm^2
- frame σ_y = 325 N/mm^2.

II DATA COLLECTION SYSTEM

At this phase it was decided to measure the response of the shell structure with strain gages and not to try to develope any special pressure transducer system.

The measuring system was based on the 14-channel tape recorder (Honeywell 5600). It was possible to measure signals from 12 strain gages and from the speed indicator at the same time. A part of measured data were also plotted with an eight-channel oscillograph to get an immediate picture. In figure II.1 the scheme of the measuring system is shown.

The strain gages on the plate field were XY-type and the measuring direction was horizontal (perpendicular to frames). The gages on the frames were fastened on the top of profiles.

The strain gages were mounted on the shell in the fore part of the ship. The breadth of the ship at the place where gages were mounted was about 58 % of the maximum breadth at the level of 3rd deck.

Two measuring point configurations were used. At the first one the points were distributed vertically as figures II.2 and II.3 show. At the second one points were distributed horizontally as figure II.4 shows. In table II.1 the places of strain gages are shown in the form of a table. In the figures II.2 and .4 the gages, which worked during measurements, are only shown.

In the vertical measuring point configuration three gages on each three spans of the fr. 96.5 were mounted. The uppermost measuring point lay about 600 mm downwards from the cwl. One gage was mounted on the crossing point between fr. 96.5 and str. IV and another on the crossing point

between fr. 96.5 and the deck beam.

The horizontal configuration extended one webframe space as figure II.4 shows. From the figure can be observed also the places of measuring points on the plate fields. The points 16 and 17 were mounted to get a picture of how the impact moves foreward.

Figure II.5 shows the mounted strain gages on the plate field between the frames 96 and 96.5.

III DATA REDUCTION SYSTEM

The measured data were converted to numerical form with the Super Nova computer. As the memory capacity of the central unit was only 18 k the data were printed on paper tapes, which were afterwards handled with the Univac 1108 computer. Figure III.1 represents the data reduction system.

The digitised data were also drawn with the Calcomp plotter to get a visualized picture of possible mistakes as for instance movement of zero level.

As it was possible to convert only seven channels at the same time due to the tape recorder, one channel was used as a reference channel.

The length of converted records was 30 s. All seven channels were sampled at a frequency of 25 Hz. So the number of samples per channel at one record was 750.

As figure III.1 shows, amplifiers were used before AD-converter to improve accuracy.

IV RESULTS OF MEASUREMENTS

IV.1 General

The measurements were made at the beginning of April, the first recording in 1976-04-01 at 02.30, the second recording at 04.30 and the third one 14.30. Figure IV.1 shows the icebreaker Urho during tests. In figure IV.3 the route of the icebreaker during measurements is presented.

The ice condition in 1976 was mild. The ice covered area in the Gulf of Bothnia was restricted to the norther part. Figure IV.3 shows the ice condition during tests. The thickness of ice on the open sea was between 40 cm and 70 cm, and at the coast about 80 cm. In figure IV.2 a picture of ice condition during measurements is shown.

The weather conditions were the following:

	04.00	16.00
Wind	North-West 6 m/s	South-East 6 m/s
Temperature	$-6^{o}C$	$-4^{o}C$

The icebreaker was maneuvered during the measurement so that the side where gages were mounted broke ice field on the side of channel and when the speed was lowered the ship was maneuvered to channel to increase the speed.

The draught of the icebreaker Urho was during measurements the following:

- fore T_F = 7.90 m --- 7.75 m
- aft T_A = 8.15 m --- 8.30 m

IV.2 Stresses as a function of time

All together 16 records were digitised from the three measurements. The length of one record was 30 s. From the first measurement (vertical configuration of measuring points) five records were taken, from the second measurement (horizontal configuration of measuring points) also five records and from the third measurement (horizontal configuration) six records.

Figures from IV.4 to IV.11 show some examples of digitised data. In figures the speed of the icebreaker is also drawn. As the speed radar has transiently lost contact with the surface of ice the correct speed is got by drawing an envelope curve to the recorded curve.

The speed of the icebreaker varied between 7.2 m/s --- 1.9 m/s and the maximum deceleration was 0.25 m/s^2. Table IV.1 presents speed data of the records.

Figures IV.4 --- IV.11 show that the response of plate fields differs from that of frames. The plate field is more sensetive to the stream of ice blocks. Stress impulses are sharper and faster for the plate field.

The digitised data show that the horizontal speed of impact between measuring points 6-14 and 15-14 was on the average equal to the speed of the icebreaker.

From figures IV.4 --- IV.11 can be found that in addition to the static dimensioning of the shell structure of an icebreaker fatigue dimensioning may become important especially when using high tensile steel.

IV.3 Statistical information about stresses

From the time based stress data the averages of the 10 highest stress amplitudes at each record were calculated. These are shown in figures IV.12, .13 and .14 in the form of pillars.

In figure IV.12 can be observed the low level of stress amplitudes above the 3rd deck compared to the measuring points under the 3rd deck. The height of stress amplitudes at the ends of brackets are equally high or even higher at some records than at the centre. In table IV.2 relative load levels of the five records are calculated supposing that the response is due to a point force. The relative load amplitudes at the span 3rd deck - str.IV have in all cases been the highest.

Figures IV.13 and IV.14 show that relative stress amplitude has been higher at the plate (measuring point 22) than at the frames. Taking into consideration that at the plate the corrosion allowance is included, the thing becomes clearer. Comparing the measuring points 22 and 20 it can be observed that the pillars at point 22 have been at every record higher. Even the height of the pillar at points 21 and 23 have been approximately equally high when comparing to point 20. The low stress amplitudes at point 15 may be due to the bulkhead lying at the next frame.

From figures IV.12, .13 and .14 it can be observed that the stress amplitudes have been highest at the measurement 3.

Table IV.3 shows the maximum stress amplitudes of the 30 s long records. It can be found that the maximum stress amplitude for a frame was $\delta 16_y = 0.43$ and for a plate $\delta 18_y = 0.48$.

Figures IV.15 and .16 show the distributions of stress amplitude at measuring points 22 and 13. The negative stress amplitudes have been left out as these are due to the reflections of nearby impacts. When comparing those two distributions it can be found that the pillars of the frame (point 13)decrease much faster as a function of stress than the pillars of the plate (point 22).

In figures IV.17 and .18 the distributions of stress level at measuring points 6 and 22 are shown. It can be found from these distributions that the stress level as an absolute value has been very low.

As it can be seen in figures IV.4 --- IV.11 the durations of impacts vary much especially at frames, but the impacts of longer duration are almost always composed of several ones. This phenomenon does not appear so often in a plate. Figures IV.19 and IV.20 show the distributions of the duration of impacts at measuring points 6 and 22. The average value of the duration of impact for the measuring point 6 is 0.38 s and for measuring point 22 is 0.28 s. The most probable value is about 0.20 s for measuring point 6 and 0.15 s for measuring point 22. The figures show clearly that the spread of the duration of impact is bigger for a frame (point 6) than for a plate (point 22).

In figure IV.21 the stress amplitude as a function of the duration of impact is shown at measuring point 6. In this figure the impacts with several peaks clearly seen have been excluded.

To get some idea about the interval time between successive impacts, the stress amplitudes under 10 N/mm^2 were eliminated. In figure IV.22.a the distribution of time interval is shown for point 6 and in figure IV.22.b for point 22. The duration of impact has of course an effect on the first pillars of the distribution. Comparing these two histograms it can be

observed that for a plate field (point 22) the frequency of getting impacts is clearly higher than for a frame (point 6). The averages of the histograms are the following:

- measuring point 6 (frame) 1.52 s
- measuring point 22 (plate) 0.90 s

In figures IV.23a and .b the distributions of the speed of structural response are shown at a frame (point 6) and at a plate (point 22). Comparing these two histograms with each other it can be recognised that for a plate the variation $\dot{z}/z_y$ is bigger and also higher values can be observed. The averages of the histograms are the following:

- measuring point 6 (frame) 0.11 1/s
- measuring point 22 (plate) 0.39 1/s

IV.4 Stress distributions on the shell

Vertical distribution

Figures IV.24, .25 and .26 show the vertical distribution of stress as a function of time. The time step in figure IV.24 is 0.12 s, in figure IV.25 0.16 s and in figure IV.26 0.20 s. In figure IV.25 the response of a fast point impact can be seen. In the two other figures the impacts have been more slow and the contact area in the vertical direction has been wider. In figures IV.24 and .26 can be observed how the load moves downwards as a function of time. The drawn distributions showed that the response of a pure point load appears seldom. The measuring point 8 shows approximately the amount of tension in the frame.

Horizontal distribution

Figures IV.27, .28 and .29 represent the horizontal distribution of the response between frames 95.5 and 97.5 as a function of time. In these figures horizontal stresses in the four measuring points of plating are also shown. The time step in figure IV.27 is 0.24 s, in figure IV.28 0.20 s and in figure IV.29 0.16 s.

The strength analysis (chapter IV.5) showed that the response of frames to a point load is concenrated to the loaded frame. Thus the first approximation can be that the frames act independently. From the distributions it can be found that on the average the load amplitude is acting on three frames at the same time. Figure IV.28 demonstrates clearly how the load moves along the shell.

The distributions of stress at the plate field show that the maximum stress amplitude appears at the midpoint. Thus the load configuration is such that the plate field cannot be considered as clamped at elastic range.

IV.5 Calculative load on the shell

From the stress distributions of the frames total load amplitudes acting between str.IV and the 3rd deck were calculated. The breadth of load area varied from one frame space to five. In the calculations the finite element method was used /1/.

The system of calculations was the following:

- an element mesh covering the double bottom - the 2nd deck and fr.s 95 - 96.5 was made. As

the main interest was at the frame 96.5, the advantage of the symmetry was used. The mesh included beam and plate elements. Different load areas were tested, the superposition of point loads proved most suitable. Figure IV.30 shows the element mesh.

- with the help of results of unit response calculations the point forces at the three points 5, 6 and 7 were solved in the following way:

$$\{F\} = [A]\{\beta\}$$

where

$\{F\}$ = point forces at points 5, 6 and 7
$[A]$ = influence coffiecients
$\{\beta\}$ = measured stresses

The superposition principle used in the calculations is shown in figure IV.31.

- the calculations showed that the stress level in the adjoining frames is about four precents of that in the loaded frame as figure IV.32 shows. Thus as a first approximation each frame can be studied independently.
  The forces at frames 95.5, 96, 97 and 97.5 are obtained with the help of a proportion.

Table IV.4 represents some calculated load amplitudes. The width of the load area has been between one frame space and five spaces. The speed of the icebreaker is also given. In figure IV.33 the loads in the form of histograms are shown. The maximum load amplitudes were the following:

- one frame space (fr. 96.5) 231 kN
- three frame spaces (fr.s 96, 96.5, 97) 379 kN
- five frame spaces (fr.s 95.5-97.5) 407 kN

In figure IV.34 the load amplitude as a function of the speed of the icebreaker is drawn. The scatter is considerable and from the figures it is difficult to draw conclusion. One explanation to the scatter may be that the speed reduction was always due to increase of ice resistance and not due to power reduction.

In figure IV.35 the effect of the horizontal extension of load on the amplitude is examined. From the curves a non-linear increase of load can be observed.

To study the load amplitudes on the plate field between frames 96 and 96.5, the unit response to the load, area 400 x 400 mm^2, was calculated. In the calculations the effect of frames was also taken into consideration. Figure IV.36 shows a scheme of load configuration and the distribution of stress in the direction of x-axis when y=0. In the figure some measured stress distributions are also drawn. The calculations give the following formula:

$$p = \frac{t^2 \times \beta}{6 \times k \times h \times s}$$

where

p = pressure
t = thickness of plate
s = width of load
h = height of load
k = constant = 0.067
β = stress at the middle of plate

In the case of a simply supported plate at same load configuration the k-constant gets value 0.084.

From table IV.3, where the maximum stress amplitudes are given, the maximum pressures on the plate at the different measurements can be derived. These are given in table IV.5. The maximum measured pressure divided by the allowed one was 0.67.

IV.6 Spectral analysis of the data with an FFT analyser

To get some idea about the dominating frequencies of the stress pulses a part of the data were analysed with an FFT analyser. The analyser was Mini-Ubiquitous 440 A.

The analysing system was the following: transient stress pulses were captured and analysed. Both the time and frequency based curves were plotted. Average rms spectrums including four and 16 records were also formed. Together about 30 samples from measuring points 6 and 22 were analysed.

In figures IV.37 to IV.42 some examples of the analysis are shown. Figures IV.37 and .40 present separate spectrums of measuring point 6, and figure IV.42 presents a separate spectrum of measuring point 22. The other figures present average spectrums of measuring point 6. All spectrums show clearly that the low frequencies under 10 Hz are dominating From the spectrums no dominating separate frequencies can be found.

In figures IV.38 and .39 it can be seen that the average spectrum approaches the spectrum of a truncated sinus wave.

Comparing figures IV.37 and .40 a big variation at the shape of spectrums can be found. The first one is much more concen-

rated to the lower frequencies than the second one.

The analysis showed that the problem of ice load on the shell can be handled as a static problem, as the natural frequencies of the shell structure of an icebreaker are much higher than the dominating frequencies of spectrums. But when dealing with the whole hull the domination frequencies of spectrums are at the same range as the first natural frequencies of the hull.

V CONCLUSIONS

The measured data show clearly that statistical treatment is needed when dealing with ice loads. In the structural response of the shell grillage dynamic effect is not found.

The measurement system was satisfactory. But with a pressure transducer system it is possible to measure the magnitude of pressure more accurately and with fewer measuring points. This system has to allow the surface of plating to be unbroken.

During measurements, efforts were made to synchronize the filming of icebreaking process and strain data, but it failed due to slashing of water and ice. It seems, however, that with another camera position this will succeed. The video system with the possibility of mixing pictures offers another intresting possibility.

These measurements gave encouraging methodical experiences to proceed the experimental studies of ice loads.

VI REFERENCES

/1/ Henshell, R.D. "PAFEC 70+" (Program Manual), Nottingham 1972.

/2/ Hakala, M.K. Jäykistämättömien ja jäykistettyjen laattojen analysointi kahdeksansolmuisilla levy- ja laattaelementeillä (An Analysis of Unstiffened and Stiffened Plates with Eight-Node Plane and Plate Elements) Thesis, Helsinki University of Technology, 1974.

VII FIGURES AND TABLES

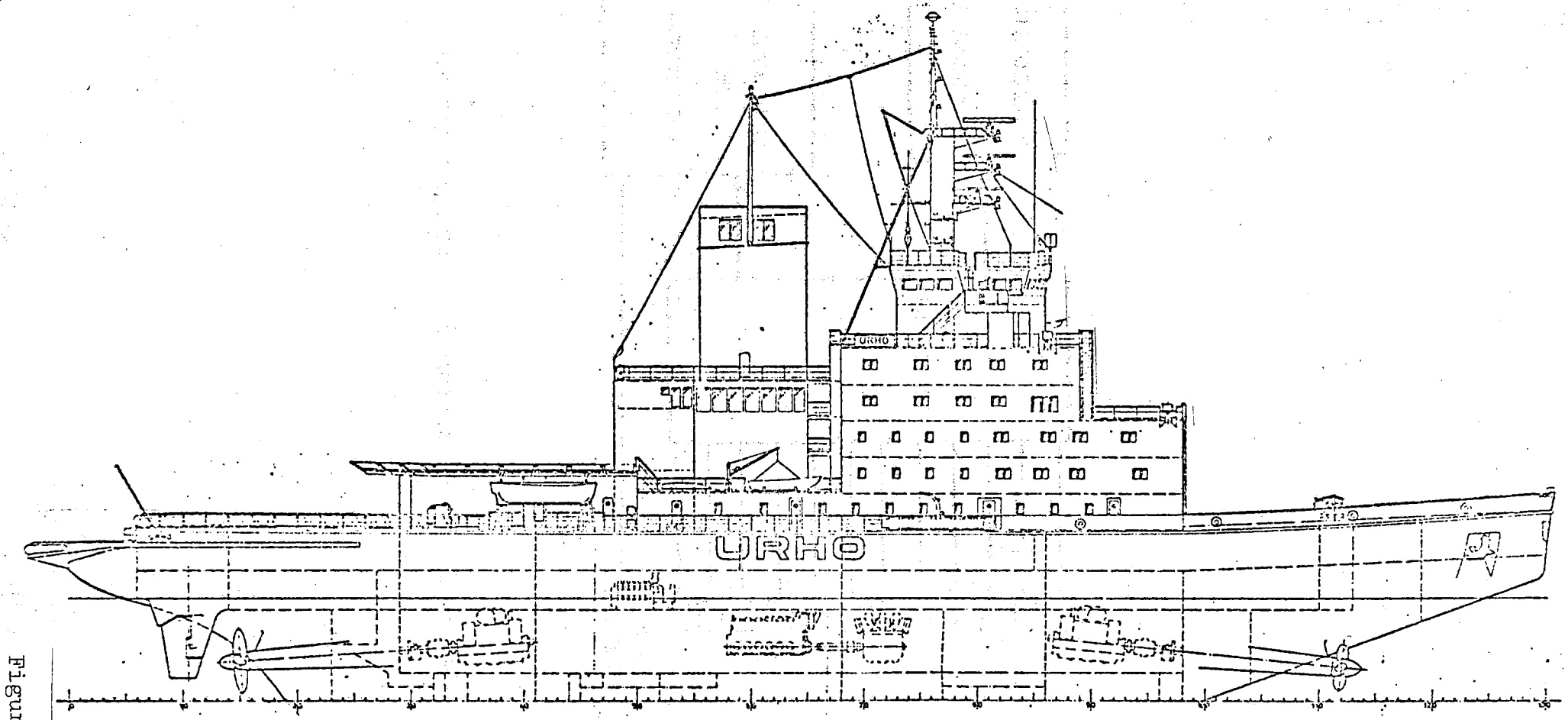

Figure I.1

Side view of the icebreaker Urho

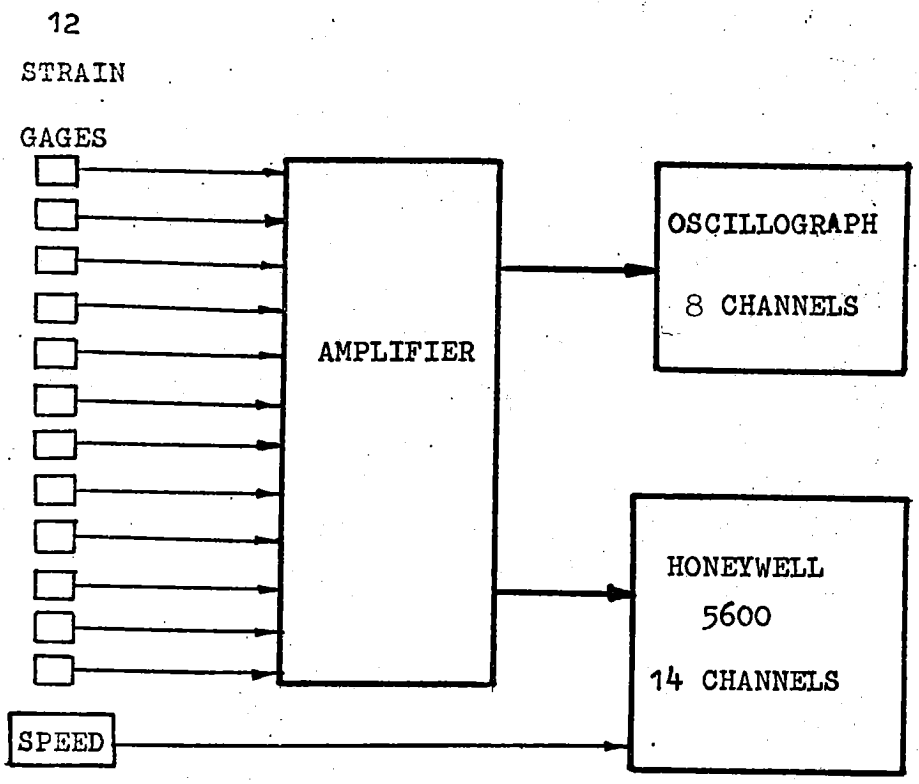

Figure II.1 The scheme of measuring system

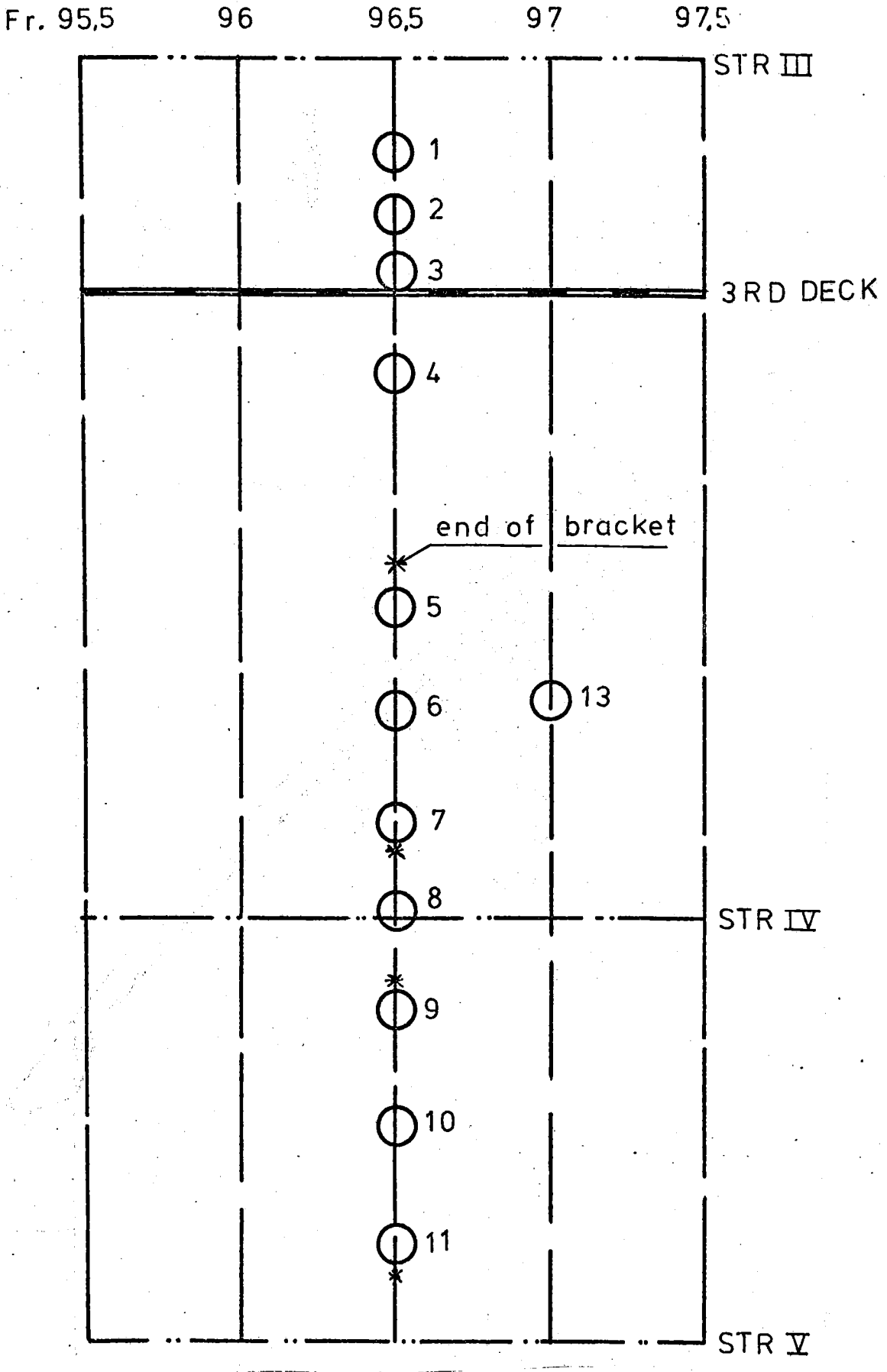

Figure II.2 The places of strain gages in measurement 1

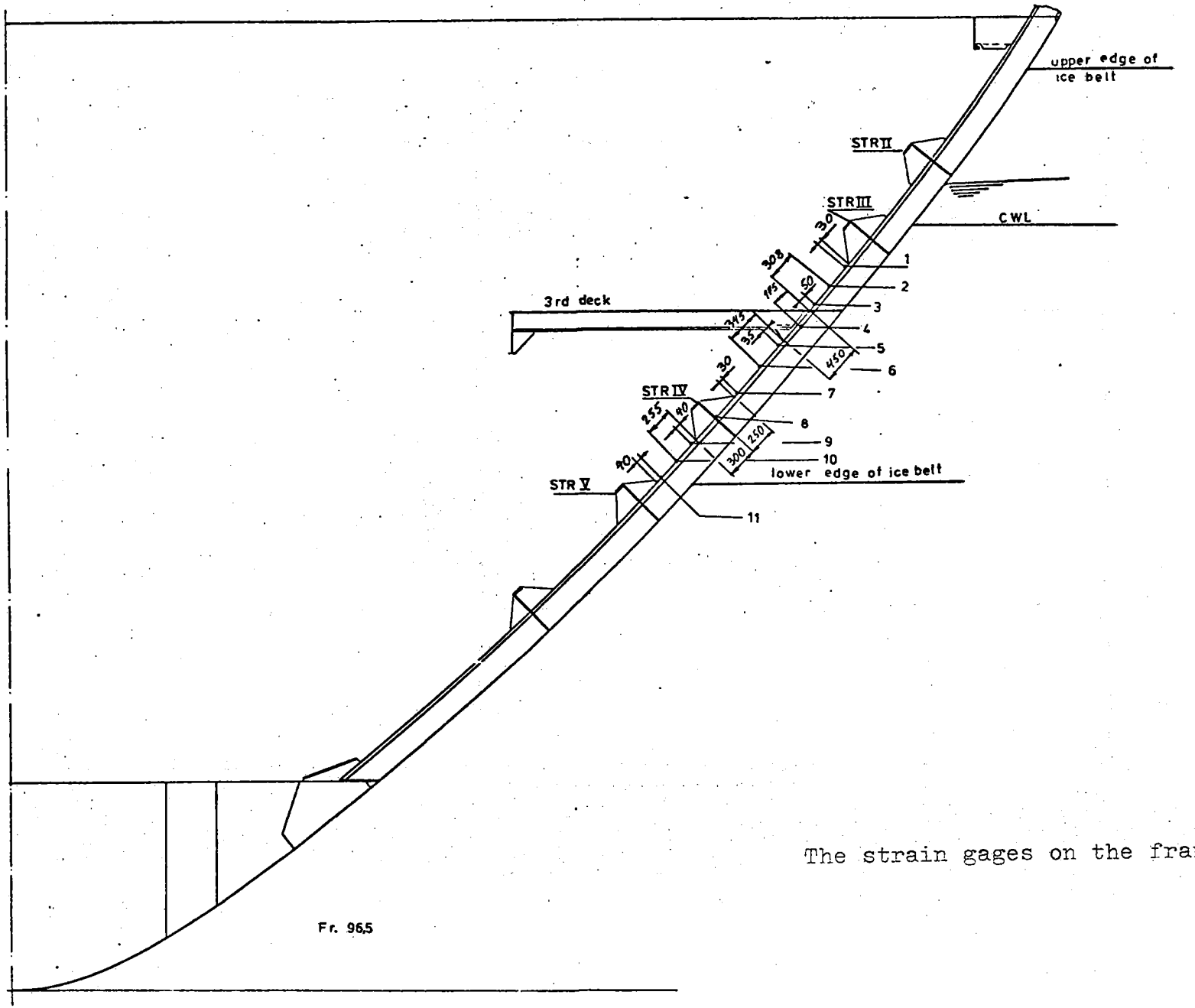

Figure II.3

The strain gages on the frame 96.5

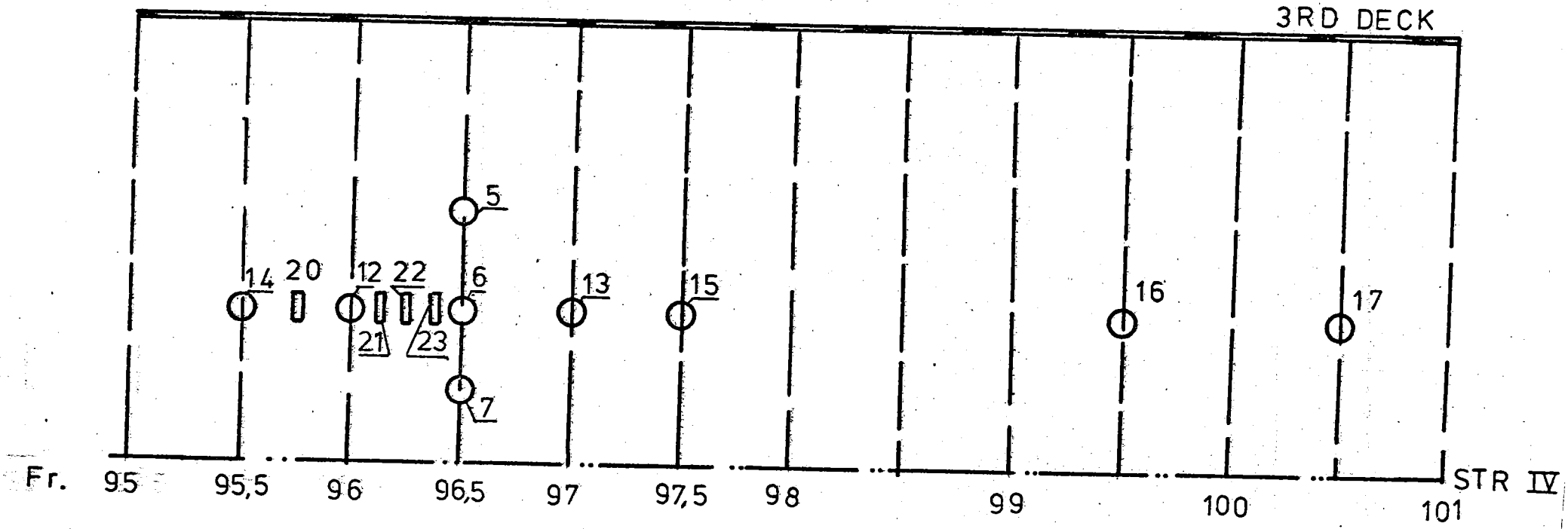

Figure II.4

The places of strain gages in measurements 2 and 3

measuring point	frame no.	dist.from BL/m
1	96.5	6.90
2	96.5	6.74
3	96.5	6.56
4	96.5	6.44
5	96.5	6.10
6	96.5	5.90
7	96.5	5.70
8	96.5	5.50
9	96.5	5.30
10	96.5	5.10
11	96.5	4.90
12	96	5.90
13	97	5.90
14	95.5	5.90
15	97.5	5.90
16	99.5	5.90
17	100.5	5.90
20	95.5 + 200	5.90
21	96 + 60	5.90
22	96 + 200	5.90
23	96.5 - 60	5.90

Table II.1 The places of measuring points

Figure II.5 Measuring points 21, 22 and 23

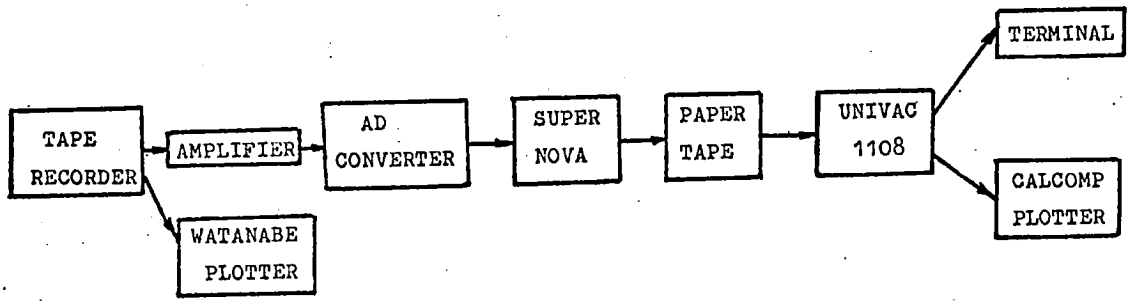

Figure III.1 Data reduction system

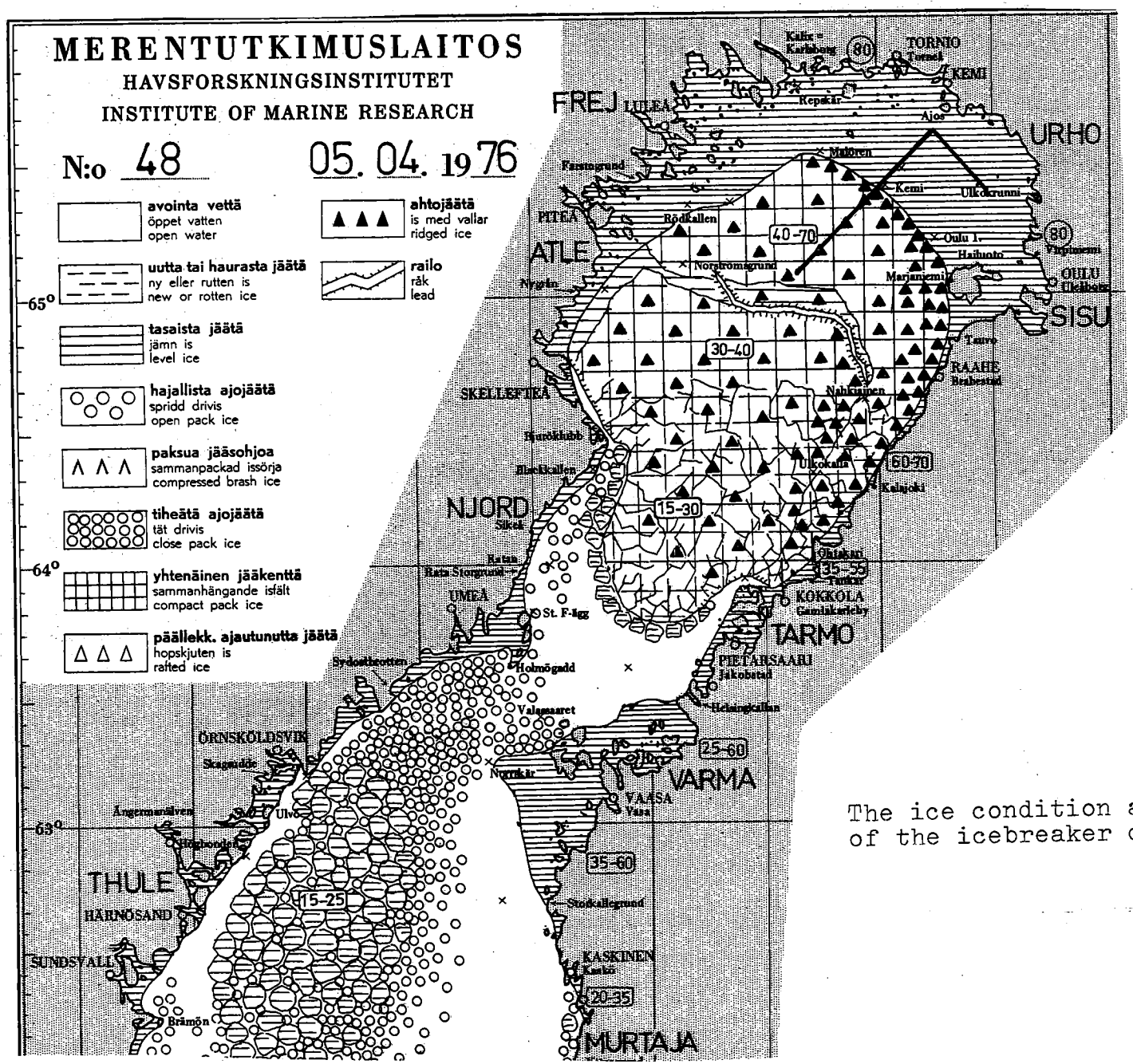

The ice condition and the route of the icebreaker during measurements.

Figure IV.3

CHANNEL 1
CHANNEL 2
CHANNEL 3
CHANNEL 4
CHANNEL 5
CHANNEL 6
CHANNEL 7
TIME SECONDS

Figure IV.4

measurement 1.5
Stresses as a function of time
measuring points 7-13 and speed
TIME SECONDS
speed [m/s]
CHANNEL 13
CHANNEL 11
CHANNEL 10
CHANNEL 9
CHANNEL 8
CHANNEL 7
[σ] = N/mm²

Figure IV.5

Stresses as a function of time
[σ] = N/mm²
TIME SECONDS
0.00
2.00
4.00
6.00
8.00
10.00
12.00
14.00
16.0
18.0
20.00
22.00
24.0
25.00
28.00
30.00
CHANNEL 20
CHANNEL 21
CHANNEL 22
CHANNEL 23
CHANNEL 5
CHANNEL 12
CHANNEL 6

Figure IV.6

Stresses as a function of time
measuring points 6, 7, 13-16
and speed
measurement 2.2
[σ] = N/mm²
TIME SECONDS
speed [m/s]
CHANNEL 13
CHANNEL 16
CHANNEL 15
CHANNEL 14
CHANNEL 7
CHANNEL 6

Figure IV.7

Stresses as a function of time
measurement 32
TIME SECONDS
0.00
2.00
4.00
6.00
8.00
10.00
12.00
14.00
16.00
18.00
20.00
22.00
24.00
26.00
28.00
30.00
CHANNEL 20
CHANNEL 21
CHANNEL 22
CHANNEL 23
CHANNEL 5
CHANNEL 12
CHANNEL 6
(1 = N/mm2)

Figure IV.8

Stresses as a function of time
measuring points 6, 7, 13-15, 17
and speed
[6] = N/mm2
measurement 32
TIME SECONDS
speed [m/s]
CHANNEL 13
CHANNEL 17
CHANNEL 15
CHANNEL 14
CHANNEL 7
CHANNEL 6

Figure IV.9

CHANNEL 20
CHANNEL 21
CHANNEL 22
CHANNEL 23
CHANNEL 5
CHANNEL 12
CHANNEL 6
0.00 2.00 4.00 6.00 8.00 10.00 12.00 14.00 16.00 18.00 20.00 22.00 24.00 26.00 28.00 30.00
TIME SECONDS

Figure IV.10

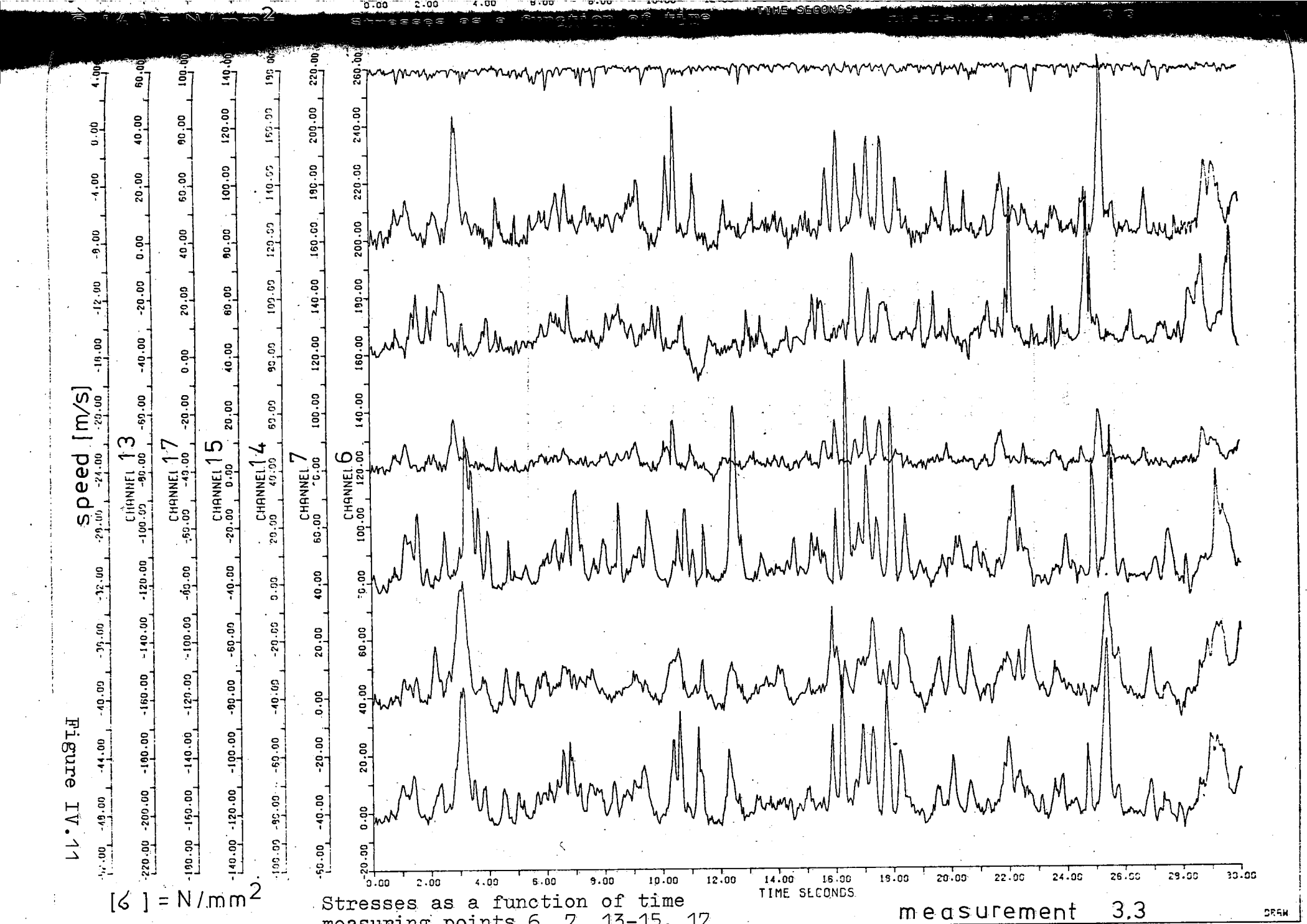

Figure IV.11

Stresses as a function of time measuring points 6, 7, 13-15, 17 and speed

measurement	speed m/s max	min	av	deceleration m/s^2
1.1	6.1	3.6	4.4	0.20
1.2	5.8	5.0	5.2	0.02
1.3	7.2	3.2	4.6	0.25
1.4	7.2	4.2	5.0	0.20
1.5	3.2	2.9	3.1	0.02
2.1	6.0	3.7	4.0	0.14
2.2	3.4	1.9	2.4	0.12
2.3	6.1	4.1	4.6	0.09
2.4	7.0	5.8	6.0	0.10
2.5	6.4	5.8	6.1	0.05
3.1	4.5	4.5	4.5	0.0
3.2	5.0	5.0	5.0	0.0
3.3	4.0	4.0	4.0	0.0
3.4	6.5	4.8	5.5	0.09
3.5	6.5	5.6	6.2	0.07
3.6	4.6	4.6	4.6	0.0

Table IV.1 Speed data of records

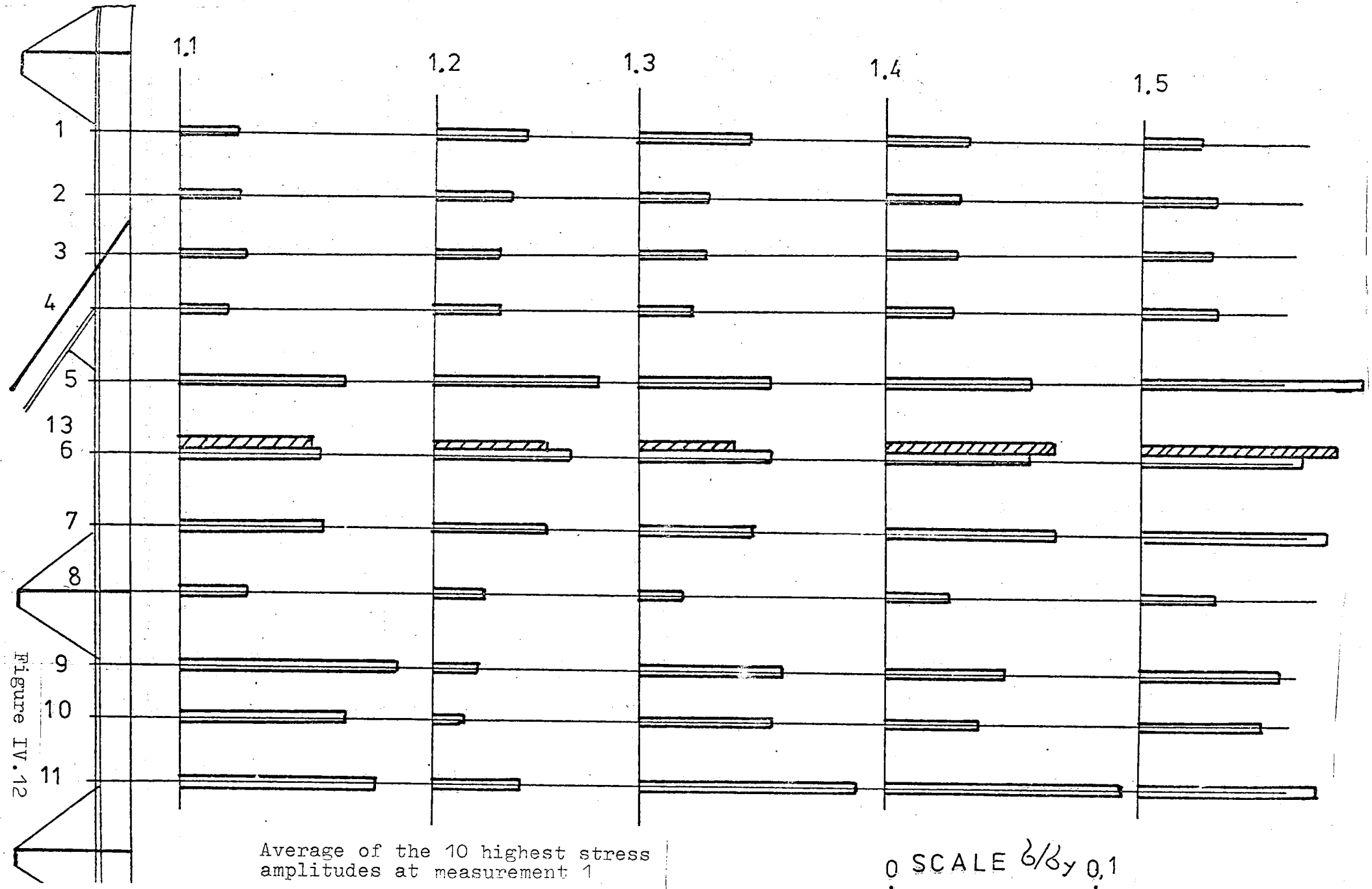

Figure IV.12

Average of the 10 highest stress amplitudes at measurement 1

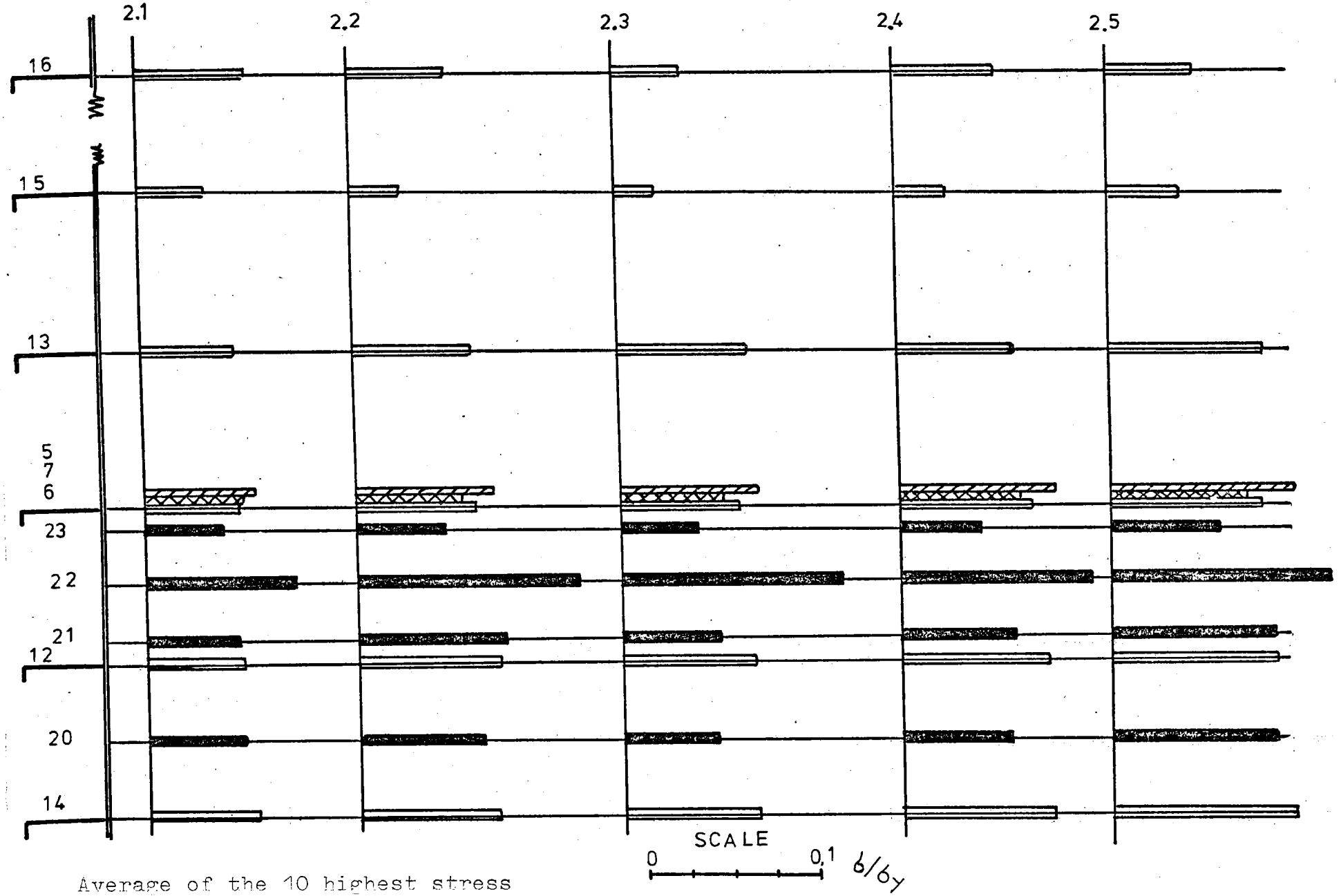

Figure IV.13

Average of the 10 highest stress amplitudes at measurement 2

amplitudes at measurement 2

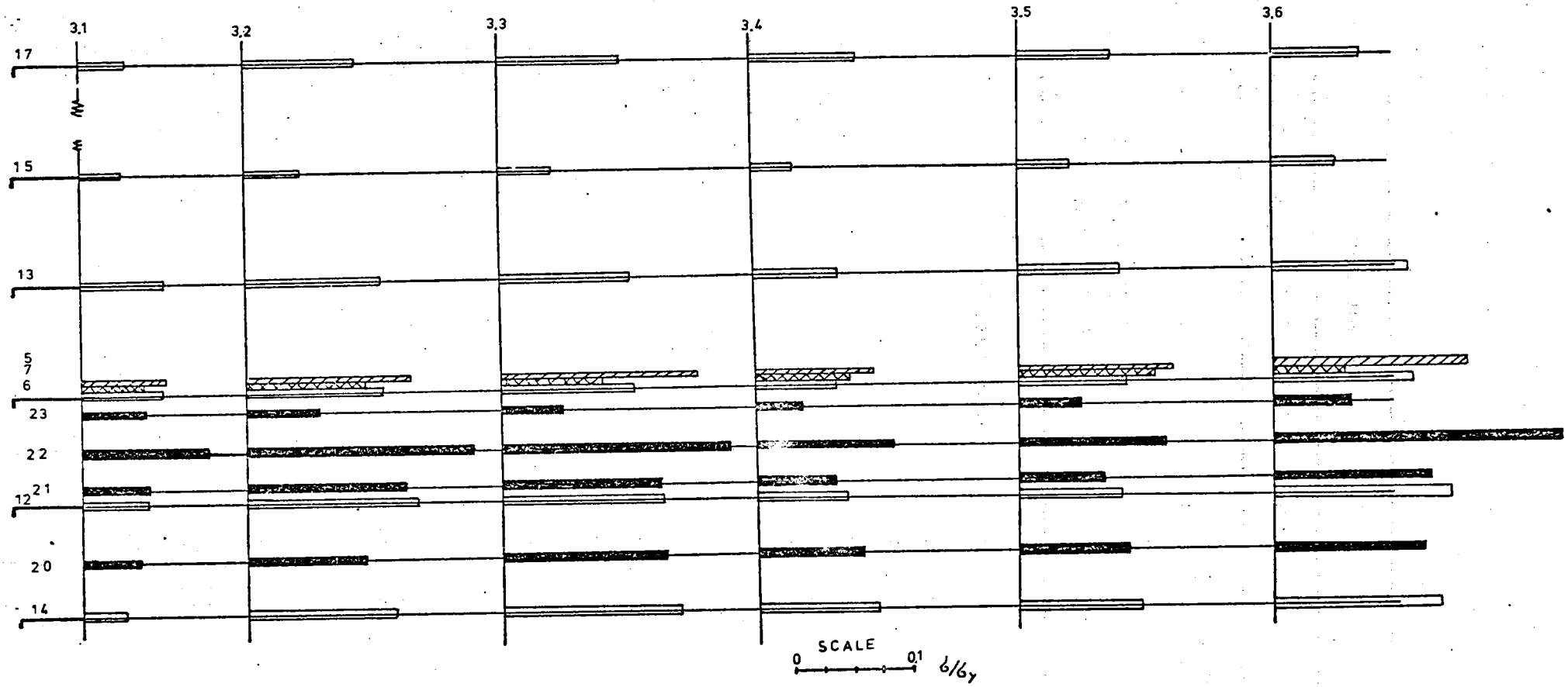

Average of the 10 highest stress amplitudes at measurement 3

Figure IV.14

	measurement				
	1.1	1.2	1.3	1.4	1.5
3rd deck - str. III	1	1	1	1	1
3rd deck - str. IV	1.5	1.1	1.3	1.3	1.5
str. IV - str. V	1.3	0.2	0.9	0.6	0.8

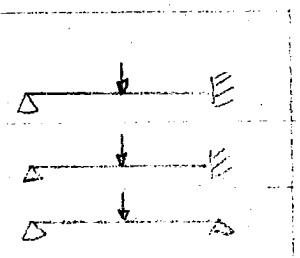

Table IV.2 Relative load levels

maximum ∂ / ∂_y - amplitude

measuring points	measurement 1.1	1.2	1.3	1.4	1.5
1	0.03	0.08	0.13	0.10	0.04
2	0.04	0.05	0.07	0.07	0.05
3	0.04	0.03	0.07	0.04	0.06
4	0.03	0.05	0.04	0.07	0.07
5	0.13	0.11	0.09	0.14	0.21
6	0.10	0.12	0.12	0.09	0.15
7	0.10	0.15	0.07	0.18	0.21
8	0.03	0.04	0.04	0.05	0.05
9	0.10	0.03	0.12	0.08	0.13
10	0.16	0.02	0.18	0.07	0.08
11	0.16	0.05	0.18	0.16	0.14
13	0.10	0.09	0.09	0.13	0.17

maximum ∂ / ∂_y - amplitude

measuring point	measurement 2.1	2.2	2.3	2.4	2.5
20	0.14	0.18	0.06	0.10	0.25
21	0.14	0.28	0.10	0.10	0.17
22	0.22	0.34	0.20	0.21	0.22
23	0.07	0.10	0.06	0.05	0.13
5	0.29	0.13	0.11	0.20	0.16
12	0.18	0.17	0.11	0.17	0.17
6	0.14	0.13	0.10	0.17	0.15
7	0.12	0.09	0.12	0.11	0.12
14	0.27	0.16	0.11	0.20	0.17
15	0.07	0.04	0.04	0.05	0.06
16	0.13	0.08	0.05	0.08	0.14
13	0.11	0.14	0.11	0.13	0.11

Table IV.3 continues on the next page

maximum σ / σ_y - amplitude						
	measurement					
measuring points	3.1	3.2	3.3	3.4	3.5	3.6
20	0.12	0.19	0.33	0.17	0.22	0.25
21	0.13	0.26	0.23	0.12	0.14	0.20
22	0.36	0.29	0.35	0.18	0.17	0.48
23	0.10	0.11	0.09	0.05	0.07	0.09
5	0.13	0.20	0.27	0.17	0.20	0.33
12	0.13	0.19	0.17	0.10	0.13	0.37
6	0.17	0.21	0.19	0.11	0.15	0.22
7	0.15	0.19	0.12	0.11	0.22	0.09
14	0.05	0.21	0.19	0.27	0.18	0.43
15	0.05	0.08	0.05	0.05	0.07	0.12
17	0.07	0.14	0.18	0.14	0.11	0.10
13	0.12	0.30	0.20	0.11	0.15	0.20

Table IV.3 Maximum stress amplitudes (σ / σ_y) of measurements 1, 2 and 3.

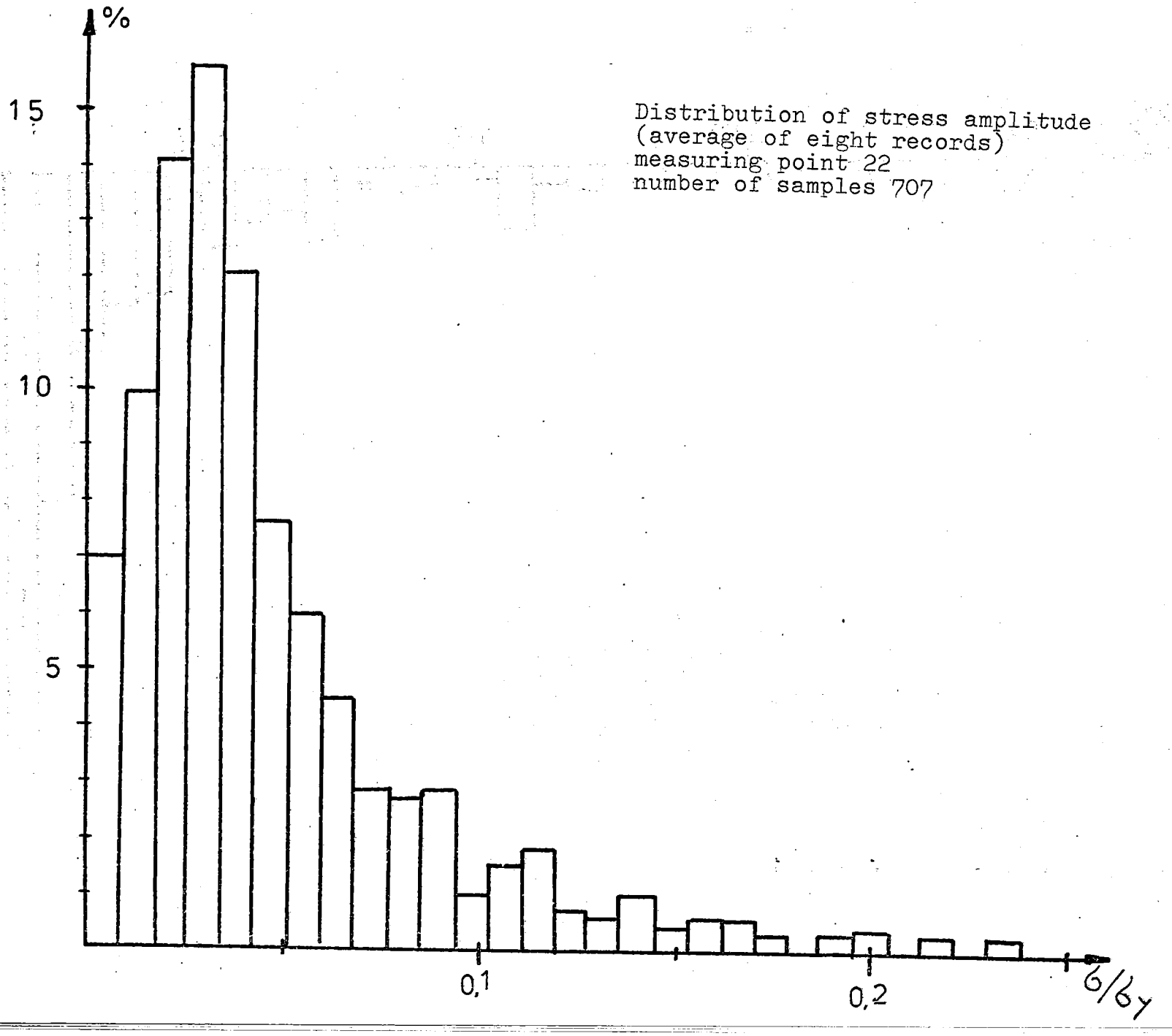

Distribution of stress amplitude
(average of eight records)
measuring point 22
number of samples 707

Figure IV.15

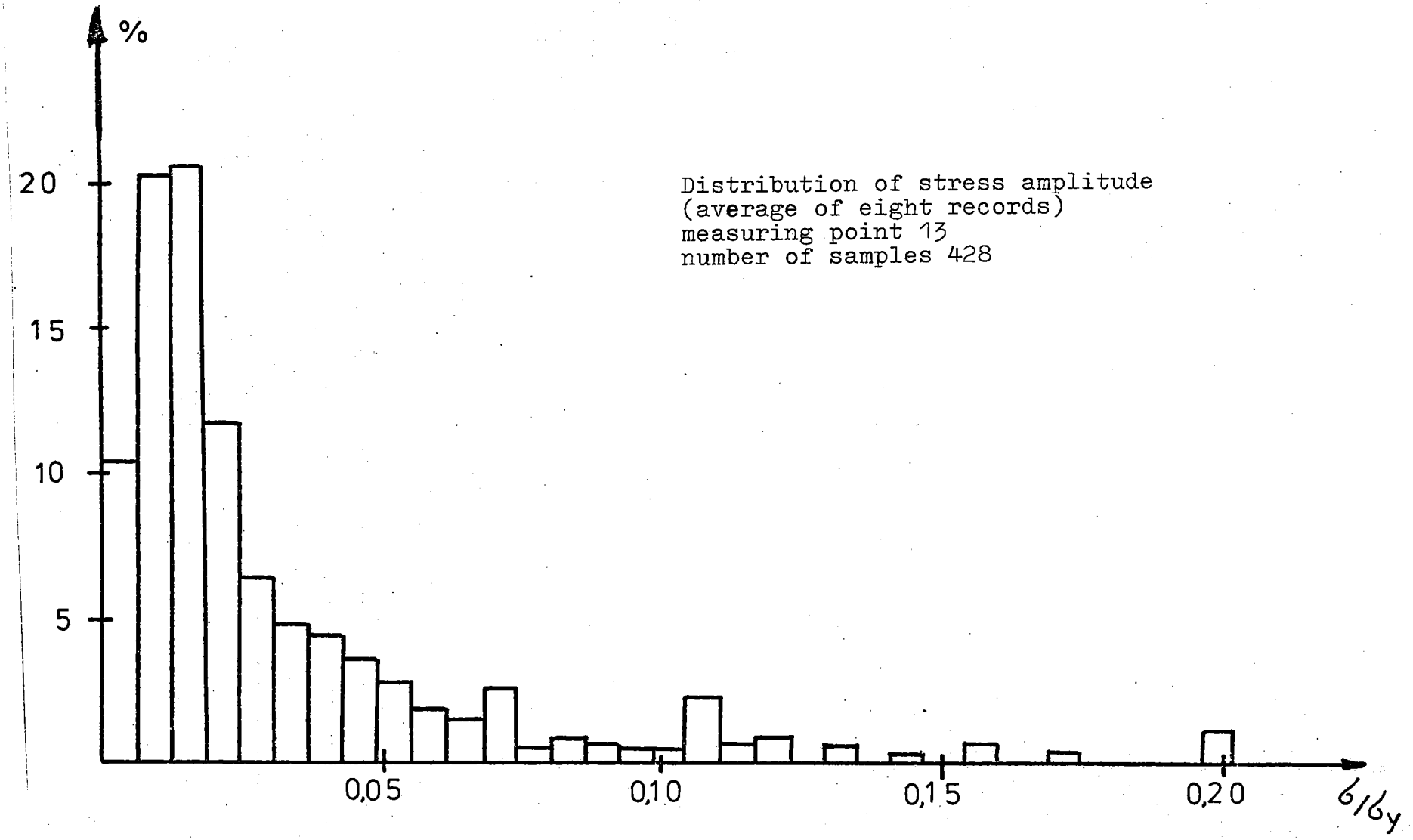

Distribution of stress amplitude
(average of eight records)
measuring point 13
number of samples 428

Figure IV.16

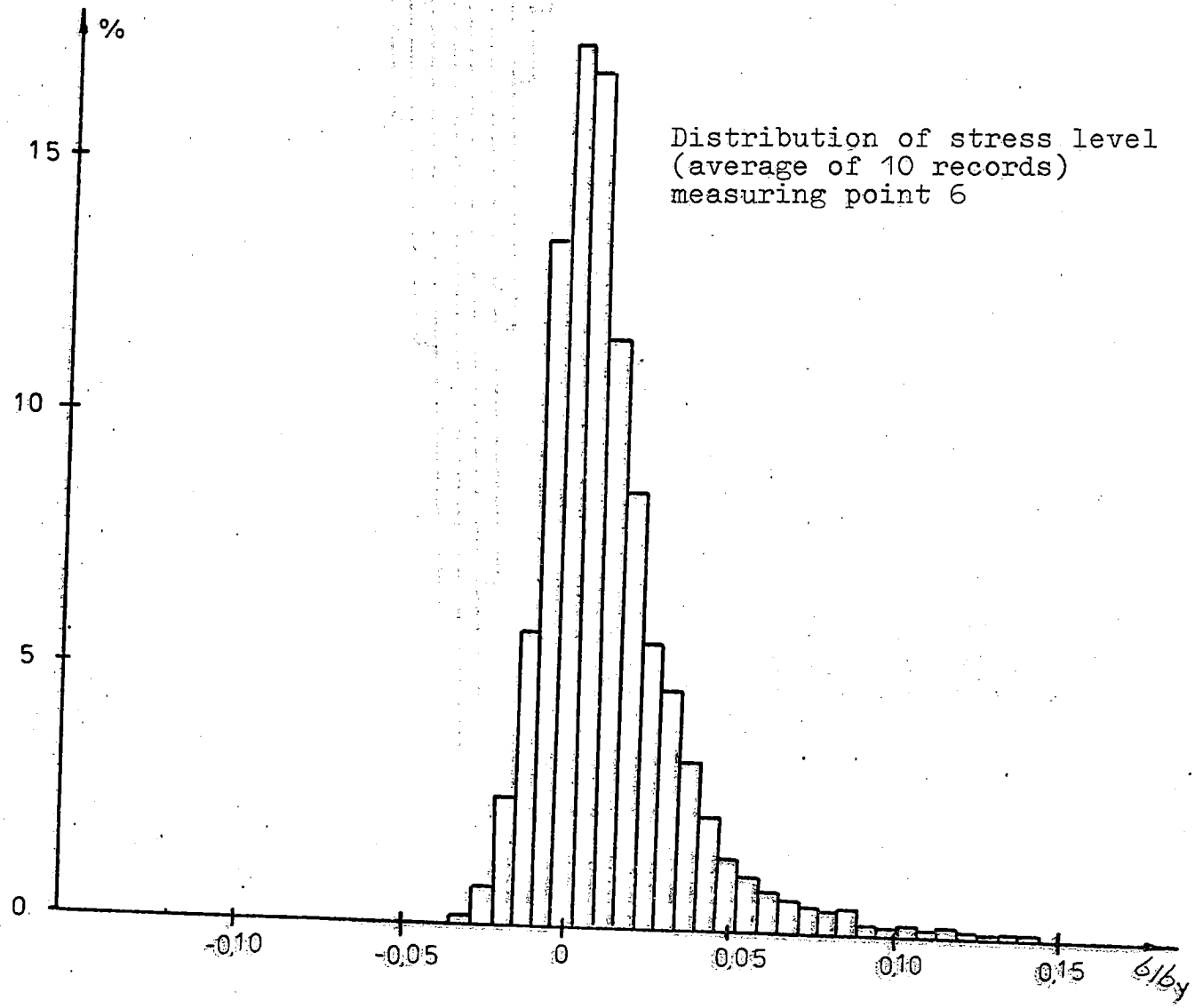

Distribution of stress level
(average of 10 records)
measuring point 6

Figure IV.17

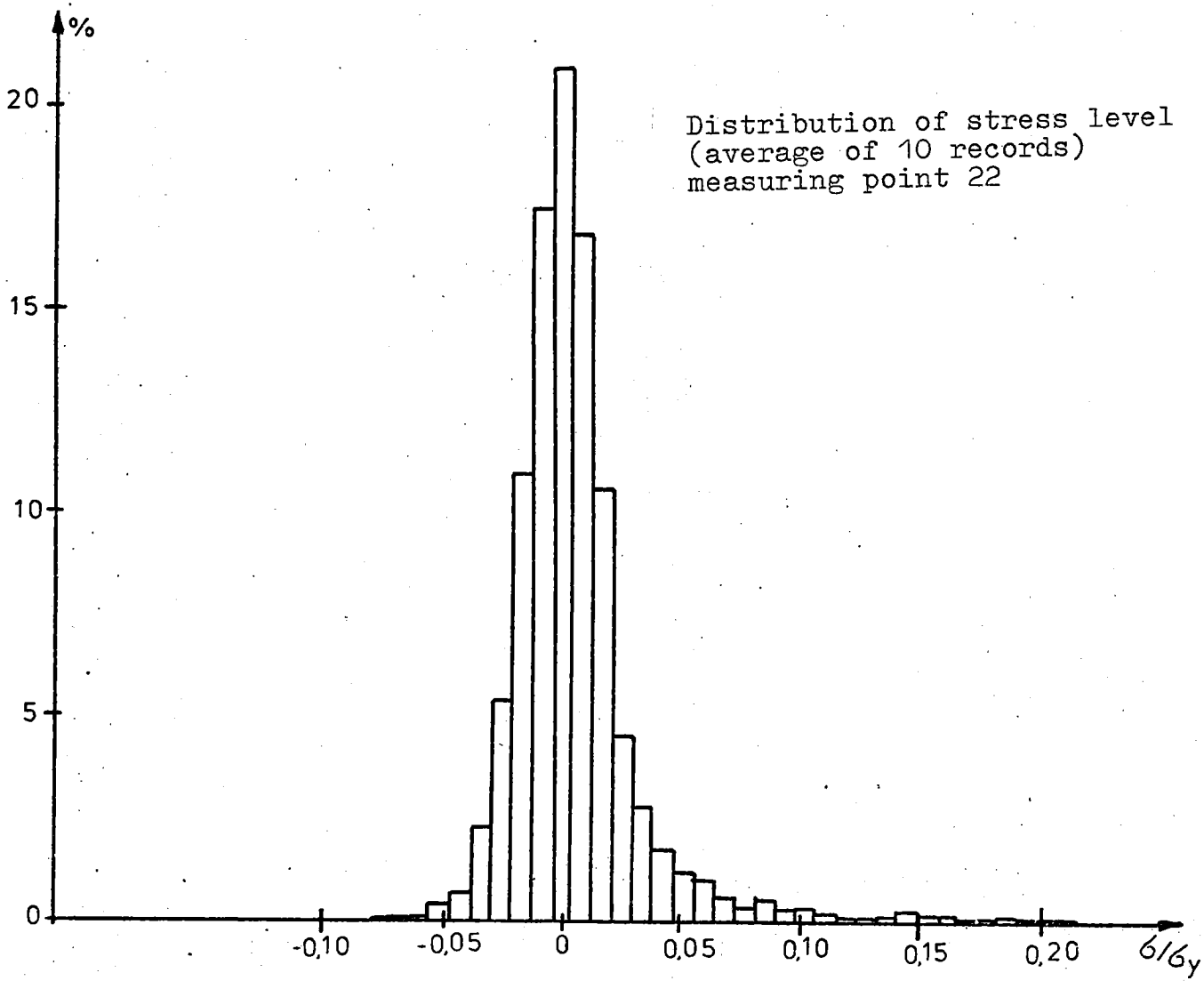

Distribution of stress level
(average of 10 records)
measuring point 22

Figure IV.18

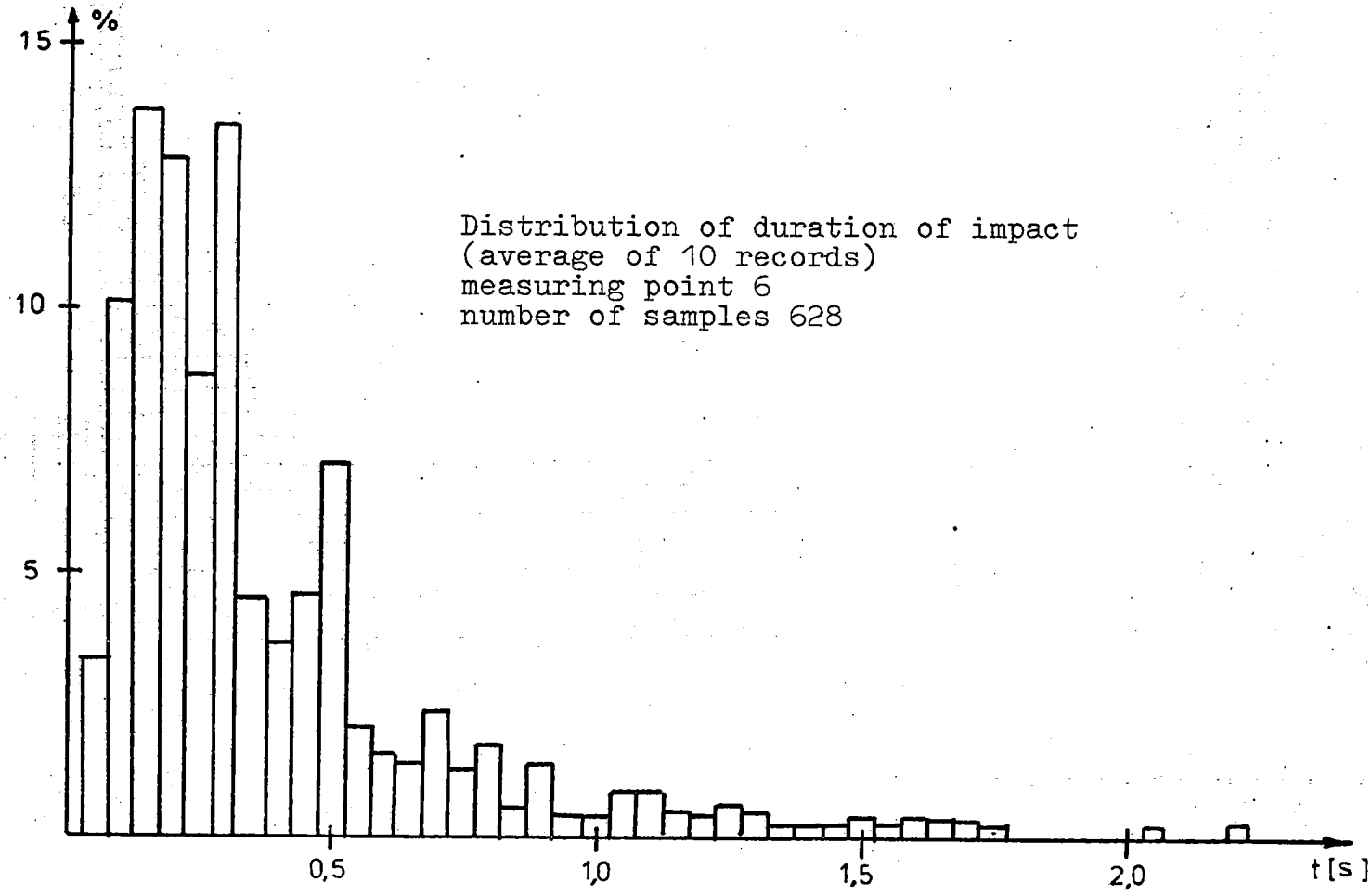

Distribution of duration of impact
(average of 10 records)
measuring point 6
number of samples 628

Figure IV.19

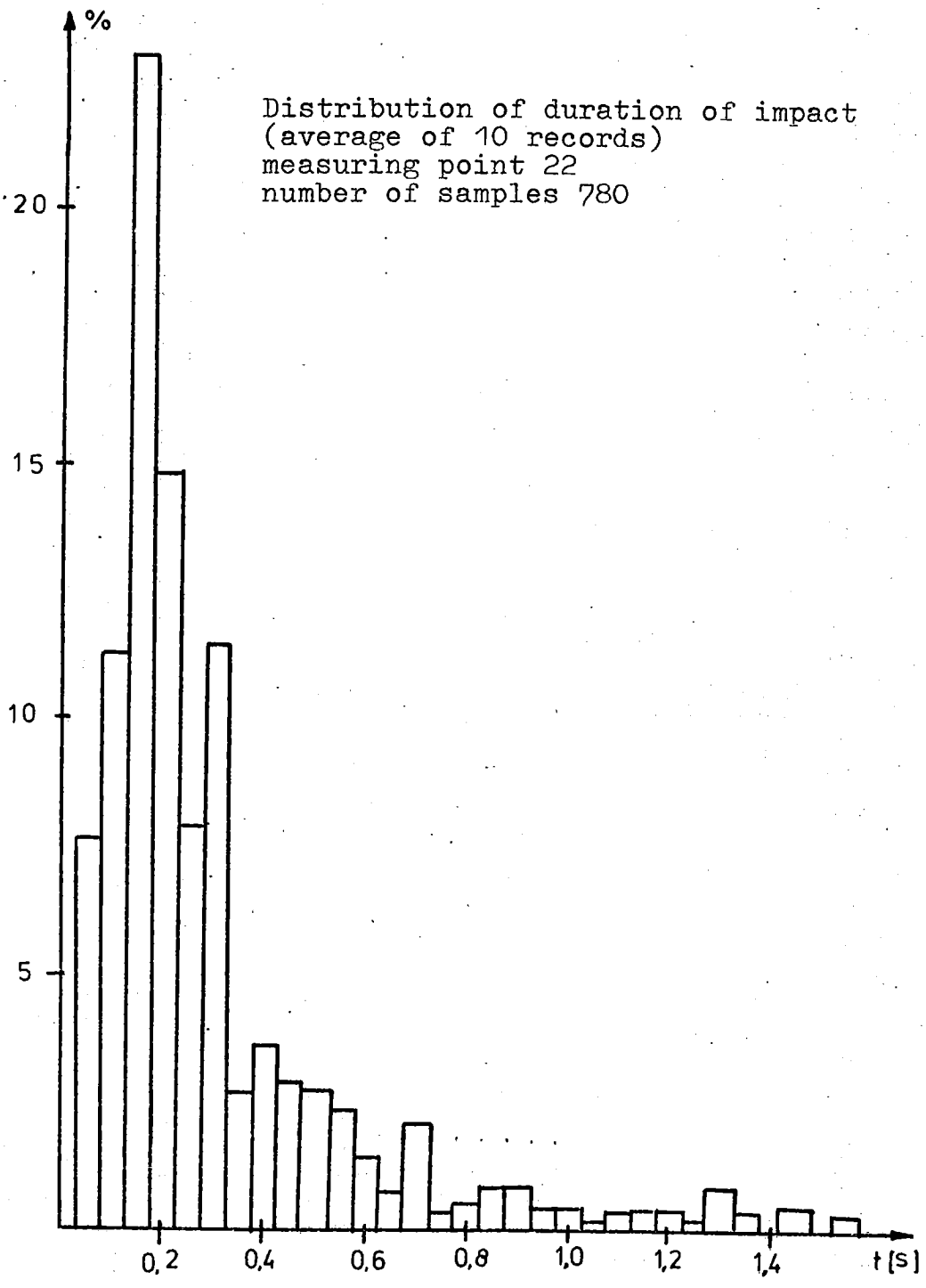
%
Distribution of duration of impact
(average of 10 records)
measuring point 22
number of samples 780
20
15
10
5
0,2
0,4
0,6
0,8
1,0
1,2
1,4
t [s]

Figure IV.20

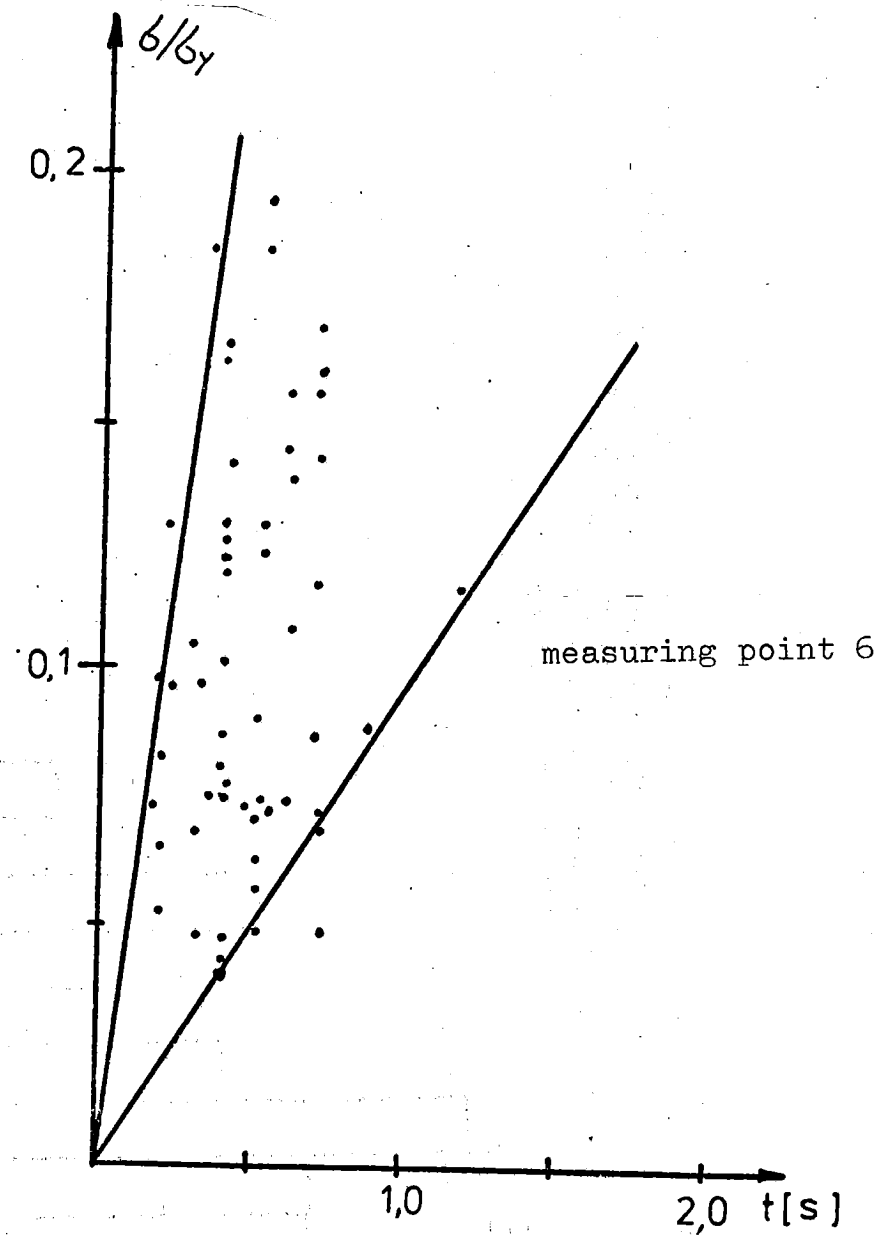

Figure IV.21 Stress amplitude as a function of duration of impact

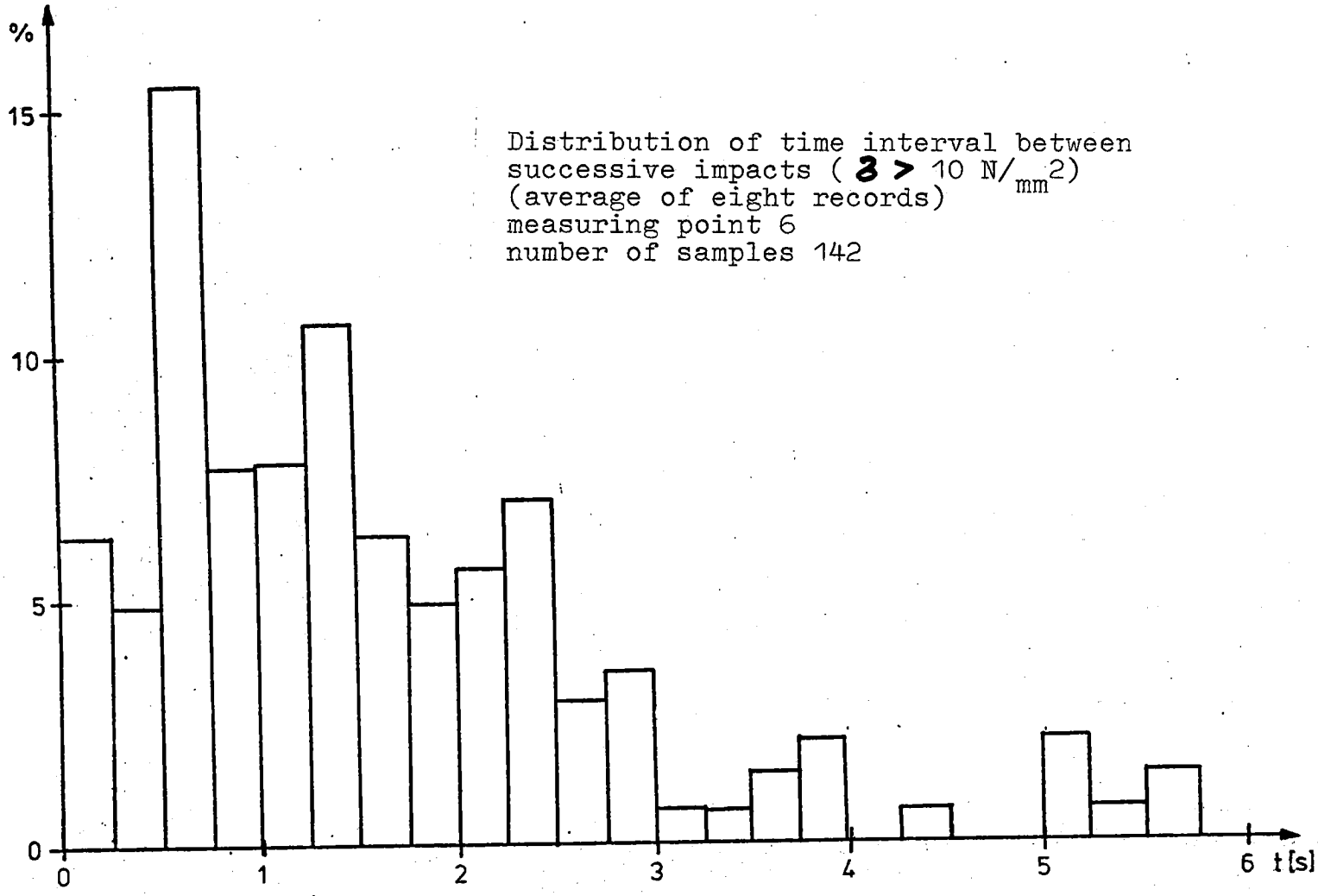

Distribution of time interval between successive impacts ($\sigma > 10$ N/mm^2)
(average of eight records)
measuring point 6
number of samples 142

Figure IV.22.a

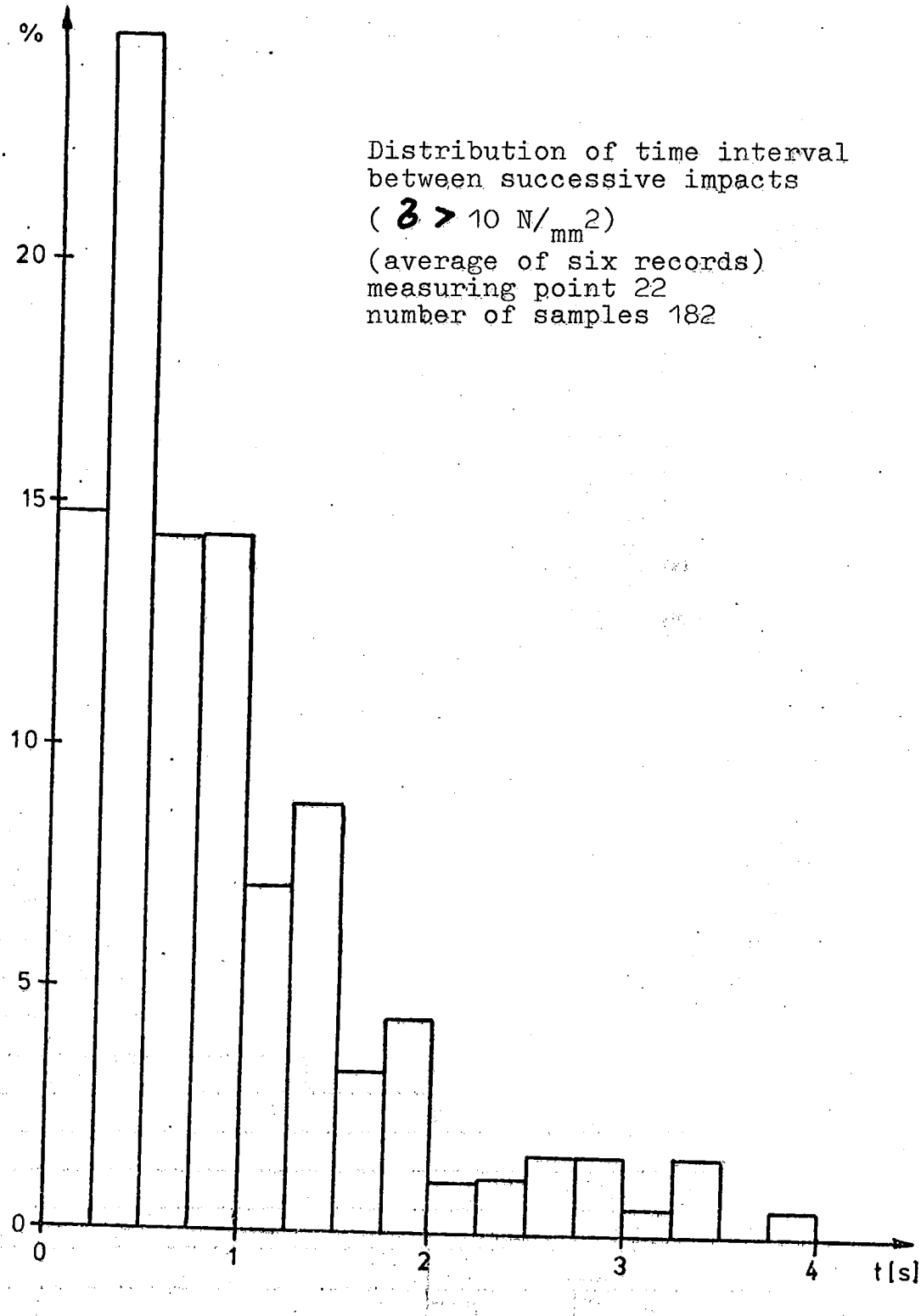

Distribution of time interval between successive impacts
($\sigma > 10$ N/mm^2)
(average of six records)
measuring point 22
number of samples 182

Figure IV.22.b

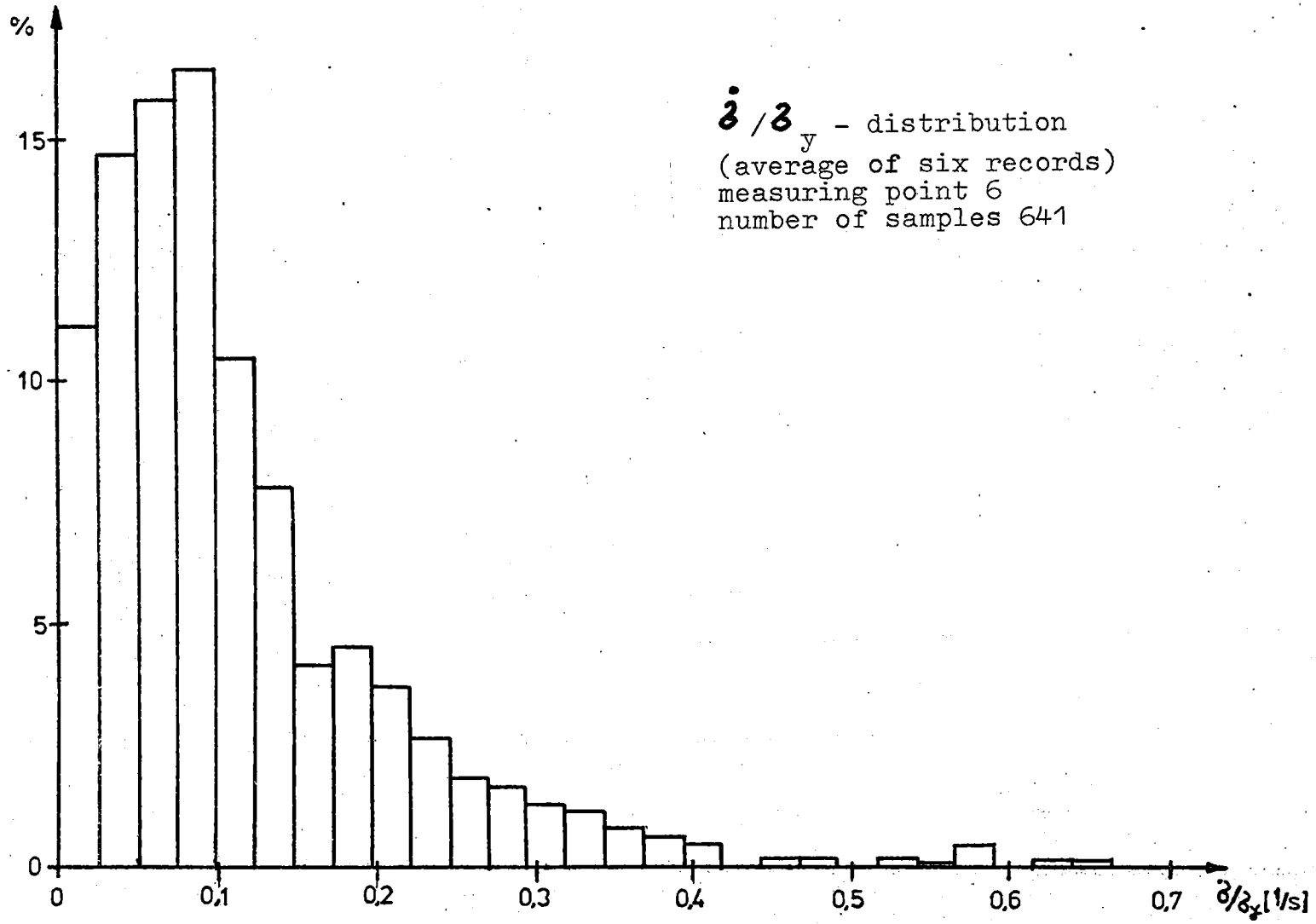

Figure IV.23.a

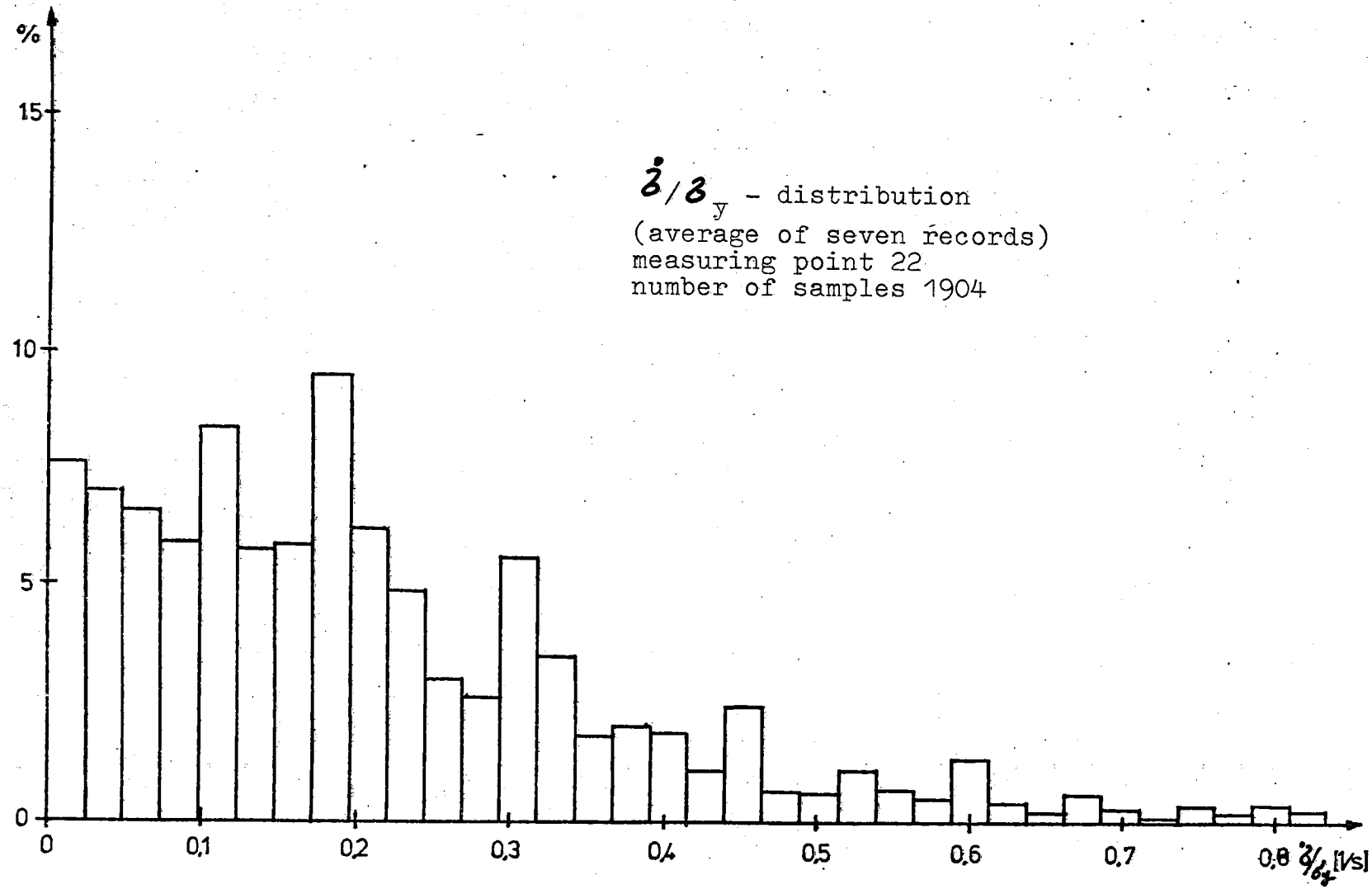

$\dot{z}/z_y$ - distribution
(average of seven records)
measuring point 22
number of samples 1904

Figure IV.23.b

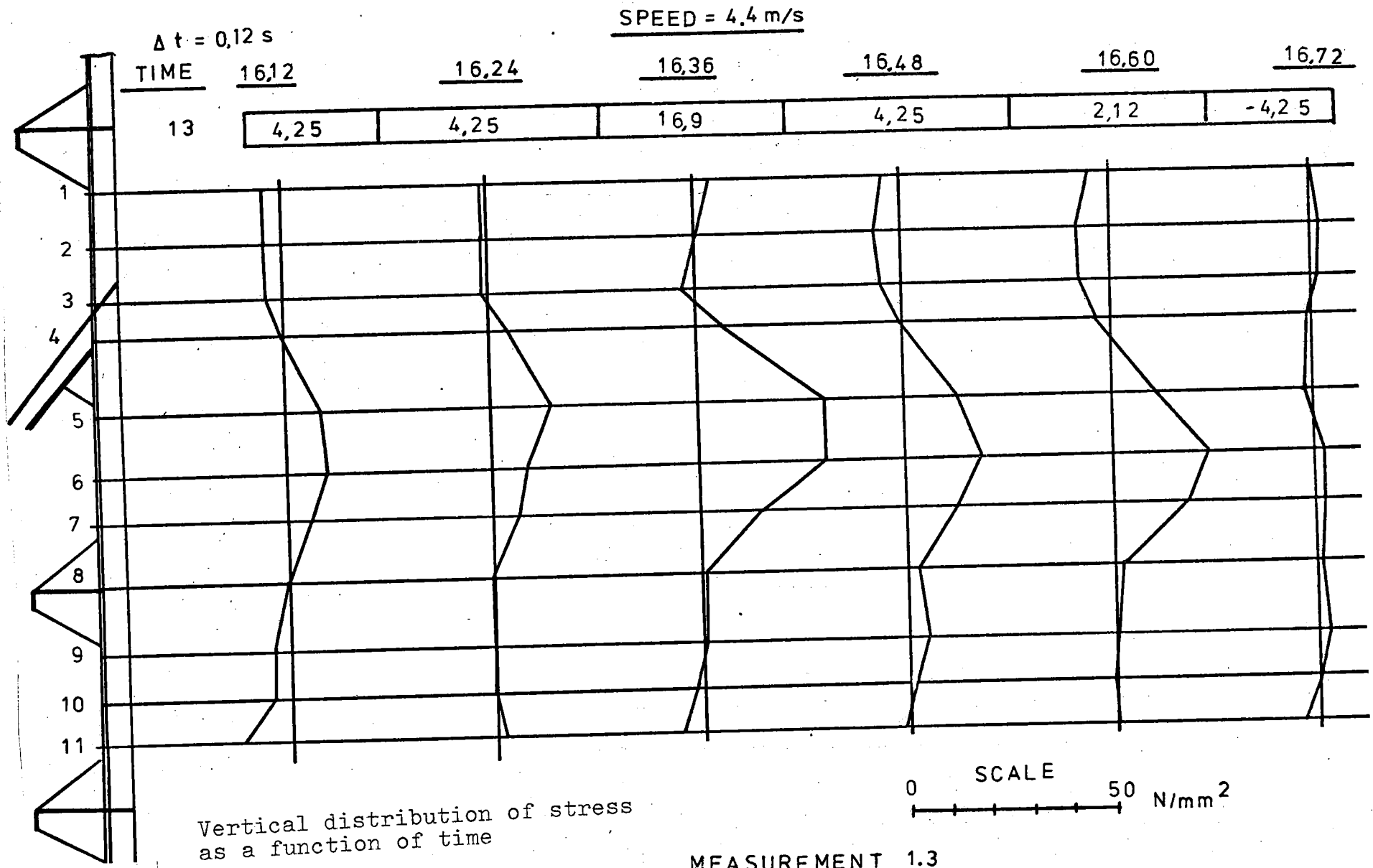

Vertical distribution of stress as a function of time

MEASUREMENT 1.3

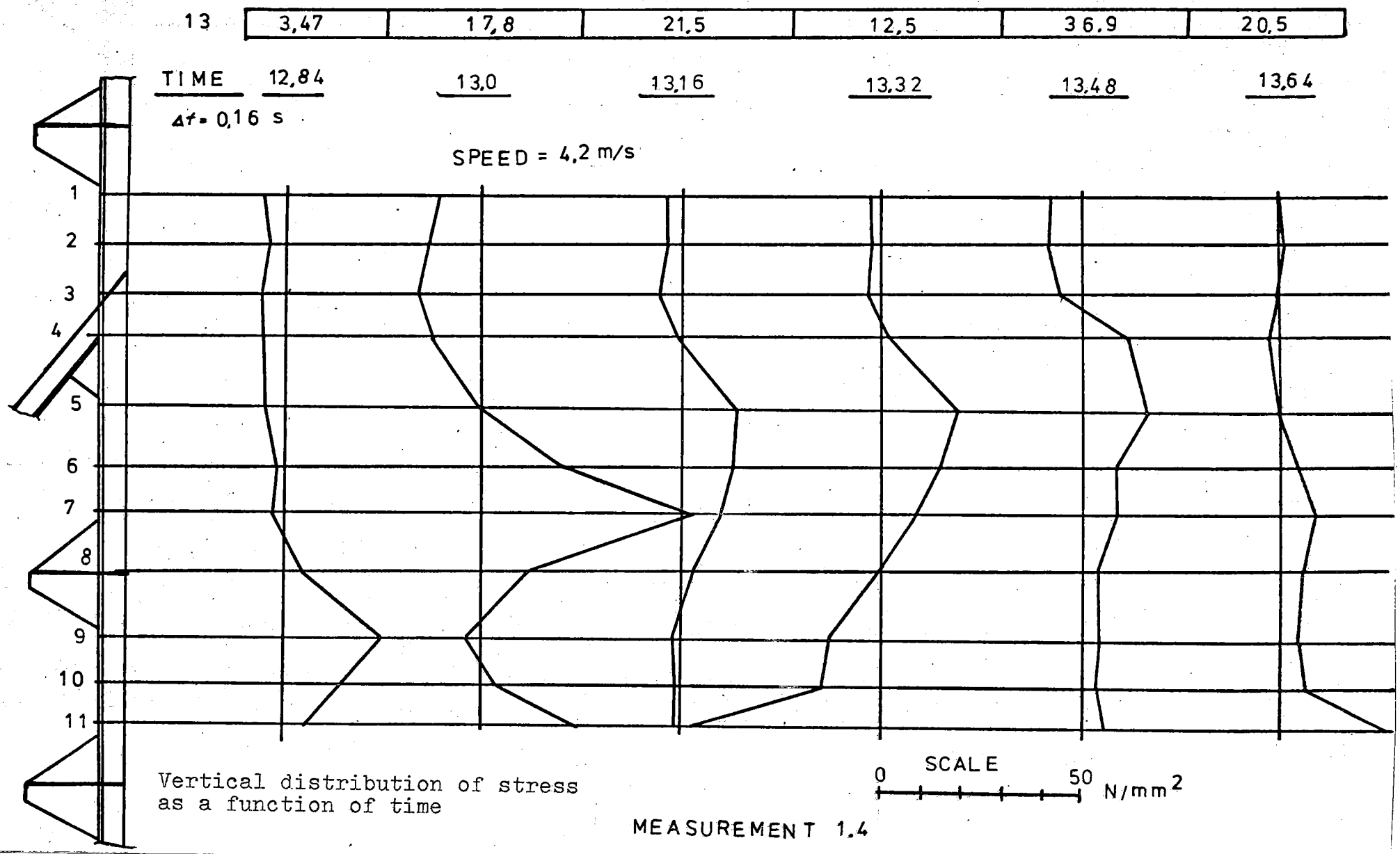

Vertical distribution of stress as a function of time

MEASUREMENT 1.4

Figure IV.25

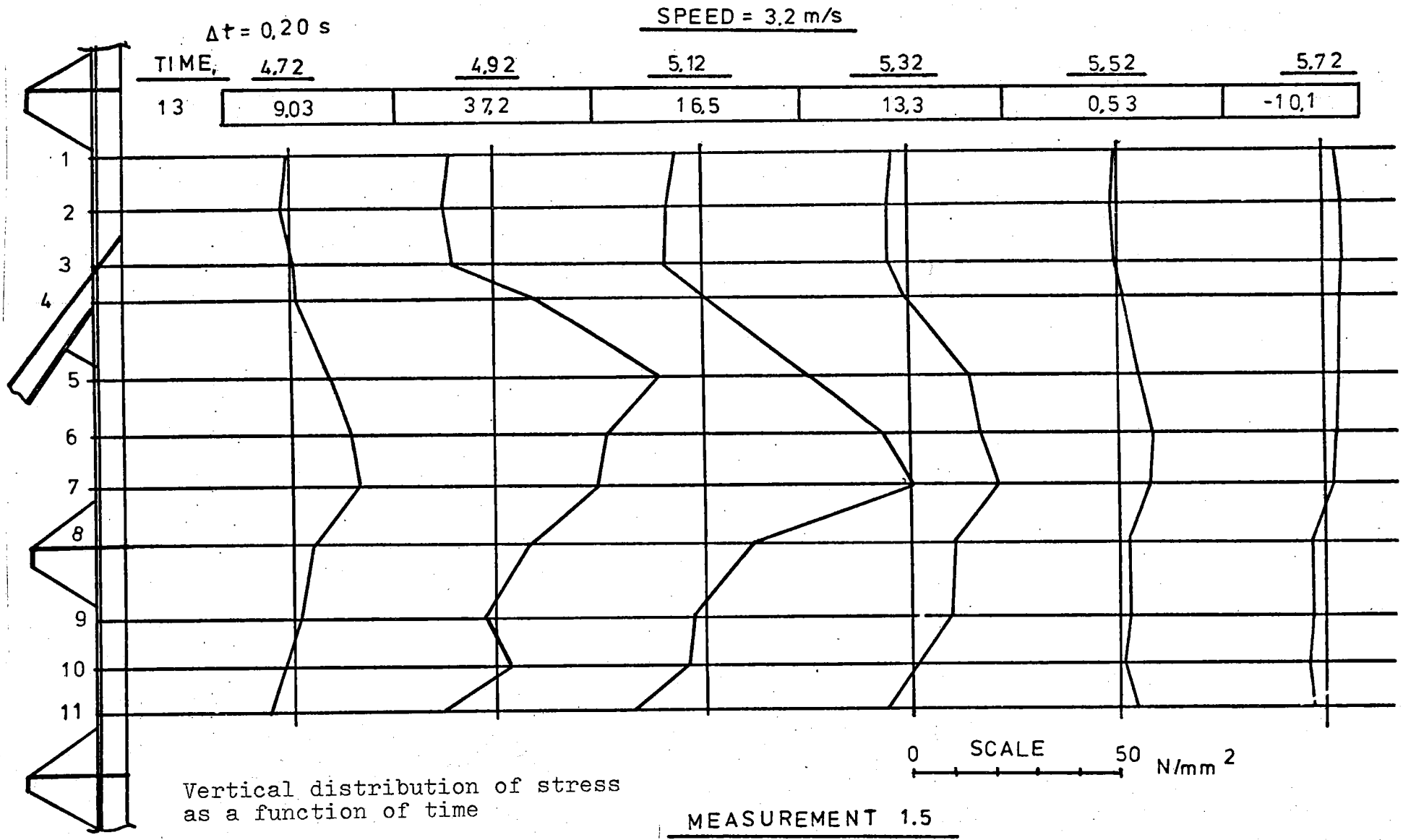

Vertical distribution of stress as a function of time

MEASUREMENT 1.5

Figure IV.26

SPEED 1.9 m/s

5	-6,0	-1,31	7,10	2,37	3,42	1,32
7	4,67	5,74	14,5	24,6	21,9	8,65
16	2,64	1,85	1,58	-1,04	-0,26	-5,20

$\Delta t = 0,24$ s

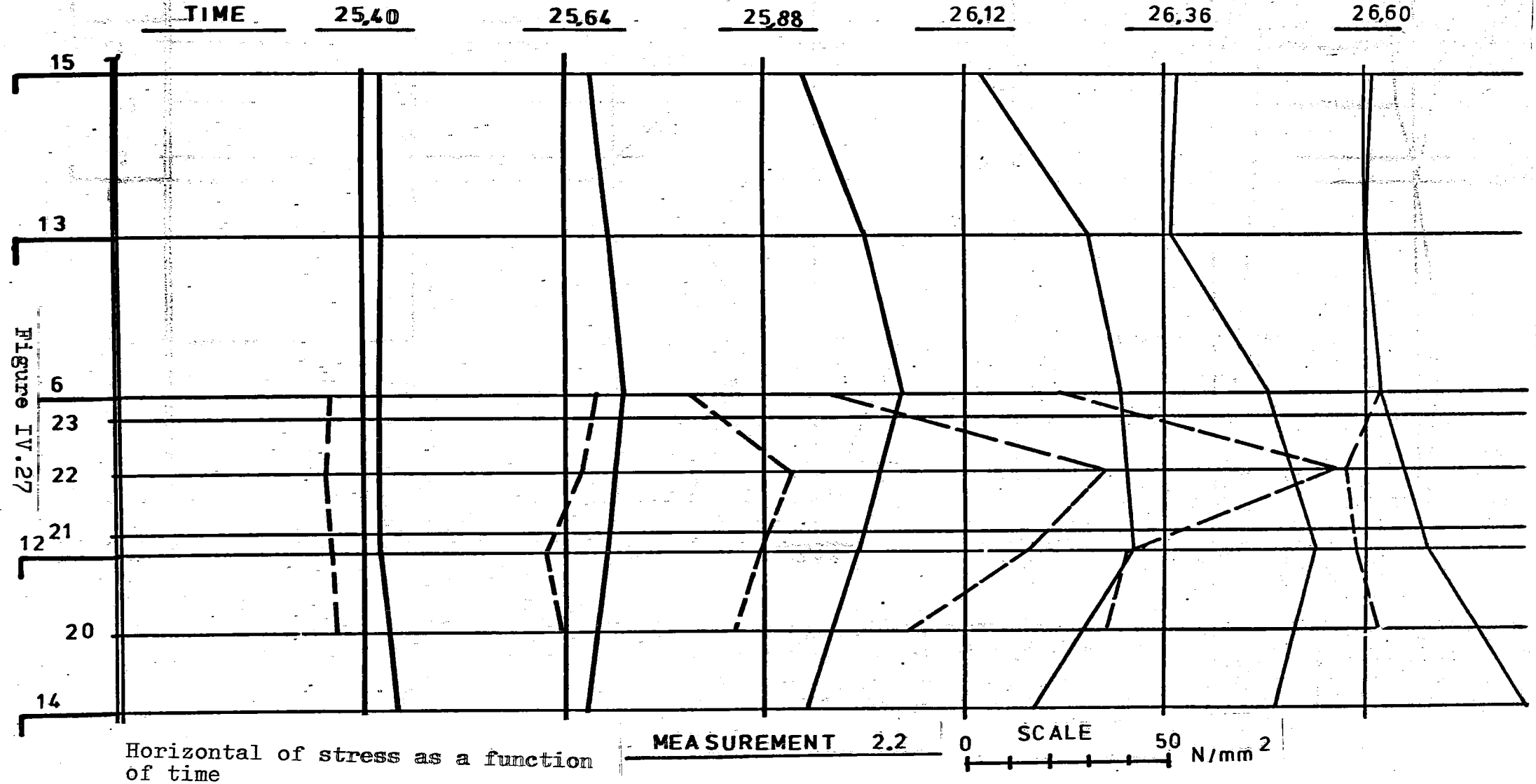

Figure IV.27

Horizontal of stress as a function of time

SPEED = 4,2 m/s

5	-3.14	13.1	27.2	9.93	36.1	-1.57
7	7,94	20,5	37.0	18.3	2,60	2.87
17	8,89	3,76	-0,84	1,59	0,51	0,78

$\Delta t = 0.20$ s

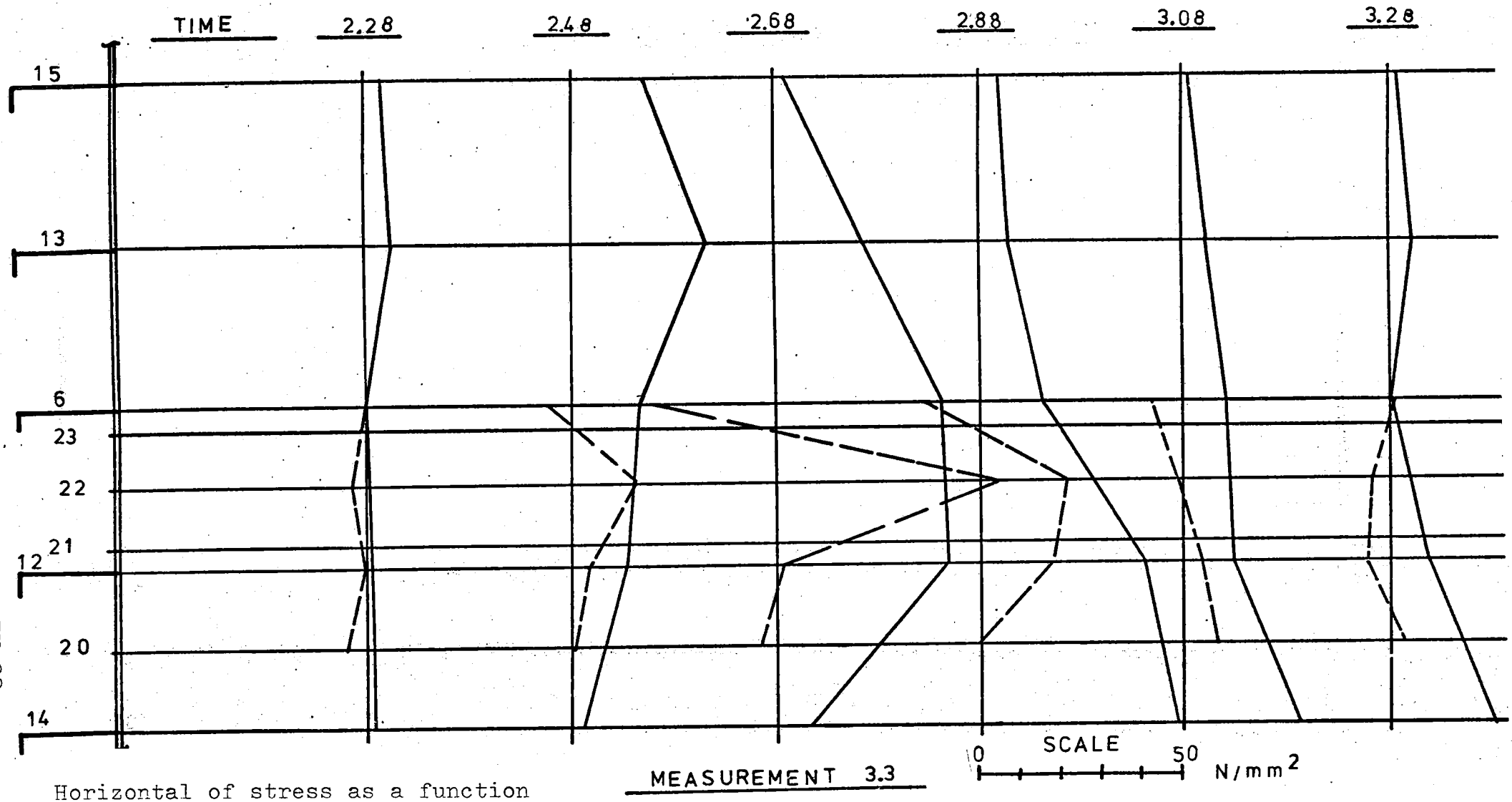

Figure IV.28

Horizontal of stress as a function of time

5	-1.66	3.05	64.7	8.27	43.8	6.71
7	- 2.31	5.07	14.7	21.9	14.9	7.47
17	14.5	6.89	- 0.14	2.84	14.5	-1.22

Δt = 0,16 s SPEED = 4,6 m/s

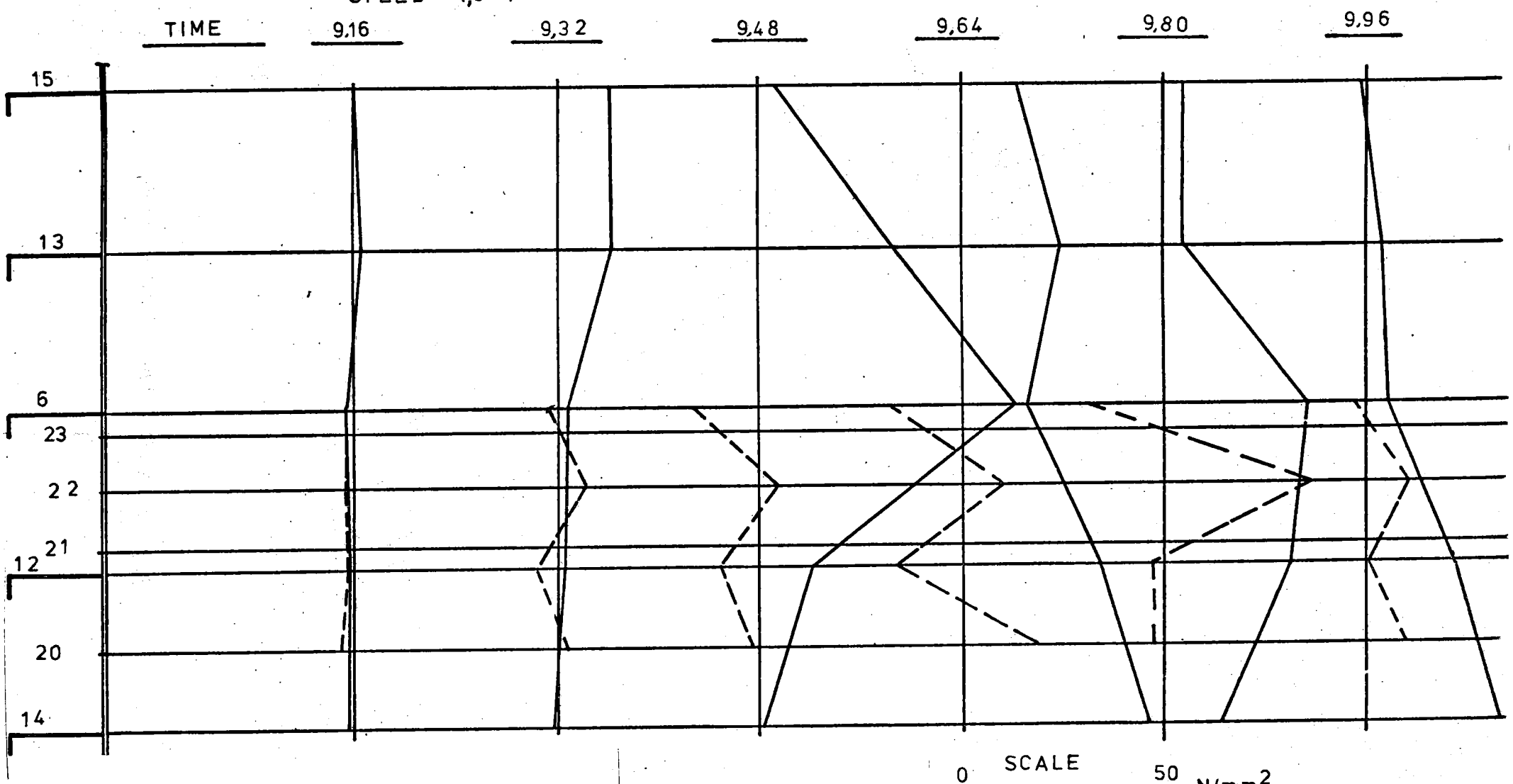

Horizontal distribution of stress as a function of time

MEASUREMENT 3.6

Figure IV.29

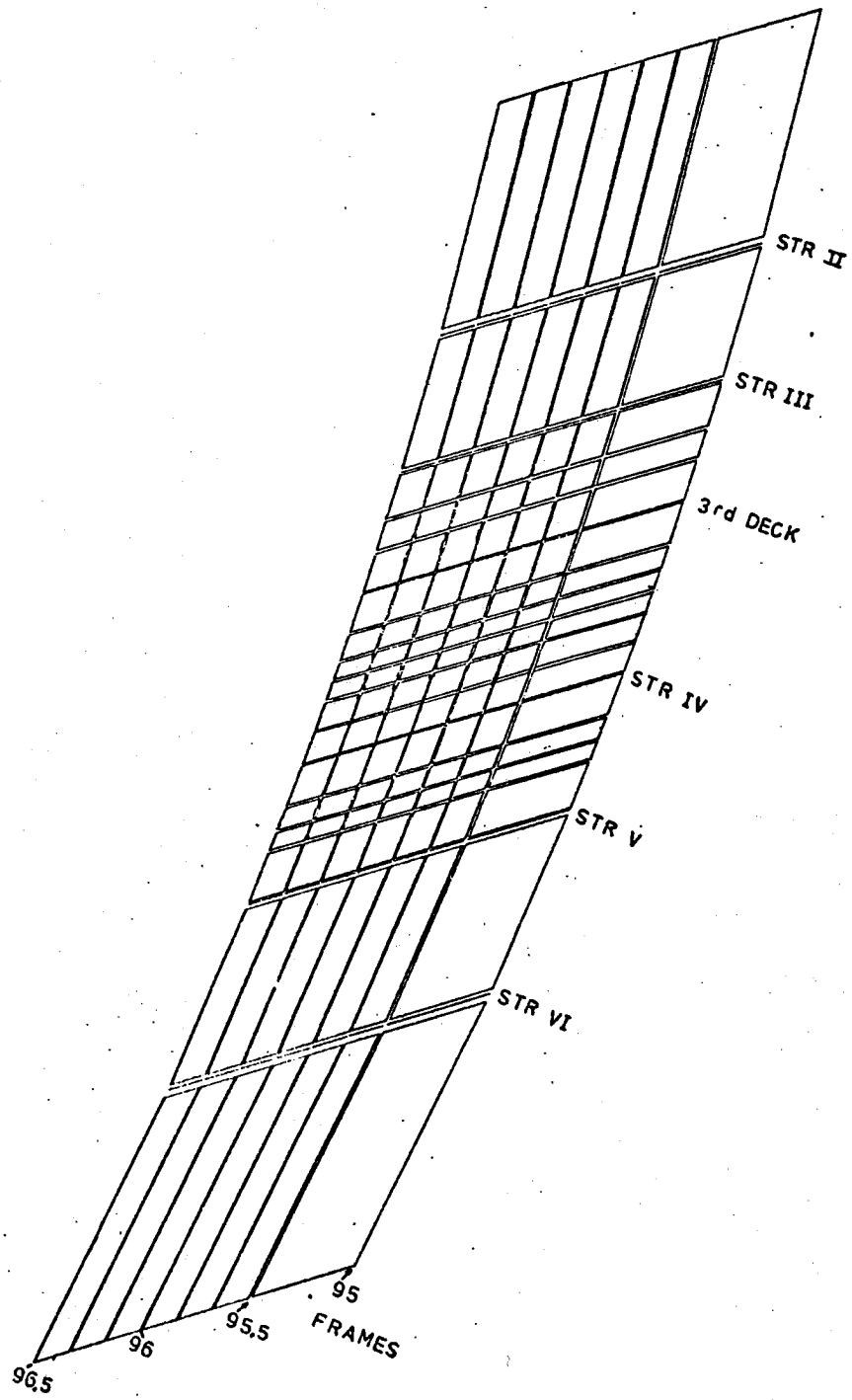

Figure IV.30 The element mesh

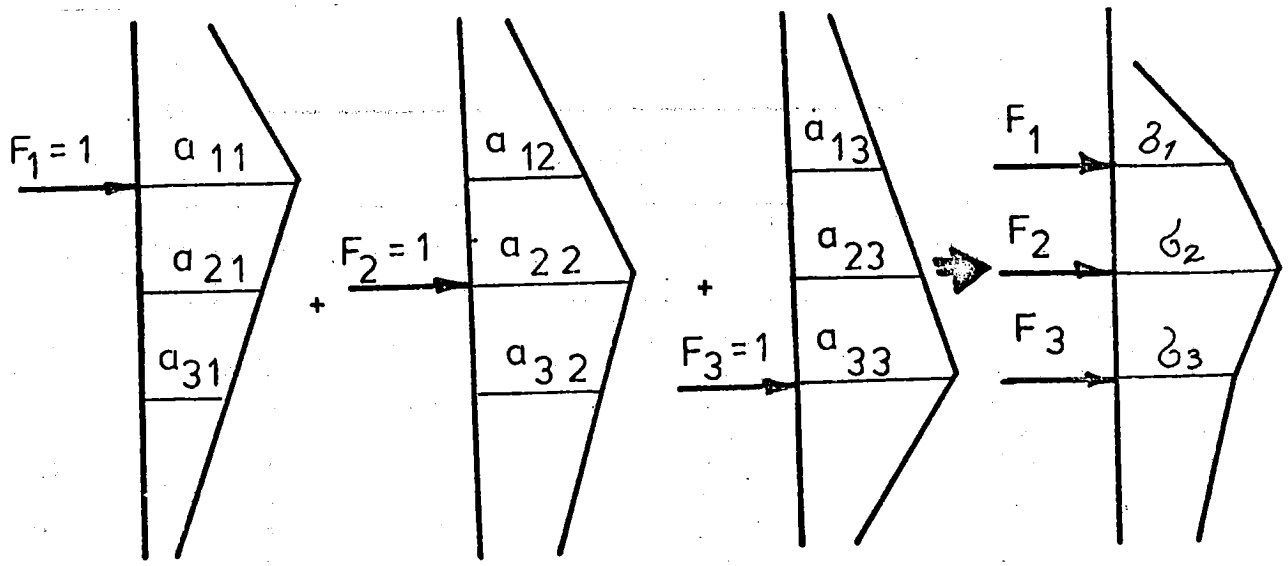

Figure IV.31 The superposition principle

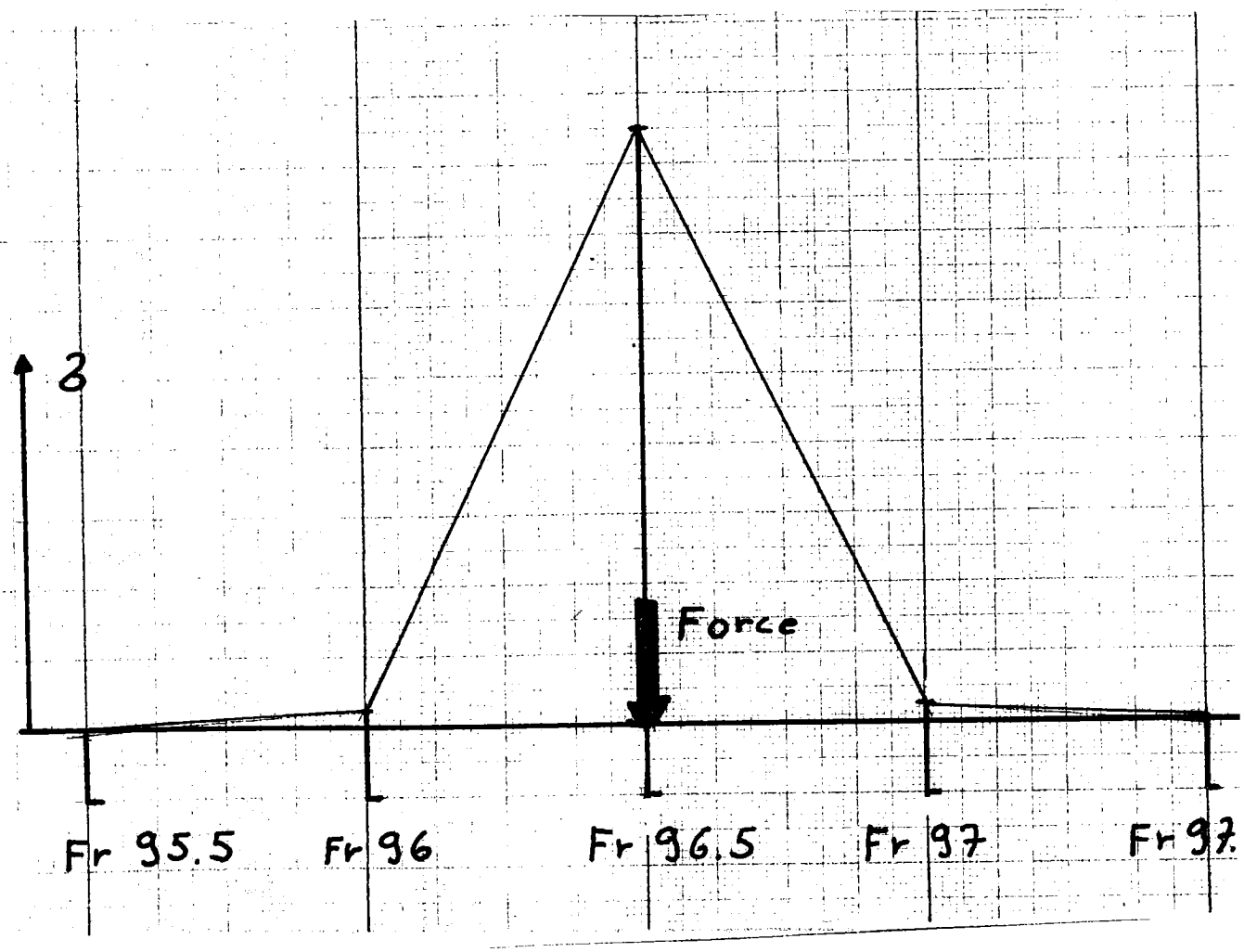

Figure IV.32 Horizontal distribution of response due to a point force

load/kN			
1 fr.sp.	3 fr.sp.s	5 fr.sp.s.	speed/m/s
97	163	-	5.1
91	185	-	4.4
73	189	-	5.5
60	106	-	3.7
147	259	-	3.2
124	220	-	5.4
85	137	-	3.0
41	91	-	3.0
59	115	-	3.0
70	106	-	2.9
63	139	-	2.9
107	259	337	6.0
99	182	200	5.2
98	206	232	4.8
164	284	300	4.6
117	198	198	4.4
101	217	247	5.4
80	160	228	5.2
231	379	407	5.2
98	201	219	5.0
81	145	170	5.0
96	244	283	6.7
128	323	360	4.2
145	302	369	5.1
77	157	179	6.7
103	270	323	6.4
111	246	295	6.3
122	288	313	6.2
90	228	260	5.8
114	320	361	5.4
118	218	252	4.4
108	205	235	4.9
103	231	247	4.9
79	158	166	5.0
109	215	225	4.4
73	210	250	2.0
91	188	194	5.9
86	151	185	4.1
155	254	254	4.2
144	291	295	4.1
153	313	343	3.9
80	193	232	5.8

Table IV.4 Calculated load amplitudes at the different load widths

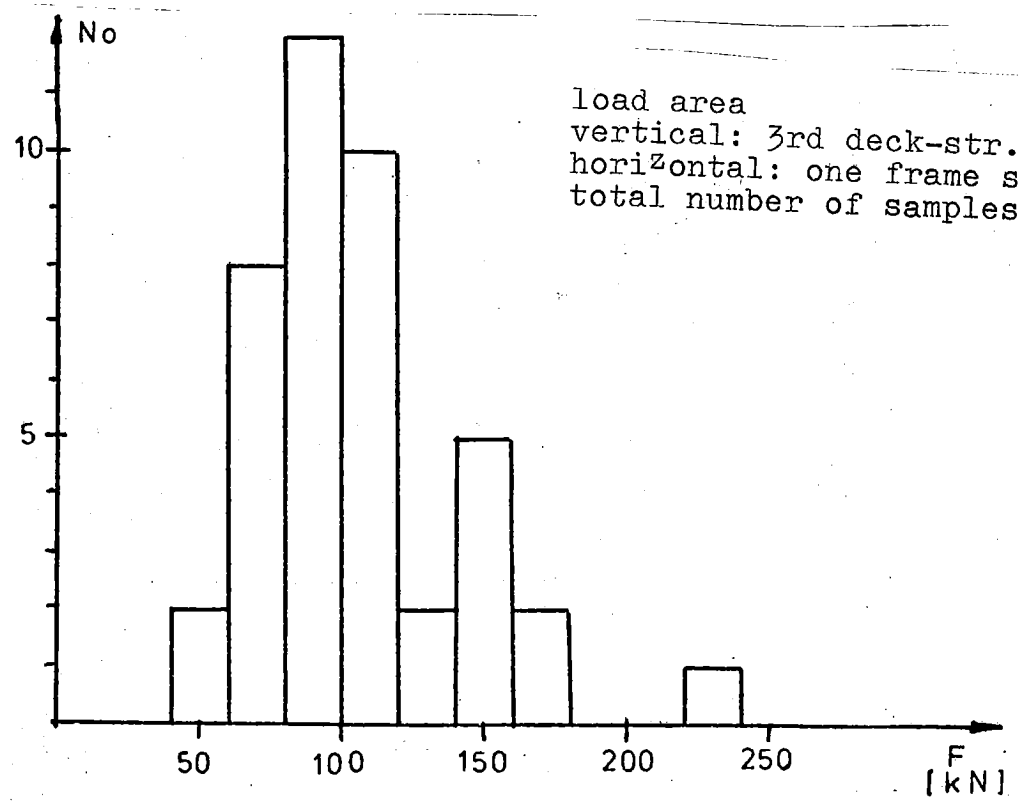

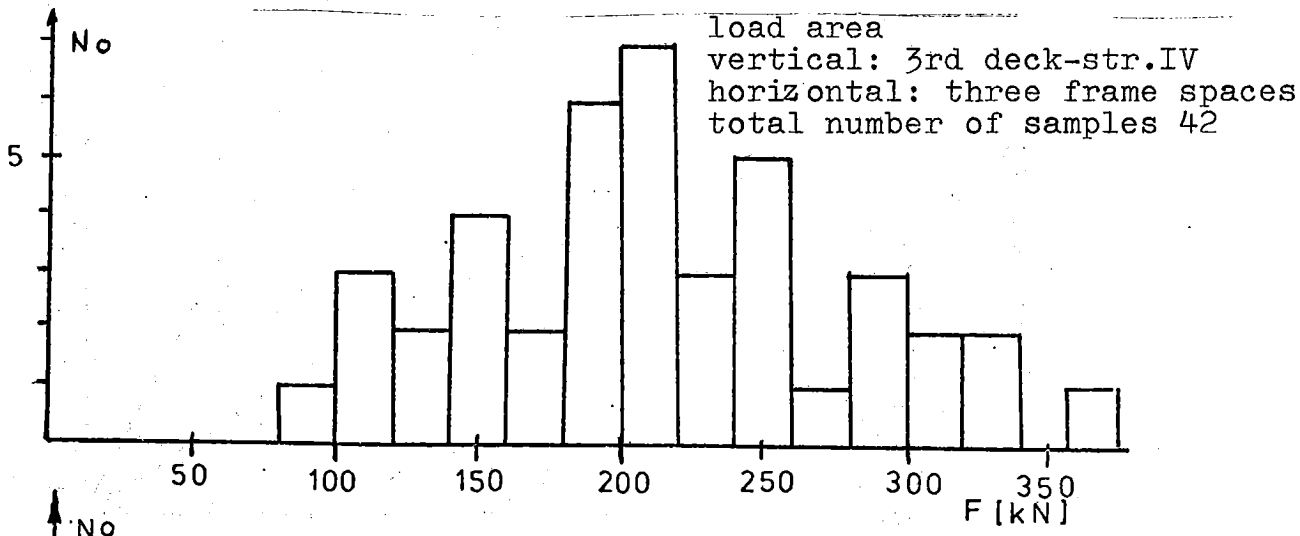

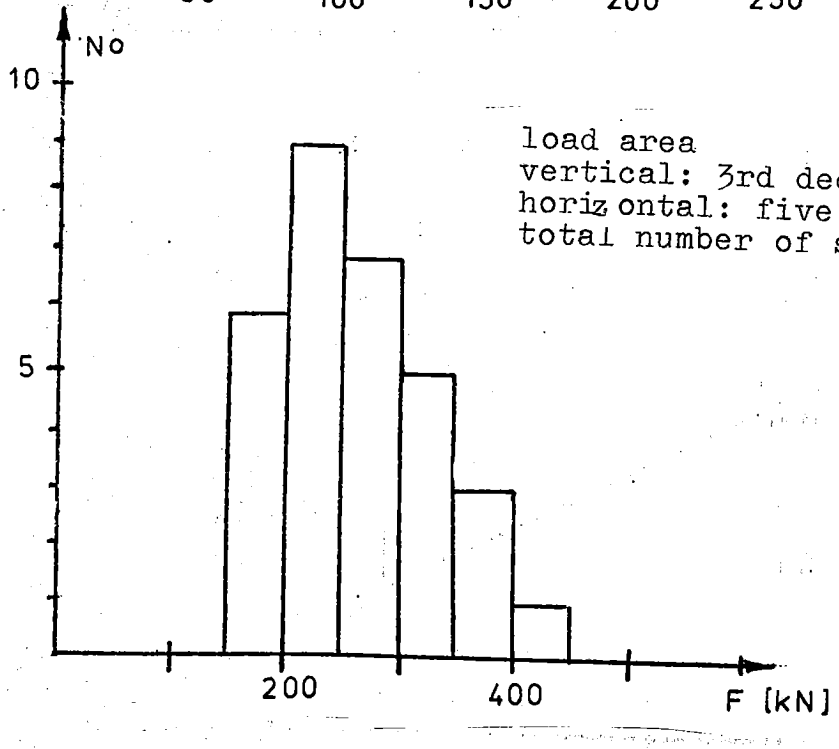

Figure IV.33 Distribution of calculated load amplitude

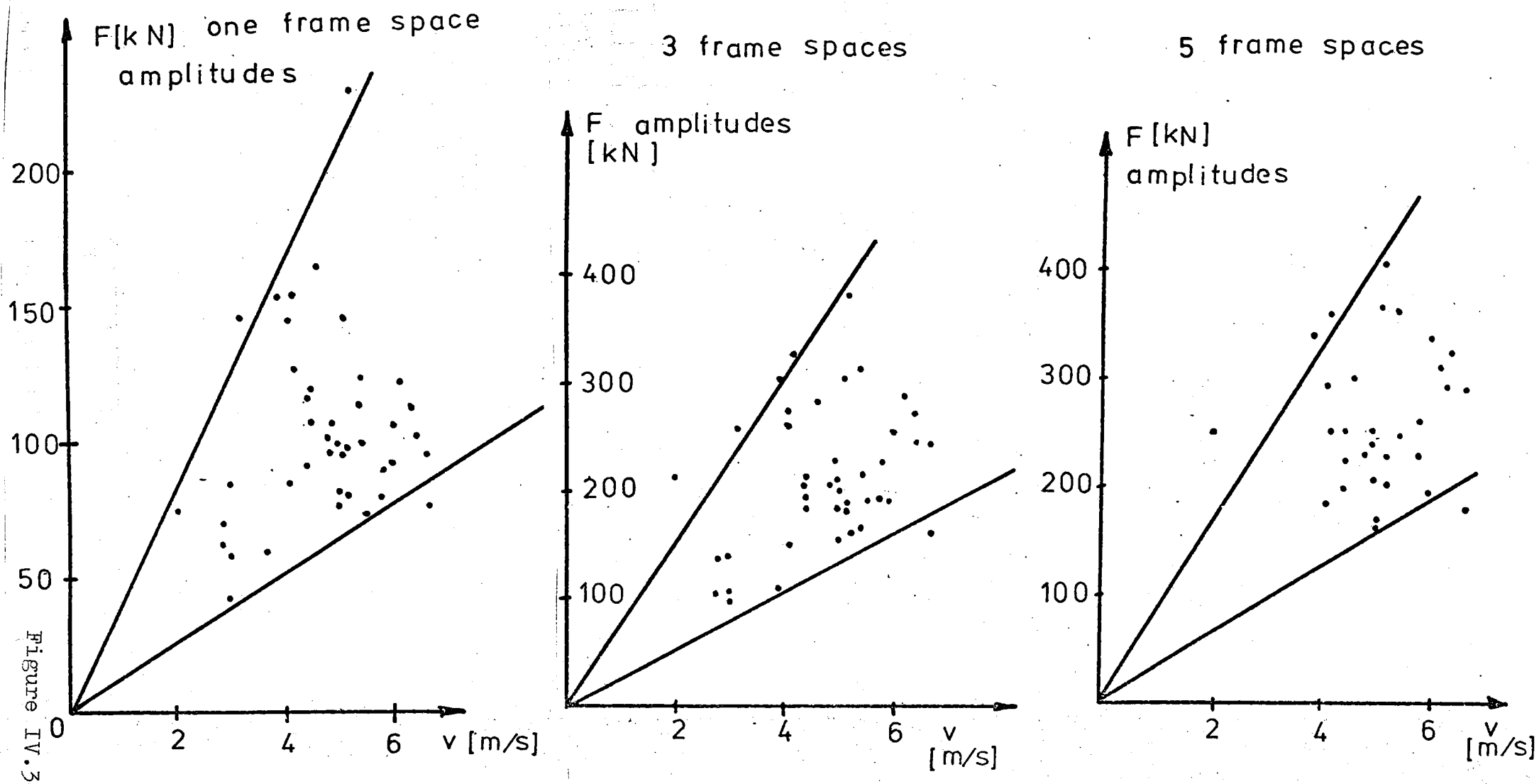

Figure IV.34

The load amplitude as a function of speed of the icebreaker

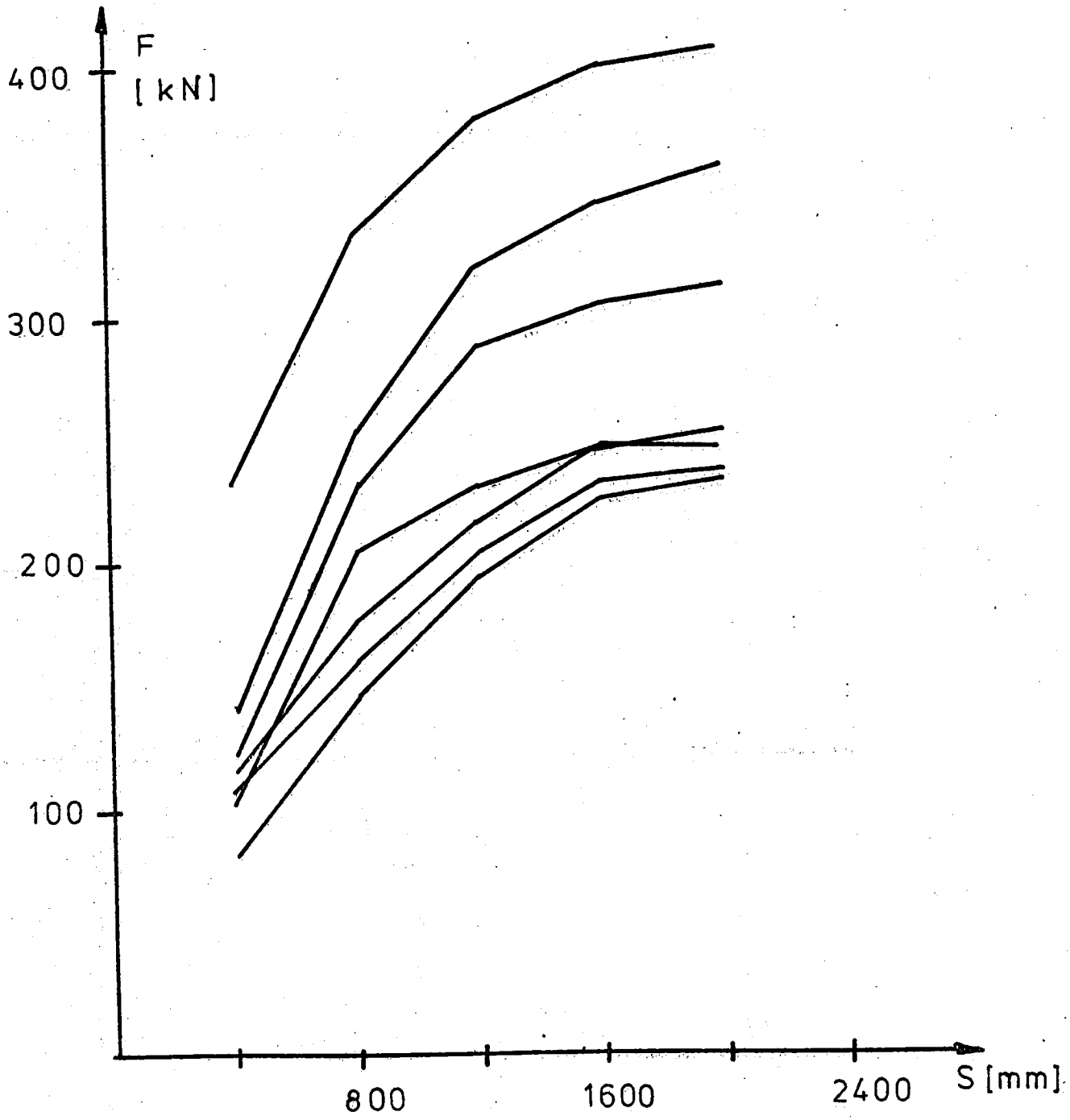

Figure IV.35 Samples of load amplitudes as a function of load width

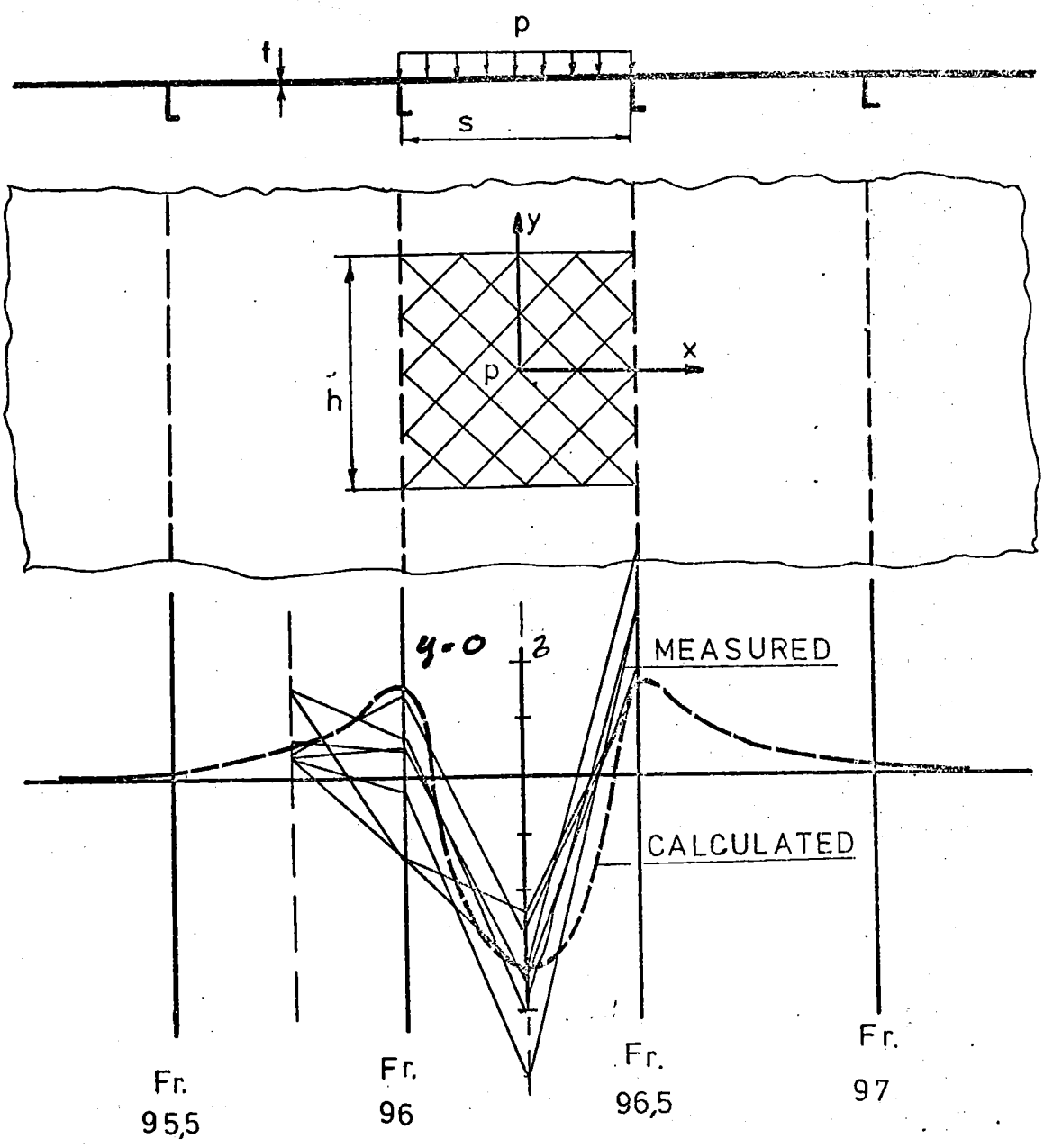

Figure IV.36 A scheme of load on the plate field and calculated and measured stress distributions

Table IV.5 Maximum pressures at different measurements

measurement	maximum pressure (p/p_a)
2.1	0.32
2.2	0.48
2.3	0.28
2.4	0.30
2.5	0.31
3.1	0.51
3.2	0.41
3.3	0.50
3.4	0.25
3.5	0.24
3.6	0.67

p_a = allowed pressure at this local configuration

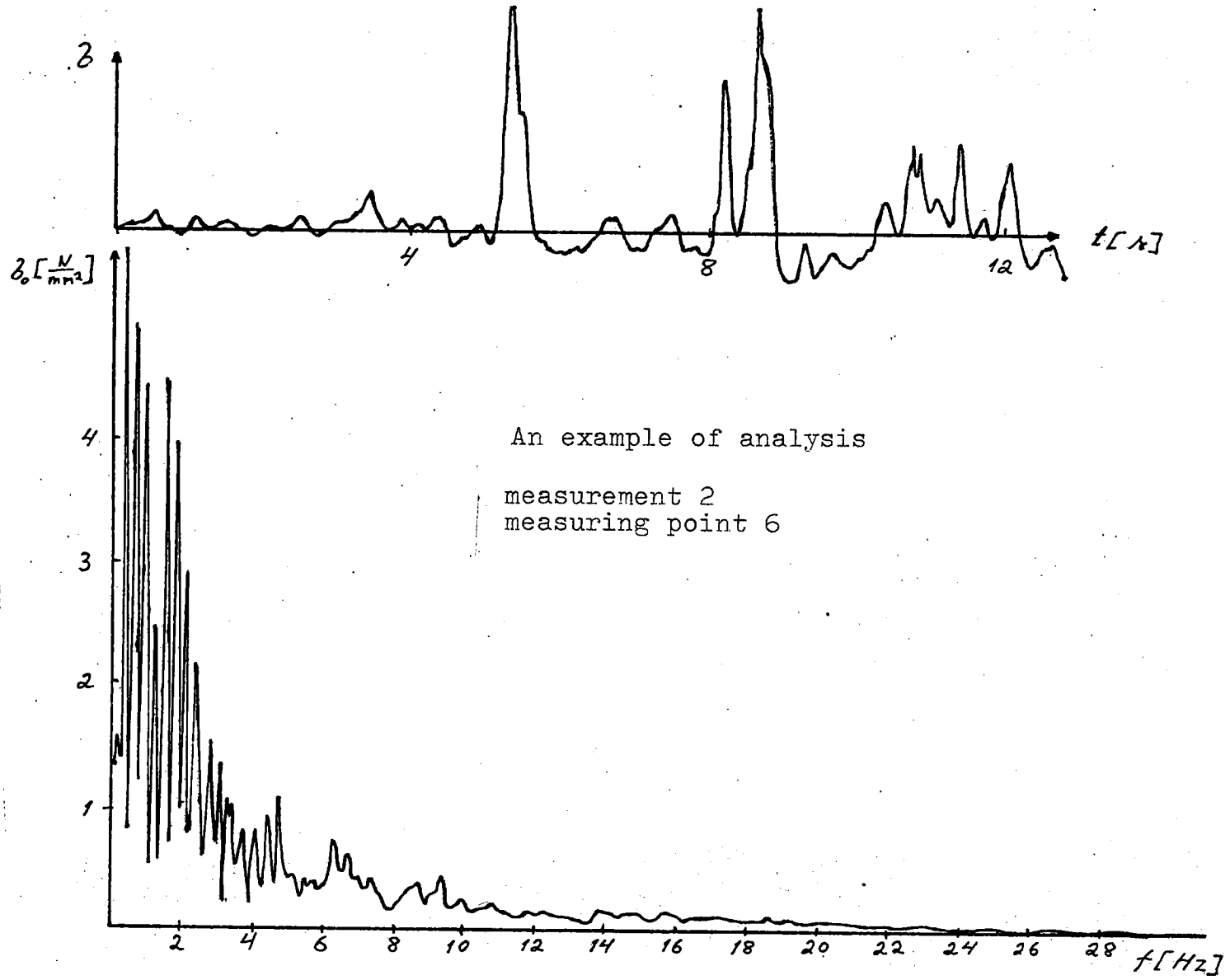

An example of analysis

measurement 2
measuring point 6

Figure IV.37

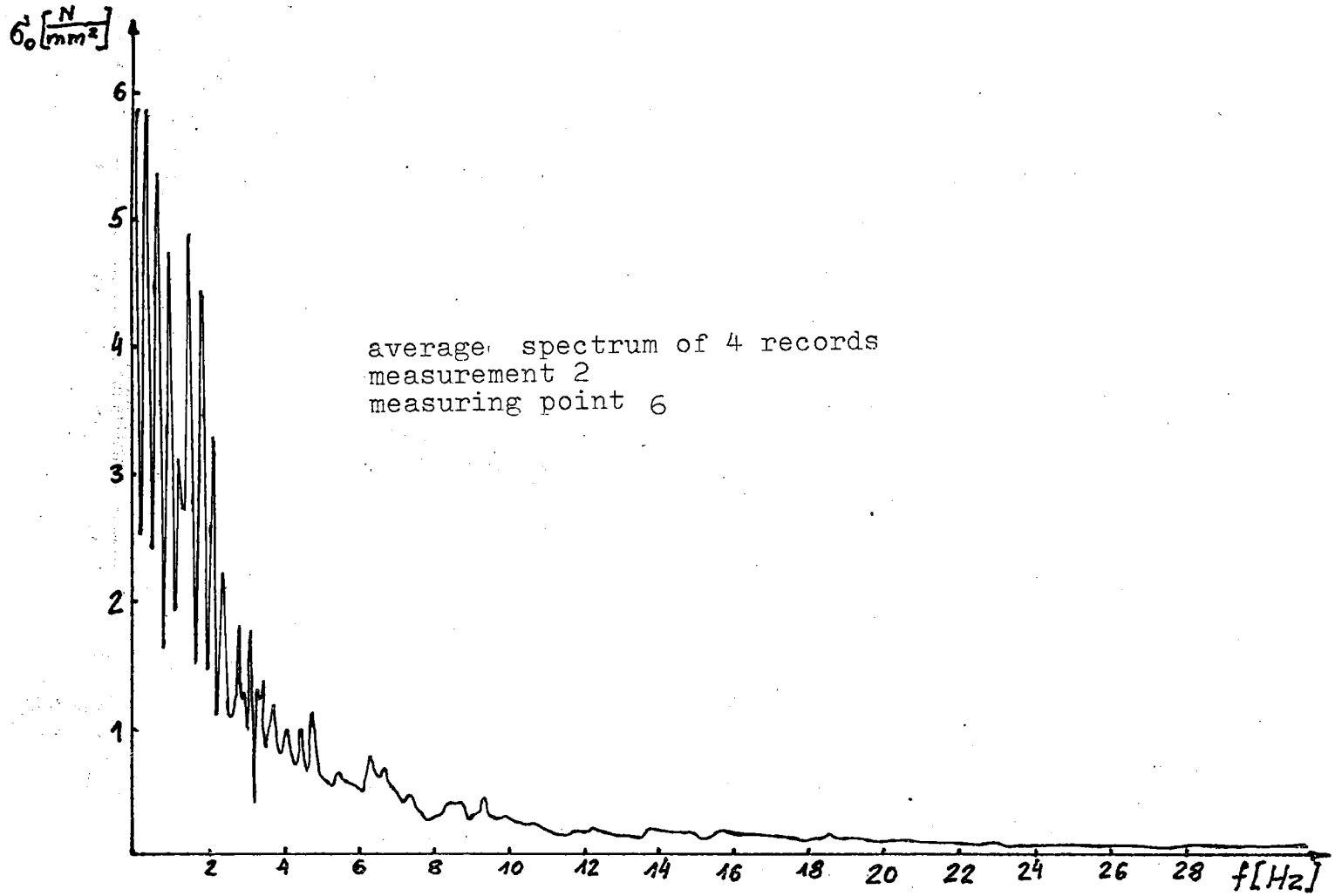
$\sigma_o \left[\frac{N}{mm^2}\right]$
6
5
4
3
2
1
2
4
6
8
10
12
14
16
18
20
22
24
26
28
f[Hz]
average spectrum of 4 records
measurement 2
measuring point 6

Figure IV.38

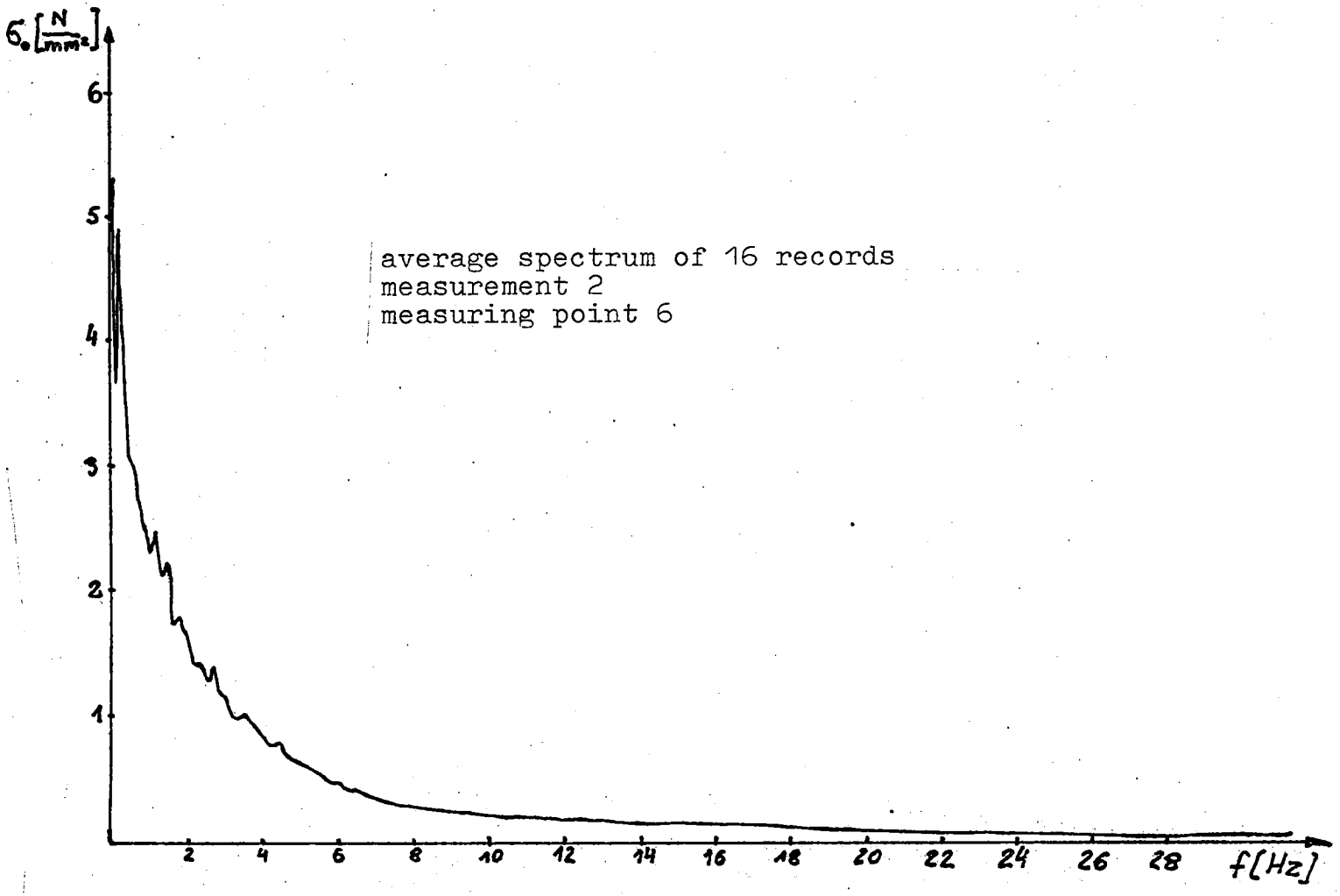

average spectrum of 16 records
measurement 2
measuring point 6

Figure IV.39

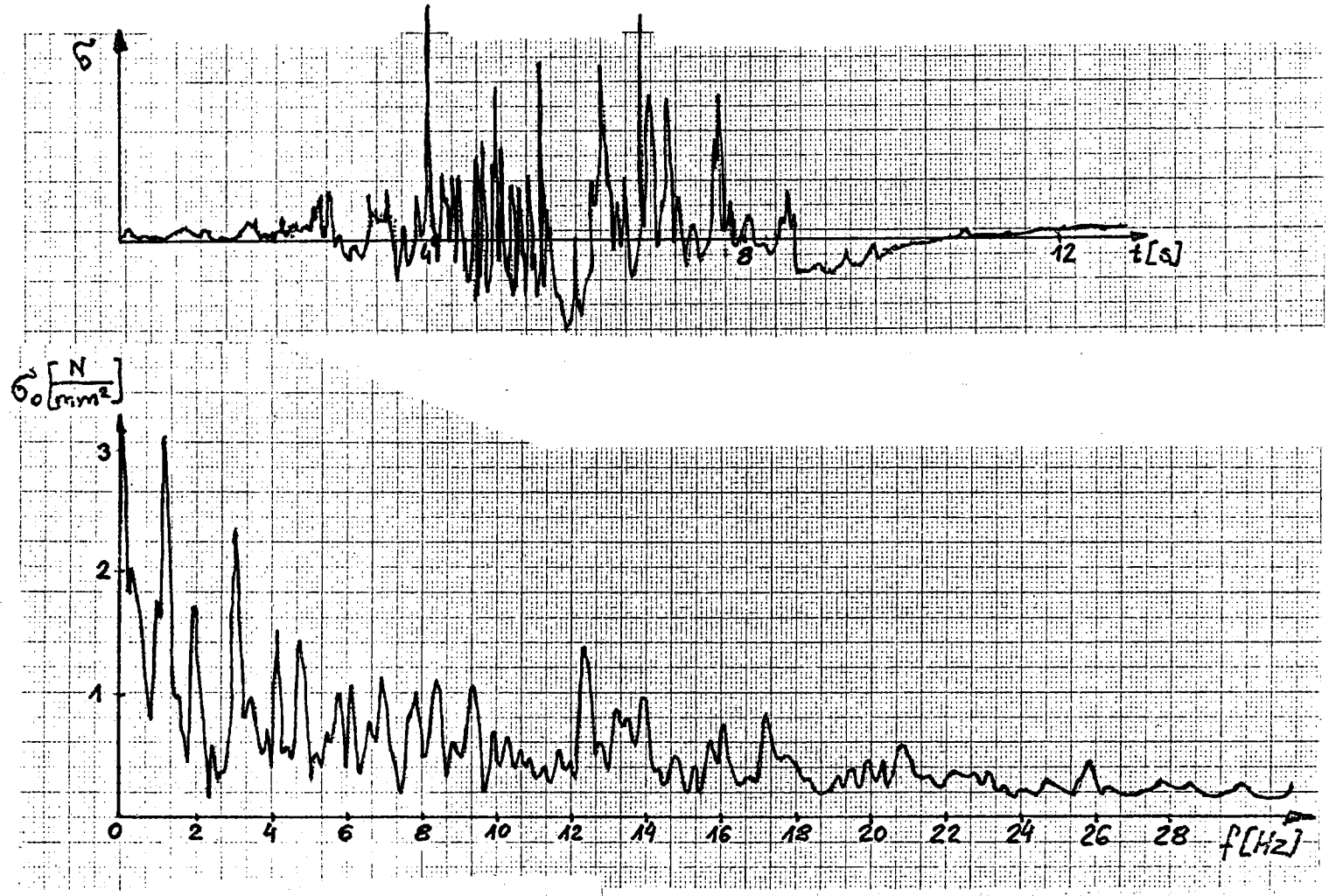

An example of analysis

measurement 1
measuring point 6

Figure IV.40

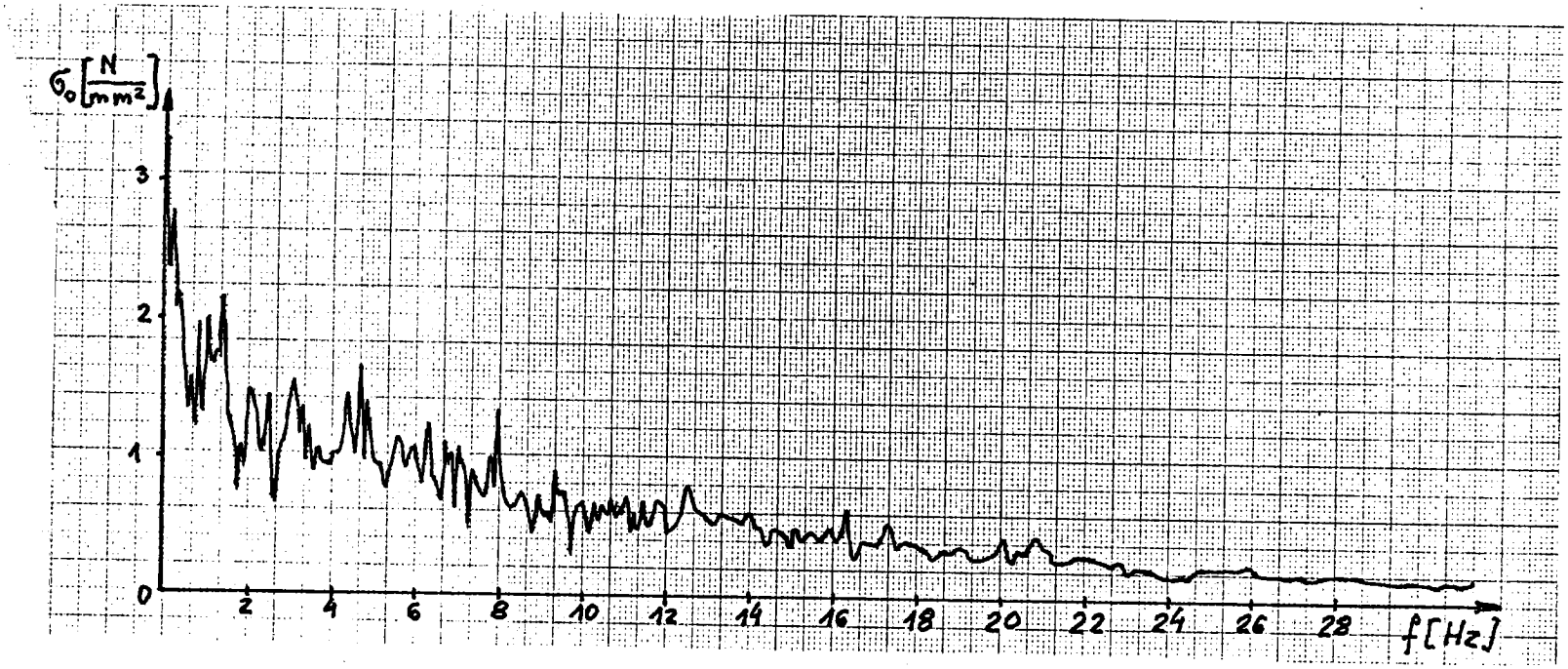

average spectrum of 4 records
measurement 1
measuring point 6

Figure IV.41

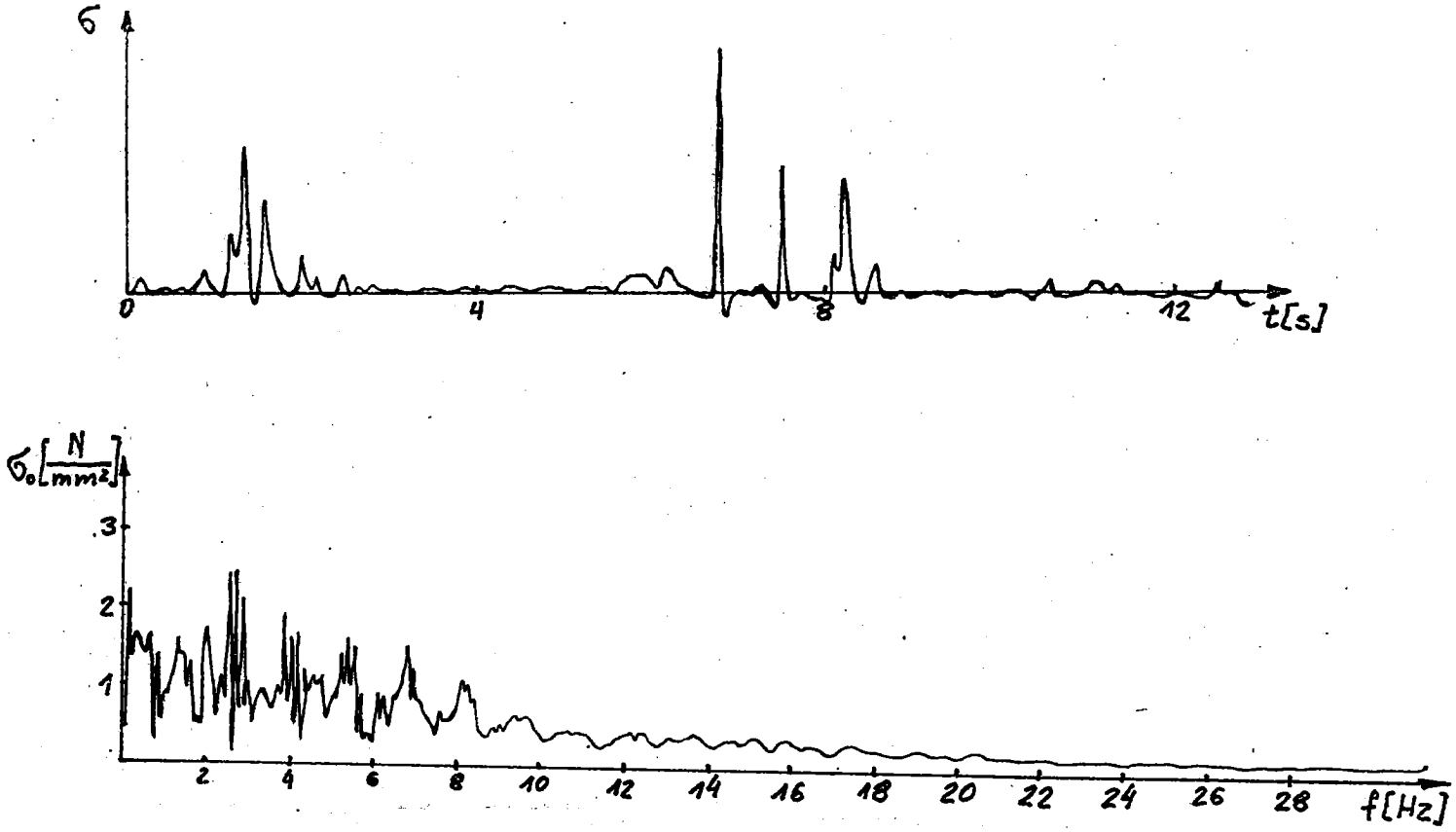

Figure IV.42

An example of analysis
measurement 2
measuring point 22

ISBN 951-46-3173-0